

"Dunărea de Jos" University of Galati
Doctoral School of Mechanical and Industrial Engineering



DOCTORAL THESIS

NUMERICAL AND EXPERIMENTAL STUDY FOR BALLISTIC PROTECTION SYSTEMS WITH ARAMID FIBRE FABRICS

EXTENDED ABSTRACT

Ph.D. Student

Eng. Larisa CHIPER (TITIRE)

Scientific coordinator

prof. eng. Lorena DELEANU, PhD

Series I6: Mechanical Engineering No. 72

Galati

2023

"Dunărea de Jos" University of Galati
Doctoral School of Mechanical and Industrial Engineering



DOCTORAL THESIS

EXTENDED ABSTRACT

NUMERICAL AND EXPERIMENTAL STUDY FOR BALLISTIC PROTECTION SYSTEMS WITH ARAMID FIBRE FABRICS

Doctorand
ing. Larisa CHIPER (TITIRE)

President	Prof. univ. eng. Cătălin FETECĂU, PhD Președintele Senatului - „Dunărea de Jos” University of Galati
Scientific leader,	Prof. eng. Lorena DELEANU, PhD "Dunărea de Jos" University of Galati
Official Referent	Prof. dr. eng. Technical Military Academy "Ferdinand I", Bucharest
Official Referent	Prof. eng. Sorin CĂNĂNĂU, PhD National University of Science and Technology "Politehnica" Bucharest
Official Referent	Prof. eng. Mihaela BUCIUMEANU, PhD "Dunărea de Jos" University of Galati

Series I 6: Mechanical Engineering No 72
Galati
2023

The PhD thesis series publicly defended in UDJG since October 1, 2013 are:

Field of **ENGINEERING SCIENCES**

- Series I 1: **Biotechnologies**
- Series I 2: **Computers and information technology**
- Series I 3: **Electrical engineering**
- Series I 4: **Industrial engineering**
- Series I 5: **Materials engineering**
- Series I 6: **Mechanical engineering**
- Series I 7: **Food engineering**
- Series I 8: **Systems engineering**
- Series I 9: **Engineering and management in agriculture and rural development**

Field **ECONOMIC SCIENCES**

- Series E 1: **Economy**
- Series E 2: **Management**

Field **HUMAN SCIENCES**

- Series U 1: **Philology - English**
- Series U 2: **Philology - English**
- Series U 3: **History**
- Series U 4: **Philology - French**

Field **MATHEMATICS AND NATURAL SCIENCES**

- Series C: **Chemistry**

THANKS

I would like to express my gratitude to those who have been next to me and guided me during the development of this PhD thesis.

I would like to express my appreciation to Professor Lorena Deleanu, PhD, who was the coordinator of my research, for her guidance and support during the years of development of my thesis.

I would like to express my gratitude to the committee that supervised the work, composed of professors phys. Gabriel Murariu PhD, eng Mihaela Buciumeanu, PhD and eng. Constantin Georgescu, PhD, for their support, their critical evaluations and constructive suggestions to both the reports and the thesis, with a high level of competence and professionalism, as well as for their quality guidance and recommendations.

I conducted the experiments with the support of phys. Simona Maria Sandu, PhD and eng. Christian Popescu, with a team of professionals from CCIACBRNE - Research and Innovation Centre for CBRN Defence and Ecology, located in Bucharest.

I would like to express my gratitude to eng. Cătălin Pîrvu, PhD, from the National Institute for Aerospace Research and Development "Elie Carafoli" - INCAS Bucharest, for his guidance in the creation of the model, as well as to eng. Ștefan Palaș from the same institute for his help in making 3D scans of the experimental samples.

I express my gratitude to phys. Alina Cantaragiu Cioromila, PhD, for her support in the careful analysis, discussion and interpretation of the SEM images obtained with the scanning electron microscope of "Dunărea de Jos" University, which provided solid arguments for the investigation of the failure mechanisms.

With love and affection, I dedicate this work to my children and my husband. With love and love I thank my mother, my in-laws, my sisters and my aunt for all their support in caring for my children.

eng. Chiper Larisa (Titire)

Galați, 19.10.2023

Contents

	Thesis	Abstract
<i>Thanks</i>	3	3
Contents	5	5
Summary	8	-
Introduction	11	9
Introduction	13	-
Notations and abbreviations	15	-
List of figures. List of tables	16	-
 Chapter 1. The State-of-the-Art of Fibre-Based Personal Protective		
Equipment.....	31	11
1.1. Introduction.....	31	11
1.2. Individual yarns. personal protection systems.....	32	11
1.3. Fibres used as ballistic impact protection.....	34	12
1.3.1. Introduction	34	12
1.3.2.Types of fibres	36	12
1.4. Ballistic fabrics	39	12
1.4.1. Introduction	39	12
1.4.2. Ballistic fabrics used in protective systems	40	12
1.5. Fibre reinforced composites.....	43	13
1.6. Research methods for ballistic impact mechanisms.....	50	13
1.6.1. Introduction.....	50	13
1.6.2. Analytical method.....	50	14
1.6.3. Numerical method.....	53	14
1.6.4. Experimental method.....	55	15
1.6.5. Empirical method.....	59	15
1.6.6. Combinations of two or more methods.....	60	15
1.7. Conclusions.....	62	16
1.8. Modern trends in the design of personal protective systems.....	63	16
1.9. Research directions	64	17
 Chapter 2. Organisation of the thesis.....		
2.1. Importance of the theme and main objectives.....	66	-
2.2. Organisation of the thesis	67	-
 Chapter 3. Projectile-target impact simulations		
3.1. Introduction	69	19
3.2. Propagation of stress waves in yarns and fabrics	73	19
3.2.1. Propagation of stresses in a yarn under ballistic impact.....	74	20
3.2.2. Stress propagation in a fabric under ballistic impact.....	76	20

3.3. Influence of the constitutive material model for aramid yarns.....	82	20
3.3.1. Introduction	82	20
3.3.2. Numerical simulation methodology for the analysis of the influence of the constitutive material model for aramid threads.....	83	20
3.3.3. Analysis of simulation results for different material constitutive models.....	89	24
3.3.4 Conclusions on the Analysis of the Influence of the Constitutive Material Model for Aramid Yarns.....	119	29
3.4. Influence of Introducing Friction into the Impact Model Projectile-Target	120	30
3.4.1. Introduction.....	120	30
3.4.2. Simulation methodology for the establishing influence of friction in the impact model	123	30
3.4.3. Analysis the results on the influence of introducing friction into the impact model.....	125	32
3.4.4 Conclusions on the influence of friction introduction in ballistic impact simulation.....	132	37
3.5. Influence of sample size in numerical simulation	134	39
3.5.1. Introduction	135	39
3.5.2. Methodology to simulate the influence of sample size in numerical simulation.....	135	39
3.5.3. Analysis of the results on the influence of sample size in the numerical simulation	136	41
3.6. Model validation	148	45
3.7. Final conclusions.....	150	47
Chapter 4. Selected fabrics for ballistic protection systems and the test campaign.....		
4.1. Introduction	153	49
4.2 Sample Procedures for Ballistics Testing: a National Institute of Justice (Ballistic Resistance, NIJ Standard-0101.06).....	157	49
4.3. Methodology of ballistic impact experiments.....	160	51
4.4. How to attach the ballistic panels.....	161	51
4.5. Fabrics used for testing of protective panels	162	51
4.6. The process of making samples of individual ballistic protection armor.....	164	52
Chapter 5. Experimental data for front panels of a vest with protection level IIA.....		
5.1. Back face signature analysis and assessment of the ability of protective systems to stop the projectile.....	169	57

5.1.1. Introduction	169	57
5.1.2. The back face signature analysis in the backing material (BFS).....	170	57
5.1.3. The back face signature analysis by 3D scanning.....	174	58
5.2 Factors influencing the performance of ballistic material in high impact scenarios	186	61
5.2.1. Introduction.....	186	61
5.2.2. Macro photo analysis of the tested panels.....	190	62
5.2.2.1 Analysis of the three fires on Twaron CT736 fabric panels.....	190	62
5.2.2.2. Analysis of the three fires on combined panels Twaron SRM509 fabric and Twaron CT736 fabric.....	218	67
5.2.3. Analysis of the Mechanism of Panel Failure on Impact Using SEM Images.....	244	72
5.2.3.1. Introduction	244	72
5.2.3.2. Multiscale material analysis for protection systems.....	244	72
5.2.3.3. Structure and morphology of aramid fibre	245	72
5.2.3.4. Failure Analysis of the Tested Panels Based on SEM Images.....	250	73
5.3 Final conclusions on the test campaign.....	257	77
Chapter 6. Final conclusions on numerical and experimental results.....	265	81
6.1. Importance of the research topic.....	265	81
6.2. Final conclusions of the thesis.....	266	82
6.3. Personal contributions.....	271	86
6.4. Research perspectives opened up by this work.....	273	91
<i>List of the author's scientific works.....</i>	<i>274</i>	<i>92</i>
<i>Bibliography</i>	<i>276</i>	<i>94</i>
<i>Attachments</i>	<i>292</i>	<i>-</i>

Introduction

Throughout global history, there have been conflicts and military battles. The degree of defence against threats to human life during uprisings and on the battlefield has advanced in tandem with the development of more powerful weaponry. Depending on the type of weapon, different materials have been used to protect against attack at different times in history. Among many other materials, wood, metal, leather and textiles were all essential for the protection of people and their possessions. In addition, these materials have been manufactured in various shapes with specific structures to maximize the protective function. For example, chain mail was used to increase the flexibility of the armor, and metal was used as a sheath to protect the torso.

After the development of firearms, soldiers faced more ballistic hazards compared to earlier weapons (Tam and Bhatnagar, 2006). A new generation of ballistic materials was sought, with an emphasis on light and strong materials. Improved weapon resistance, reduced weight and flexibility were brought about by this technology of personal protection development (Dunn, 2008). Since then, PPE engineering has been dominated by fiber-based materials. As textile-reinforced composites advance, fibre-based composites are becoming more important as body materials for aviation and military vehicles. When more cutting-edge fibrous materials were developed in modern times, such as aramid fibers (such as Kevlar and Twaron), ultra-high molecular weight polyethylene (UHMWPE) fibers (such as Dyneema and Spectra), PBO fibers (such as Zylon) and PIPD fibers (such as M5), this approach to engineering ballistic materials attracted much attention. However, Zylon is not recommended for use in ballistic protection as it is reportedly prone to hydrolytic and photolytic degradation (US Department of Justice, 2005). Since this is the case, aramid and UHMWPE fibres are most commonly used for ballistic protection.

Body armour is essential defence gear that helps the human body fend off many types of assaults. The projectile's ballistic impact is one of the most frequent causes of attacks among the many others. The body armor-related ballistic impact is a fast-moving event that happens in 50–200 μ s. Therefore, armour constructions must react and withstand high-velocity strikes successfully during this period. Mobility and performance are critical factors when it comes to body armour. Traditionally, the primary materials used to make body armour were steel and ceramic, which gave them a hefty, hard appearance. Besides, the human body's joints, shoulders, and necks could not be protected by these inflexible body armours. Researchers turned their attention to body armour made of textiles in order to get around these restrictions. The National Institute of Justice's (NIJ) standard divides body armour into two categories: soft body armour, which is categorised at protection levels I, IIA, II, and IIIA, and hard body armour, which is rated at protection levels III and IV (from NIJ standard 0101.06). Depending on how they are made, body armour made of textiles may be

either soft or rigid. Soft body armour is created by sewing together many layers of high-performance fabrics in textile-based body armour. Conversely, the creation of hard armour involves strengthening the various layers of high-performance fabric inside a polymer matrix. Because they are inflexible, hard body armours limit the wearer's range of motion. Soft body armour, on the other hand, is more flexible and lighter than this.

The aim of this work was to study materials for personal protective systems to increase penetration resistance by making a recent documentation for personal protective systems, making Twaron CT 736 fabric panels and Twaron CT 736 fabric and Twaron SRM 509 fabric panels (hybrid panels) for protective systems, applying a laboratory test methodology based on NIJ Standard-0101.06, using the finite element method to simulate projectile-panel impact and analysing damage/failure mechanisms of ballistic panels.

Chapter 1 includes an overview of personal protective systems, the architecture of ballistic vest systems, ballistic vest development technology, fibres used as ballistic impact protection, a description of fabrics used in protective systems, and recent literature on protective systems and ballistic impact by grouping them by research methods. These research methods are: analytical method, numerical method, experimental method, empirical method and combinations of two or more methods.

Chapter 2 describes the organisation of the thesis, the importance of the topic and the main objectives of the thesis.

Chapter 3 presents projectile impact simulations on the influence of several criteria influencing the ballistic impact mechanism. This chapter starts with a theoretical study regarding the ballistic impact mechanism of a projectile and a ballistic target and continues with three sub-chapters that aim to analyse the parameters influencing the ballistic impact mechanism. In this chapter the validation of simulated models with experimental models is done.

Chapter 4 presents a description of the materials tested, two ballistic materials, how to make the samples tested, how to compose the panels, the size of the panels, how to attach the layers, the thickness of the panels and the velocities of the projectiles.

Chapter 5 presents the results of the experimental tests by analysing the macro photographs, analysing each layer individually to determine the number of broken wires, how the wires broke, the behaviour of the wires that did not break, and the analysis of the polymer substrate and the silicon carbide substrate. The yarn breakage mode is also analysed by SEM photographs. Print depth in the ballistic clay analysis for the samples is performed according to the Ballistic Resistance of Body Armor NIJ Standard-0 101.06, but print depth is also analysed using high precision 3D scans.

Chapter 6 contains final conclusions and personal contributions. These conclusions are essential for assessing the impact of the research and for understanding the importance of the findings in terms of ballistic protection.

Chapter 1. The State-of-the-Art of Fibre-Based Personal Protective Equipment

1.1. Introduction

Due to the existence of war, man has been concerned to protect himself from various hazards such as projectiles and sharp objects. To protect themselves from the many hazards, people wore clothing made of several types of materials: animal skins, wood, stones, copper and steel. Numerous textiles and laminates made of conventional fibers such as linen, cotton, silk and nylon were used as protective materials against various hazards, including ballistic hazards [Scott, 2005], [Saxtorph, 1972], [Sun, 2016], [Abtnew, 2019].

After the invention of gunpowder and firearms, body armor has continuously developed with a new concept of being lighter and stronger to protect from penetration of different calibers. During World War I, body armor was not used; however, experiments began on some later designs. An improved version was reported in 1916 to protect the wearer's chest, but it was heavy due to the use of steel plates. The U.S. Patent and Trademark Office lists registrations dating back to 1919 for various designs of bulletproof vests and armor-type garments.

The development of protection systems has shifted from traditional methods to computer-aided engineering analysis because of the economic and time-saving advantages. However, challenges remain in accurately modelling the behavior of materials under extreme conditions, and one of the key issues is the lack of comprehensive material models that take into account multi-scale phenomena in materials, particularly in the case of armour-grade composite materials. Addressing these challenges is important for improving the performance of protective systems.

1.2. Individual Yarns. Personal Protection Systems

Personal protection consists of vests, armor and helmets. The materials used for personal protective systems are woven, knitted or non-woven materials, laminates and composites [İşmal, 2019], [Hu, 2022].

Personal protective armor can be classified according to textiles, into two categories: soft armor and hard armor [İşmal, 2019], [Tahir, 2022]. It can also be classified according to its flexibility, how it is worn (under or over clothing) and in what situations it is worn. Body armor worn under clothing is thin and may be referred to as concealed body armor.

Concealed body armor is used for a not very high level of protection. Body armor worn over clothing is made of hard panels.

The ballistic vest system consists of a soft armor that is designed to dissipate the force generated during impact and a reinforced component that is designed to further dissipate the force generated during impact, the component that is positioned at the rear [Beck, 2014].

1.3. Fibres Used as Ballistic Impact Protection

1.3.1. Introduction

Fibres are the main elements of a fibre-reinforced composite material. The fibres occupy most of the volume of a composite laminate and share the load acting on the composite structure. The characteristics of a composite laminate are influenced by the correct selection of fibre type, fibre volume fraction, fibre length and fibre orientation [Mallick, 2007a]. The characteristics of a composite laminate are:

- density,
- tensile strength,
- compressive strength,
- fatigue resistance and fatigue failure mechanisms,
- electrical and thermal conductivity,
- price.

1.3.2. Types of Fibres

The two well-known high performance fibers that produce protective textile material due to their high impact resistance [Yavaşa, 2015], [Zhang, 2006] are:

- aramid fibres;
- very high molecular weight polyethylene fibres.

Other commonly used high performance fibre brands are Zylon (Toyobo), Spectra (Allied Signal), M5 Vectran (Hoechst Calanese), Technora (Teijin), Nextel (3 M Ceramic Fiber Products).

1.4. Ballistic Fabrics

1.4.1. Introduction

Textile fabrics are the materials used, in two forms, soft or rigid, for protection systems against various types of ballistic and impact yarns [Abtew, 2009].

The essential requirements for selecting the required textile fabrics are:

- reduced weight,
- high protection performance,
- reduced price,
- comfort [Lane, 2005].

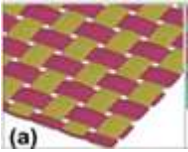
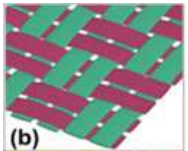
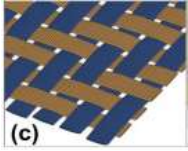
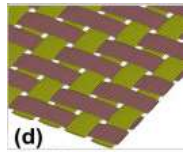

Types of architectures for ballistic fabrics:

- unidirectional (UD),
- two-dimensional (2D),
- three-dimensional (3D).

1.4.2. Ballistic Fabrics Used in Protective Systems

The basic types of 2D fabric are plain weave, bias weave, satin weave and leno weave (Table 1.1).

Table 1.1. Types of ballistic fabrics [Bilisik,2017; Yang, 2015]

Type of fabric	Construction	Properties	Images
Plain weave	each warp yarn runs alternately under and over each weft yarn.	- symmetrical, - directional stability, - high wrinkling, - difficult to mould during casting.	
Basket weave	is a derivative of plain weave which has two or more warp yarns interlaced alternately with two or more weft yarns	- less incremented/corrugated, - a good grip, - unstable.	
Diagonal weave yarns	one or more warp yarns alternately pass over and under two or more weft yarns in a regularly repeated manner.	- smoother surface, - reduced ripple, - good wettability, - good drapability, - low stability compared to plain weave.	
Satin fabric	one or more warp yarns run alternately over and under two or more weft yarns to make fewer intersections	- smooth surface, - good wettability, - a high degree of capability, - low ripple, - low stability, - asymmetric structure.	
Leno fabric yarns	adjacent warp yarns are twisted around consecutive weft yarns	thick and rough surface with high porosity.	

1.5. Fibre-Reinforced Composites

Fibre-reinforced composites are made from fibres and a matrix, the matrix acting as a binder for the fibres. Coupling agents, layers of material and fillers can also be used in composite materials. The coupling agents and material layers are applied to the fibres to improve their connection with the matrix (fibre-matrix bonding) [Mallick, 2007a].

During ballistic missile impact, composite materials for protective systems are tracked:

- slowing down the projectile,
- deformation of the projectile as it passes through the panel or layers,
- stopping the projectile,
- deformation of the back face (Bhatnagar et al., 2006)

1.6. Research Methods for Ballistic Impact Mechanisms

1.6.1. Introduction

High velocity impact resistance is a requirement, of major importance during ballistic impact. Extensive research has been carried out to better understand the ballistic impact mechanisms of different materials with different parameters. Different parameters

and fibre properties influence the final ballistic resistance performance of the target material [Abtew, 2009].

The external and internal parameters that influence the final ballistic resistance performance of the target material are the characteristics of the ballistic material system in terms of:

- yarn properties,
- type of fabric,
- density,
- number of layers,
- impact parameters such as:
 - impact velocity,
 - angle of impact,
 - projectile geometry,
- boundary conditions etc.

1.6.2. Analytical Method

One technique used to analyse, examine and understand the distinct ballistic impact processes of different materials is the analytical method [Mohammed, 2021].

The analytical method has the following objectives [Naik, 2016]:

- to indicate the energy absorbed by different mechanisms,
- to the contact force,
- to the speed of the projectile during partial or total penetration,
- the displacement of the projectile tip at each moment in time,
- determination of residual velocity.

Zhang et al. [Zhang, 2023] studied an analytical model of UHMWPE laminates under ballistic impact in order to determine the deformation/rupture mode of UHMWPE layers. Their proposed analytical model indicates the residual projectile velocity and the ballistic limit.

Dogan et al. [Dogan, 2023] present a new analytical formulation for reducing the impact velocity of projectile-type projectiles based on in-plane tensile break energy absorption, including a new approach, representing energy absorption due to friction.

Liu et al. [Liu, 2023] developed an analytical model to predict BFS for a hybrid panel composed of modified aramid fabrics and unidirectional ultra-high molecular weight polyethylene (UHMWPE) films, which is based on two-step damage evolution: shear blocking and tensile dissipation.

Choudhury et. al [Choudhury, 2023] developed an analytical model for GFRP composite that takes into account the strain rate dependence and temperature effects of the matrix material, including the cohesive zone model.

1.6.3. Numerical Method

In order to establish projectile-panel simulation models and to obtain the ballistic impact performance of materials, many researchers have preferred and used a numerical modeling approach that relies on techniques such as finite element and finite difference

methods, using commercial packages such as Abaqus, Dyna3D, LSDyna, ANSYS, etc. [Pawel, 2022], [Zishun, 2021], [Mark, 2018], [Nilakantan, 2018], [Zhu, 2014], [Tarfaoui, 2001], [Kumar, 2010], [D'Amato, 2003], [Lim, 2003], [D'Amato, 2005], [Royslance, 1995], [Tarfaoui, 2001], [Ghazlan, 2023], [Xie, 2023], [Wu, 2022], [Rezasefat, 2023], [Vescovini, 2021], [Fuqiang, 2023]. Due to the fact that it reduces the work required for sample testing, this method is usually more efficient than the experimental one in terms of time and money.

Marques et al. [Marques, 2021] studied three different armor materials, such as carbon fibre reinforced polymer (CFRP), Kevlar and steel, by numerical modelling, using ANSYS software, considering the bullet made of brass.

Caçoilo et al. [Caçoilo, 2021] use numerical simulation (finite element analysis) to predict the consequences of the impact on bullets military helmet, producing human injuries.

1.6.4. Experimental Method

One of the most reliable techniques for examining the ballistic impact performance of various materials is the use of experimental methods, the obtained data being useful for to improving ballistic applications [Cunniff, 1992], [Karahan, 2015], [Song, 2011] , [Hassanpour, 2019], [Mudric, 2016]. When using experimental methods, it is possible to study how different target configurations and mechanical qualities affect the ballistic performance of the material when impacted by different conventional bullets or fragment simulation projectiles (FSP) at different velocities [Almohandes, 1996].

Bajya et al. [Bajya, 2021] studied the ballistic protection performance and breakage modes of soft armor panels (SAPs) made of different structures, including woven and laminated unidirectional (UD) fabrics.

Pinkos et al [Pinkos, 2023] conducted an experimental investigation of human body injuries protected by biaxial and triaxial fabric ballistic packages, during a non-penetrating impact from a Parabellum 9 mm and 19 mm Full Metal Jacket (FMJ) projectile, at a velocity of 406 ± 5 m/s.

1.6.5. Empirical Methods

An empirical and semi-empirical method is one of the simplest and most important methods for investigating ballistic material performance, which mainly focuses on data from experimental work to investigate ballistic material impact responses, various failure mechanisms [Cunniff, 1992], [Gu, 2004], [Shim, 2001] and dependences on the influencing factors (package thickness, impact velocity).

1.6.6. Combinations of Two or More Methods

Using only one of the methods (experimental, empirical, numerical or analytical) is very difficult to fully understand and describe the ballistic impact process. For a better understanding of ballistic impact mechanisms combinations of methods (experimental, empirical, numerical and analytical) are used [Signetti, 2022], [Gilson, 2021], [Gregori, 2020], [Asemani, 2021], [Shim, 1995], [Chen, 2013], [D'Amato,2001], [Chandekar, 2014], [Soydan, 2018], [Chen, 2014], [Sikarwar, 2012], [Mohamadipoor, 2018], [Shaktivesh, 2015], [Lee, 2001], [Tabiei, 2002].

Jafari et al [Jafari , 2023] investigated the ballistic performance of a composite armour composed of ceramic-polyurea-aluminium layers. First, to validate the simulation results, they used two reference targets and the coated with ceramic-aluminium and polyurea-aluminium layers were investigated.

Hakan et al [Hakan , 2023] experimentally and numerically investigated the dynamic response of functionally graded plates subjected to normal and oblique ballistic impact. According to numerical and experimental studies, the impact angle and material composition were found to be significant influencing the damage and deformation of functionally graded plates.

1.7. Conclusions

Flexible protection systems are preferable for their performance and advantages over hard ones, given their low weight, wearer is comfort and mobility. The optimal design of an armour system should balance three conflicting characteristics: effective protection, mobility and comfort. Armour comfort is affected by all parameters that influence both protection performance and mobility. The mechanism of armour failure under bullet impact was investigated by considering the theories of deformation propagation under bullet impact and the effect of fabric structure in single and multi-layer armoured structures. The effect of some parameters on ballistic velocity is presented. In some armour designs, hard plates are used as inserts in flexible armour to increase the protective capacity.

1.8. Modern Trends in the Design of Personal Protective Systems

Advances in materials science have led to the development of protective systems made from materials, such as aramid fibres and ultra-high molecular weight polyethylene (UHMWPE). These materials provide protection while reducing the overall weight of the protective system, making it more comfortable for wearers.

Another trend is the design of protective systems that allow much greater mobility and comfort for the wearer. Modular armor systems have become more popular, allowing users for tailoring their protection to the mission or to the yarn level.

In addition to ballistic protection, individual protection system designs have focused on mitigating the effects of explosions and fragmentation from explosive devices. This includes the development of blast-resistant materials and designs to reduce the risk of traumatic brain injury.

1.9. Research Directions

This PhD thesis aims to study ballistic panels based on layered aramid fibre fabric and to analyse the impact behaviour by simulation using the finite element method and by testing with a single type of projectile (9 mm FMJ bullet).

For this thesis, the research directions are:

- a study of the influence of the number of layers on back face signature (BFS),
- numerical modelling to evaluate the behaviour of a meso-modelled level for the panel (isotropic and homogeneous yarns) to significantly reduce experimentation and design costs,

- laboratory testing of panel pull-outs,
- the study of failure processes at different levels (macro, meso and micro) of the panels tested,
- a state-of-the-art of reported products from Teijin Aramid Netherlands (which still has very few experimental reports on ballistic protection of various types).

In today's world and national conditions, the protection of personnel in the army and state institutions in the fields of police, justice, gendarmerie, intelligence services is important and research results are needed for product design, and approval, for innovative solutions that include the latest developments in the field.

Chapter 2. Organisation of the thesis

The figure below summarises the activities carried out for this research theme.

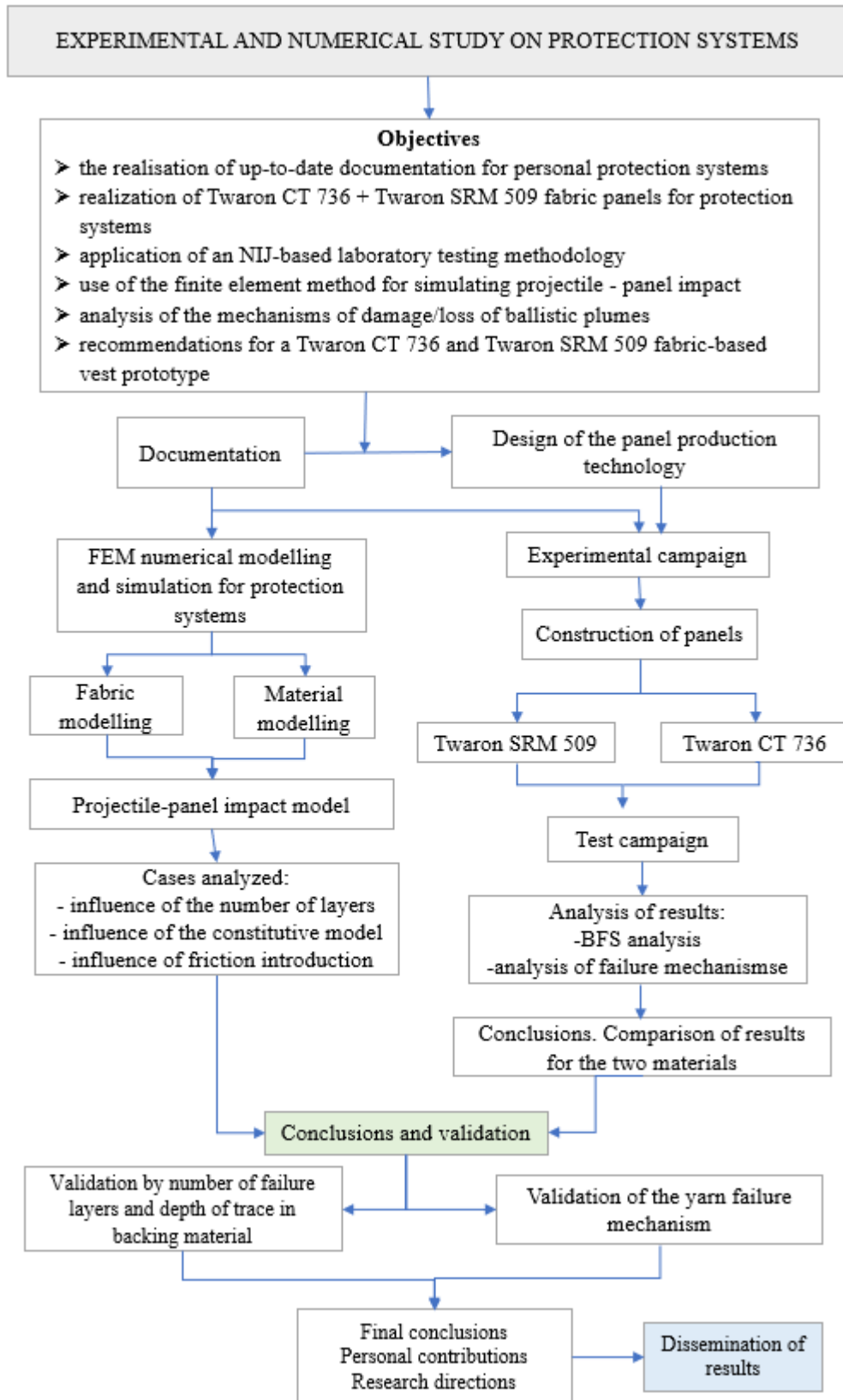


Fig. 2.1. Thesis diagram

Chapter 3. Projectile - Target Impact Simulations

3.1. Introduction

The design and realization of protective material systems can be accelerated and made more cost-effective by using the lightweight protective material development flowchart that is given in Figure 3.1. The design and testing process is replaced by rapid iterations of modeling and simulation, with ballistic evaluation used selectively to verify satisfactory designs. The aim of this diagram is to design superior protective system and accelerate their implementation in armour systems. This armour design process provides an improved and closer link between the materials research and development side and the modelling and simulation side, resulting in a significant reduction in the time to develop new protective systems.

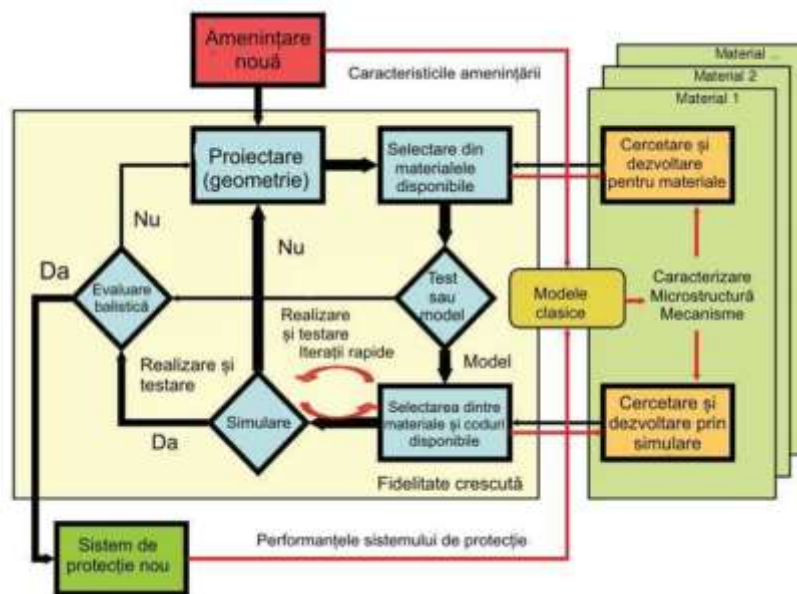


Figure 3.1. Diagram of the design, simulation, testing and implementation of a protection system [National Research Council. Opportunities in Protection Materials Science and Technology for Future Army Applications; The National Academies Press: Washington, DC, USA, 2011. <https://doi.org/10.17226/13157>, <http://nap.edu/13157>]

3.2. Propagation of Stress Waves in Yarns and Fabrics

During impact, the projectile creates a transverse deflection in the main yarns, while longitudinal stress waves propagate from the point of impact along the axes of the main yarns with the velocity of sound in this material. The number of warp/weft yarns hit by the projectile makes the process of absorbing fabric energy very complicated because the projectile can hit on the yarns, or in the space between the yarns. When the projectile hits only a few yarns on the affected zone, the results will be very complicated to be modelled.

3.2.1. Propagation of Stresses in a Yarn Under Ballistic Impact

The investigation of the transverse impact behaviour of a single yarn or fibre is done to understand the different impact behaviours of fabrics. When a single yarn is subjected to

projectile impact, a cone-shaped transverse deflection has formed in the yarn, growing in time. This is because the yarn is forced to advance with the projectile, while, at the same time, a longitudinal wave gradually builds up in the yarn and propagates rapidly from the centre of impact, at the speed of sound, out of the fabric, travelling in the direction of the yarn axis. In front of the longitudinal wave, the yarn material is set inwardly moving towards the centre of impact due to stretching. The inward flowing material continues to feed the advancing transverse deflection until the deformation of the yarn reaches its breaking limit.

3.2.2. Stress Propagation in a Fabric Under Ballistic Impact

When the projectile strikes a single layer of fabric, almost momentarily, stress is transferred to a circular area of the fabric in the direct contact zone. This is immediately followed by the start of a radially increasing longitudinal wave and a slower transverse wave that increases to form a rising cone that has the projectile at its tip.

The energy lost by the projectile and absorbed by the fabric panel depends on various energy damage and absorption mechanisms:

- yarn extraction, from the fabric
- plastic deformation of fibres, fibre breakage [David,2009], [Sadegh,2012],
- type of fibre (material, shape),
- linear density of the yarn,
- fabric architecture yarn,
- finishing the fabric surface,
- the dimensions of the fabric sample,
- number of layers of the fabric,
- the assembling technique for the protection system [Zhang, 2014], [Tabiei, 2008], [Hasanzadeh, 2014].

3.3. Influence of the Constitutive Material Model for Aramid Yarns

3.3.1. Introduction

Understanding how the variation in the yield strength of aramid fibres influences the mode of deformation within a ballistic protection panel is important for optimising its design for personal protective systems.

3.3.2. Numerical Simulation Methodology for Analysing the Influence of the Material Constitutive Model for Aramid Yarns

A very useful classification of the models used in impact simulation is given in [Grujicic, 2016], the author outlining the advantages and limitations of each level.

In recent years, there has been an increasing emphasis to study the behavior of aramid fabrics, filament scale, to investigate the various deformation and energy dissipation mechanisms, at the micro scale [Sockalingam, 2017]. There is still a large gap between filament-yarn and fabric scales in modelling the behaviour of the entire system

Based on the image in Figure 3.2, the yarn cross-section can be realistically represented by lenticular model and the wave path can be considered as constructed of two lenticular arcs.

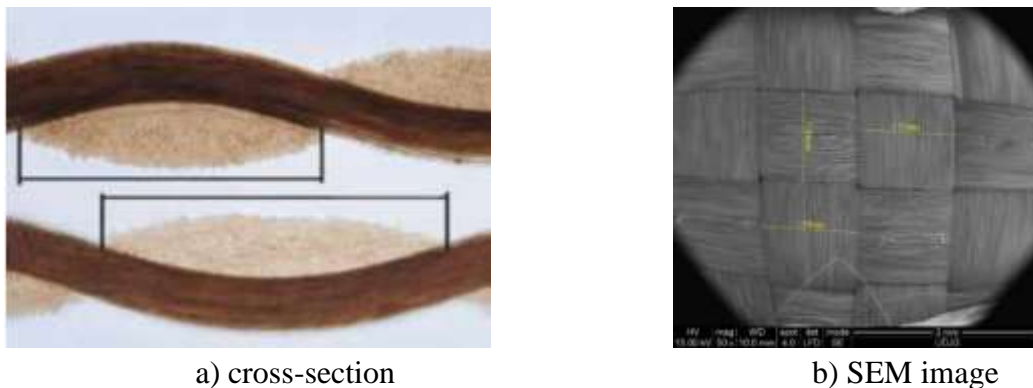


Figure 3.2. Cross and longitudinal section of Twaron fabric yarn [TEIJIN]

The model geometry includes projectile and fabric dimensions (Figure 3.4). Since the model level is meso, the yarn geometry is given in Figure 3.3, very close to the actual yarn. The cross-section of the yarn has the shape of a convex double lens, with chords of $R=1.95$ mm and a length of 1.5 mm. The thickness of the yarn is 0.3 mm. The cross sections of the warp and weft yarns are the same. This shape is close to the lenticular shape obtained by using the generalized power ellipse with exponent $n=2$ [Endruweit, 2018], as modelling the yarn shape is important in obtaining a realistic weave.

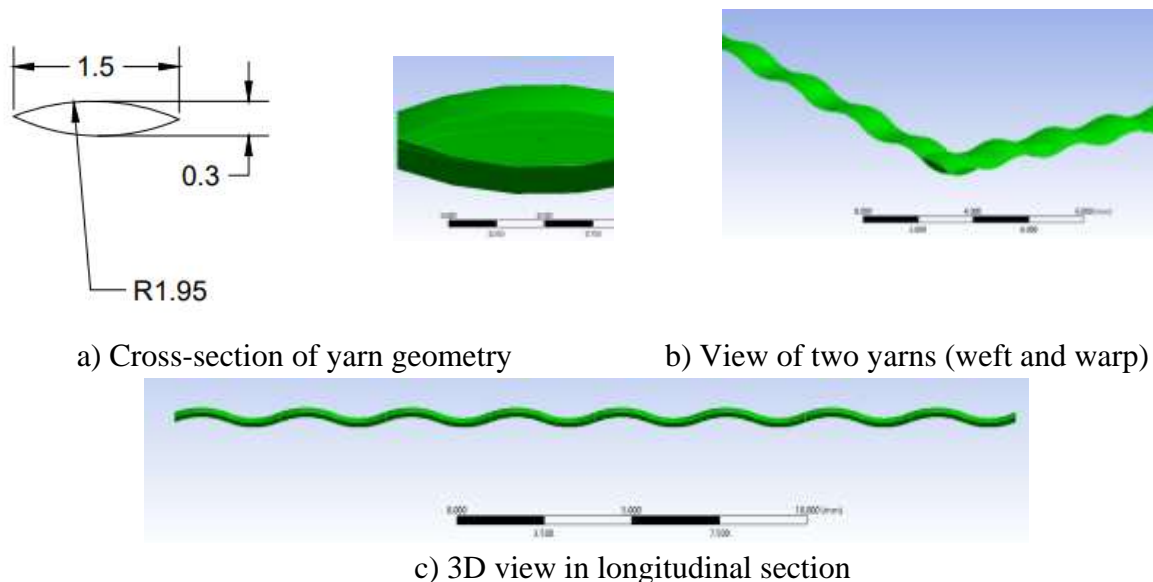


Figure 3.3. Yarn geometry

The lens model was also proposed by [Grujicic, 2010], but with lateral segments. The initial conditions are:

- $v_0 = 420$ m/s, this is a level that characterizes the FB2 level,
- the distance between the tip of the projectile and the first yarn is 0,03 mm.

Boundary conditions imply that each yarn has fixed lateral cross sections. Contact conditions take friction into account:

contact with friction:

- for yarn-yarn contact, the friction coefficient $COF=0.25$ is considered constant,
- for yarn-projectile contact, $COF=0.25$.

The model uses the Lagrangian formulation to simulate the behaviour of both the projectile and the 1/1 woven panel. The linear equation of state (EOS) is applied to describe the response of the material under different states or conditions.

The model incorporates both projectile geometry and 1/1 woven panel geometry.

The behaviour of the yarn material is described using a bilinear constitutive model.

The yield criterion for the yarn is EPS (equivalent plastic strain). The yield criterion for the projectile jacket is Johnson Cook and for the projectile core is also EPS.

The values of the parameters for the projectile component equations are given in Table 3.2 and Table 3.3. Table 3.1 gives the values of the yarn characteristics.

Figure 3.5 shows the impact area, main yarns and secondary yarns.

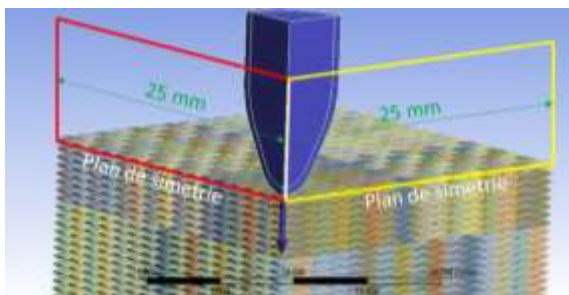


Figure 3.4. Panel size with two planes of symmetry

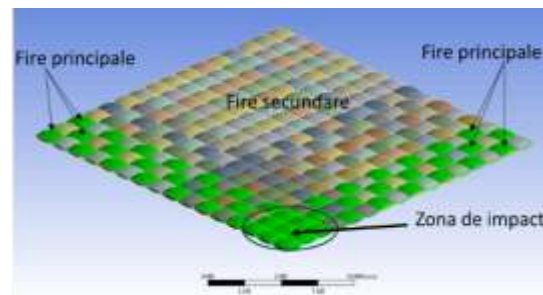


Figure 3.5. Main yarns, secondary yarns and impact area

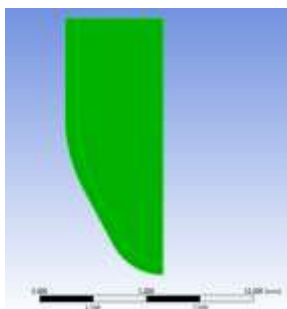


Figure 3.6. Projectile geometry

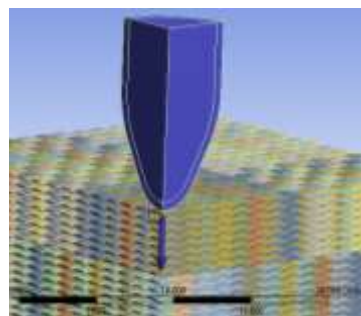


Figure 3.7. Yarn and projectile geometry

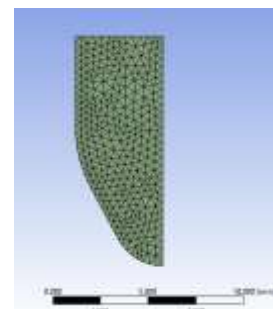


Figure 3.8. Projectile meshing network

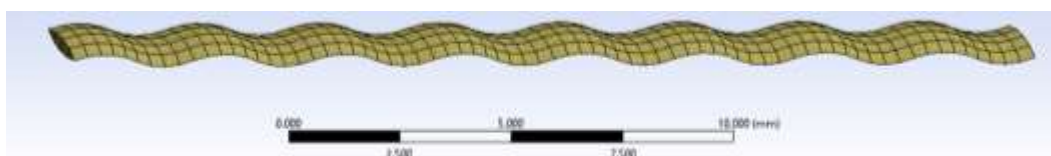


Figure 3.9. Yarn meshing network

Table 3.1. Yarn properties [Pirvu, 2018], [Yang, 2019] [Pirvu, 2014].

Property	Variant				Measure unit
	1	2	3	4	
Density	1440				kg m ⁻³
Young modulus	90000				MPa
Poisson ratio	0.35				-
Bulk modulus	1×10 ¹¹				Pa
Shear modulus	3.333×10 ¹⁰				Pa
Temperature	22				°C
Bilinear isotropic hardening model					
Yield limit	2000	2500	3000	3600	MPa
Tangent modulus	1000				MPa
Maximum equivalent plastic strain, EPS	0,04				-

Table 3.2. Material properties for projectile jackett [Peroni, 2012]

Property	Variant				Measure unit
	1	2	3	4	
Density	8300				kg m ⁻³
Young modulus	1.17×10 ⁵				MPa
Poisson ratio	0,34				-
Bulk modulus	1.218×10 ¹¹				Pa
Shear modulus	4.365×10 ¹⁰				Pa
Temperature	22				°C
Bilinear isotropic hardening model					
Yield limit	70				MPa
Tangent modulus	1150				MPa
Maximum equivalent plastic strain, EPS	1				-

Table 3.2. Material properties for the projectile core [López, 2016], [Peroni, 2012], [Mohotti, 15].

Property	Variant				Measure unit
	1	2	3	4	
Density	11340				kg m ⁻³
Young modulus	16000				MPa
Poisson ratio	0,44				-
Bulk modulus	4.444×10 ¹⁰				Pa
Shear modulus	5.555×10 ¹⁰				Pa
Temperature	22				°C
Johnson Cook constitutive model					
Initial yield stress	24				MPa
Hardening constant	300				MPa
Hardening exponent	1				°C
Strain rate constant	0.1				-
Thermal softening exponent	1				
Melting temperature	760				K
Maximum equivalent plastic strain, EPS	0.75				

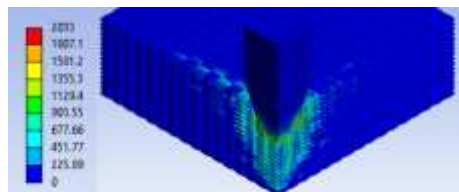
3.3.3. Analysis of the Results on of the Influence of the Constitutive Material Model for Aramid Yarns

In order to get a clear picture of the impact for variations in the yield strength of the aramid yarn on the behaviour of the fabric panel during impact with a projectile (9 mm FMJ), we performed numerical simulations for four different values of this yield strength. These values were considered to represent four distinct test variants, as follows:

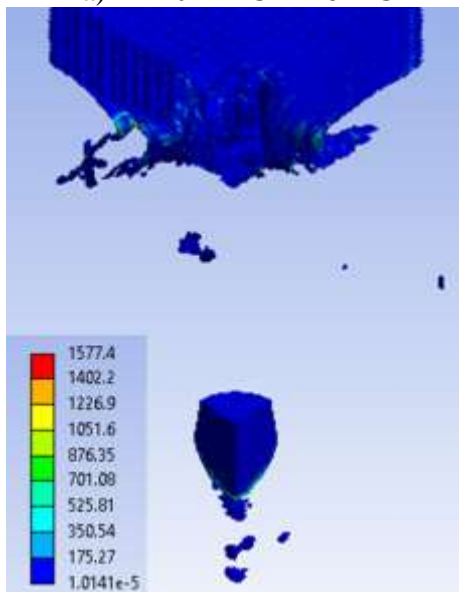
- **Variant 1:** an aramid yarn yield strength of 2000 MPa,
- **Variant 2:** an aramid yarn yield strength of 2500 MPa,
- **Variant 3:** the yield strength of the aramid yarn of 3000 MPa,
- **Variant 4:** an aramid yarn yield strength of 2000 MPa.

For the following images from the simulations, each have its own colour scale to highlight the equivalent stress distribution.

Figure 3.10 gives the von Mises stress distribution for the panel consisting of 16 fabric layers, simulated variant 1, with yield strength 2000 MPa, at time moment, $t = 7.5 \times 10^{-6}$ s (Figure 3.10a), and for the time moment $t = 1.5 \times 10^{-4}$ s (Figure 3.10b). First moment of impact, $t = 7.5 \times 10^{-6}$ s, records a von Mises stress distribution beneath the projectile in the impact zone, with von Mises stress wave propagation through the thickness to the last layer (Figure 3.10a). The last layer at this time moment, $t = 7.5 \times 10^{-6}$ s is not stressed, yet. At time $t = 1.5 \times 10^{-4}$ s, a maximum von Mises stress value of 1577 MPa is recorded. At time moment $t = 1.5 \times 10^{-4}$ s, all layers are broken (Figure 3.10b).

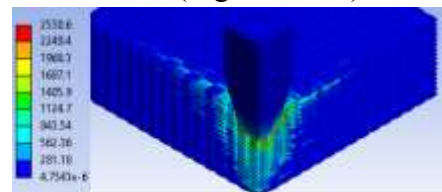


a) $t = 7.5 \times 10^{-6}$ s

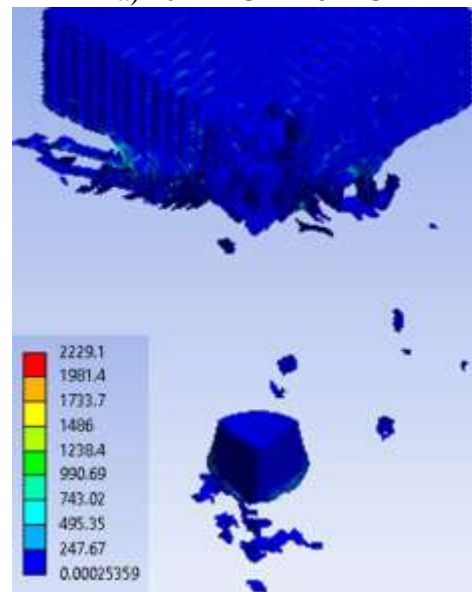


b) $t = 1.5 \times 10^{-4}$ s

Figure 3.10. Distribution of von Mises stress (in MPa) for 16-layer fabric panel, simulated variant 1, yield strength 2000 MPa



a) $t = 7.5 \times 10^{-6}$ s



b) $t = 1.5 \times 10^{-4}$ s

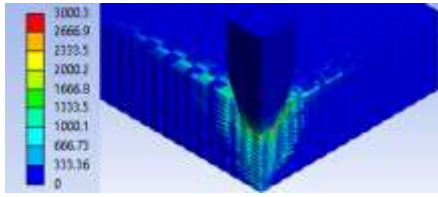
Figure 3.11. Distribution of von Mises stress (in MPa) for 16-layer fabric panel, simulated variant 2, yield strength 2500 MPa

Figure 3.11 gives the von Mises stress distribution for the panel consisting of 16 fabric layers, simulated variant 2 with yield strength 2500 MPa, at the time moment, $t = 7.5 \times 10^{-6}$ s, and for the time moment $t = 1.5 \times 10^{-4}$ s. First moment of impact, $t = 7.5 \times 10^{-6}$ s, records a von Mises stress distribution under the projectile in the impact zone, with stress wave propagation over half the length of a main yarn, through the first two layers and through the thickness to the last layer (Figure 3.11a). The last layer at this time moment, $t = 7.5 \times 10^{-6}$ is not stressed yet. The last moment of the simulation records a von Mises stress value of 2229 MPa. At this time moment, $t = 1.5 \times 10^{-4}$ s, all layers are broken (Figure 3.11b) and the destroyed yarns of these layers show a strong bending due to the penetration speed of the projectile. The projectile, in this case, shows a larger deformation.

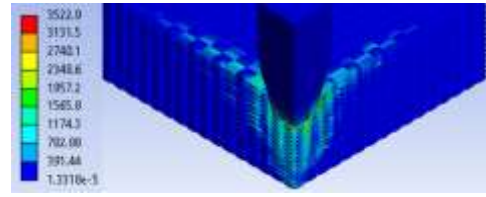
Figure 3.12 gives the von Mises stress distribution for the panel consisting of 16 fabric layers, simulated variant 3, with yield strength 3000 MPa, at time moment, $t = 7.5 \times 10^{-6}$ s and for the time moment $t = 1.5 \times 10^{-4}$ s which is the last moment of the simulation. The duration of the simulated impact between the 9 mm FMJ projectile and the 16-layer fabric target is $t = 1.5 \times 10^{-4}$ s. First moment of impact, $t = 7.5 \times 10^{-6}$ s, records a von Mises stress distribution beneath the projectile, in the impact zone, with stress wave propagation through the thickness up to layer 15 (Figure 3.12a). The last layer at this time point, $t = 7.5 \times 10^{-6}$ s is not stressed. The last time moment of the simulation records an equivalent stress value of 1854 MPa, a value recorded in the area where the destroyed yarns are strongly bent. At this moment in time, $t = 1.5 \times 10^{-4}$ s all layers are broken (Figure 3.12b).

Figure 3.13 gives the von Mises stress distribution for the 16-layer fabric panel, simulated variant 4, with yield strength 3600 MPa, at time moment $t = 7.5 \times 10^{-6}$ s and for the time moment $t = 1.5 \times 10^{-4}$ s. The duration of the simulated impact between the 9 mm FMJ projectile and the 16-layer fabric target, simulated variant 4 is $t = 1.5 \times 10^{-4}$ s. First moment of impact, $t = 7.5 \times 10^{-6}$ s, records a von Mises stress distribution under the projectile in the impact zone, with wave propagation through the thickness up to layers 14-15 and von Mises stress propagation in the longitudinal direction of the main yarns on the first two layers and (Figure 3.13a). The last layer at this time moment, $t = 7.5 \times 10^{-6}$ s, is not stressed. At this time moment, $t = 1.5 \times 10^{-4}$ s, the projectile remains trapped in the fabric layers (Figure 3.13b).

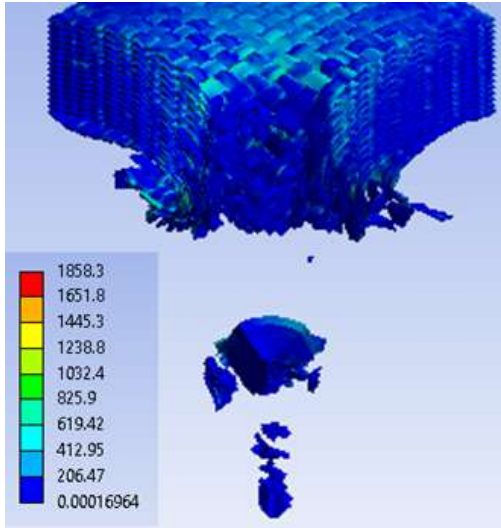
Figure 3.14 gives the von Mises stress distribution of the panel consisting of 32 layers of fabric, simulated variant 1, yield strength 2000 MPa, at time moment, $t = 7.5 \times 10^{-6}$ s which is the first moment of the simulation and for the time moment $t = 1.5 \times 10^{-4}$ s, which represents the last moment of the simulations. The duration of the simulated impact between the 9 mm FMJ projectile and the 32-layer Twaron CT736 fabric target is $t = 1.5 \times 10^{-4}$ s. At first moment of impact, $t = 7.5 \times 10^{-6}$ s, there is a stress distribution under the projectile, in the impact area, with a wave propagation through the thickness of the first 15 layers (Figure 3.14a). The last 17 layers at this time moment, $t = 7.5 \times 10^{-6}$ s are not stressed. The last time of the simulation records an equivalent stress value of 1957 MPa, just under the yield limit of 2000 MPa. Last moment in time, $t = 1.5 \times 10^{-4}$ s, records the rupture of the 32 layers of the panel (Figure 3.14b).



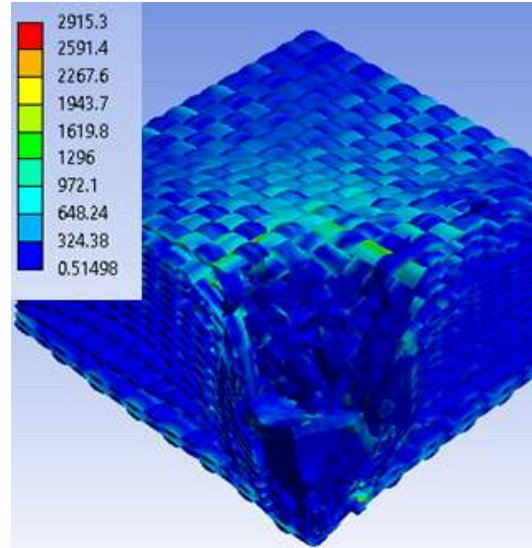
a) $t = 7.5 \times 10^{-6}$ s



a) $t = 7.5 \times 10^{-6}$ s



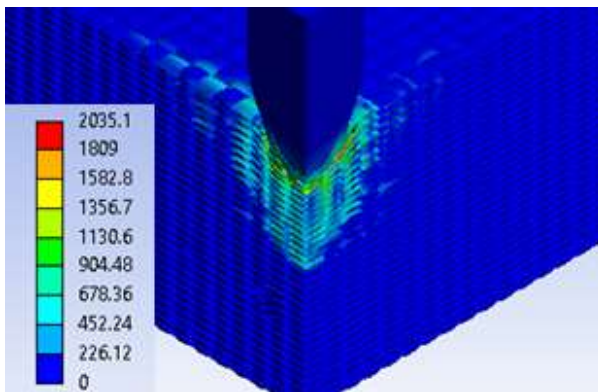
b) $t = 1.5 \times 10^{-4}$ s



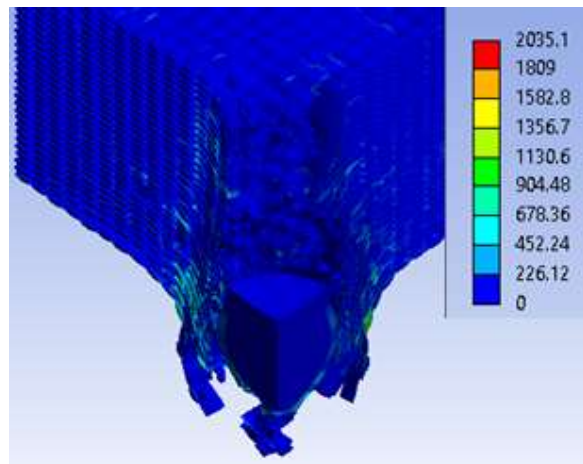
b) $t = 1.5 \times 10^{-4}$ s

Figure 3.12. Distribution of von Mises stress (in MPa) for 16-layer fabric panel, simulated variant 3, yield strength 3000 MPa

Figure 3.13. Distribution of von Mises stress (in MPa) for 16-layer fabric panel, simulated variant 4, yield strength 3600 MPa



a) $t = 7.5 \times 10^{-6}$ s



b) $t = 1.5 \times 10^{-4}$ s

Figure 3.14. Distribution of von Mises stress (in MPa) for 32 fabric layer panel, variant 1, yield strength 2000 MPa

Figure 3.15 gives the von Mises stress distribution for the panel consisting of 32 layers of fabric, variant 2, simulated at the time moment, $t = 7.5 \times 10^{-6}$ s and for time $t =$

1.5×10^{-4} s. The duration of the simulated impact between the 9 mm FMJ projectile and the target consisting of 32 fabric layers is $t = 1.5 \times 10^{-4}$ s. First moment of impact, $t = 7.5 \times 10^{-6}$ s, records a von Mises stress distribution beneath the projectile, in the impact zone, with stress wave propagation through the thickness of the first 16 layers (Figure 3.15a). The last 16 layers at this time moment, $t = 7.5 \times 10^{-6}$ s are not stressed. The projectile for this simulated variant does not penetrate the fabric, it shows partial penetration (Figure 3.15b).

The projectile exhibits significant deformation in the case of simulated variant 2 of the 32-layer fabric panel, which shows partial penetration. This includes changes in its shape and dimensions, pushing/bending of projectile fragments and even breaking it into smaller pieces. This deformation significantly affects the projectile's ability to penetrate deeper into the target material and to cause damage to it.

After the projectile has partially penetrated and remained trapped in the target material, some of the projectile's kinetic energy remains. This residual kinetic energy contributes to subsequent deformation and damage of the target material and causes fragmentation of the material around the projectile.

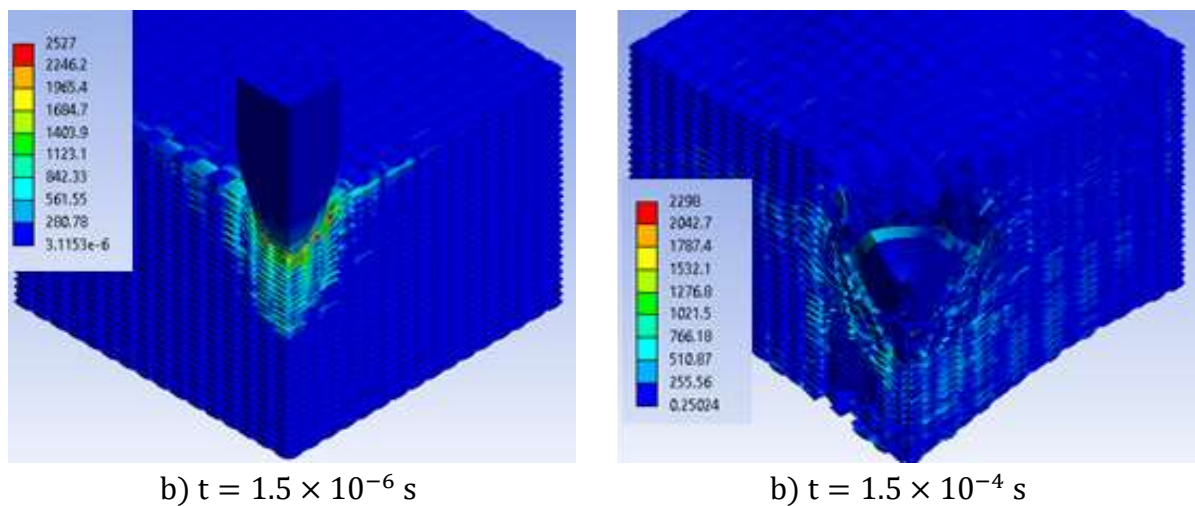


Figure 3.15. Distribution of von Mises stress (in MPa) for 32 fabric layer panel, variant 2, yield strength 2500 MPa

Figure 3.16 gives the von Mises stress distribution of the 32-layer fabric panel, simulated variant 3, at the time moment, $t = 7.5 \times 10^{-6}$ s which is the first moment of the simulation and for time $t = 1.5 \times 10^{-4}$ s, which represents the last moment of the simulations. The duration of the simulated impact between the 9 mm FMJ projectile and the target consisting of 32 layers of fabric is $t = 1.5 \times 10^{-4}$ s. First moment of impact, $t = 7.5 \times 10^{-6}$ s, records a stress distribution under the projectile in the impact zone, with wave propagation through the thickness of the first 17 layers (Figure 3.16a). The last 15 layers at this time moment, $t = 7.5 \times 10^{-6}$ s are not stressed. The last time of the simulation records a stress value of 1640 MPa. The projectile, for this simulated variant, does not penetrate the fabric, showing partial penetration (Figure 3.16b).

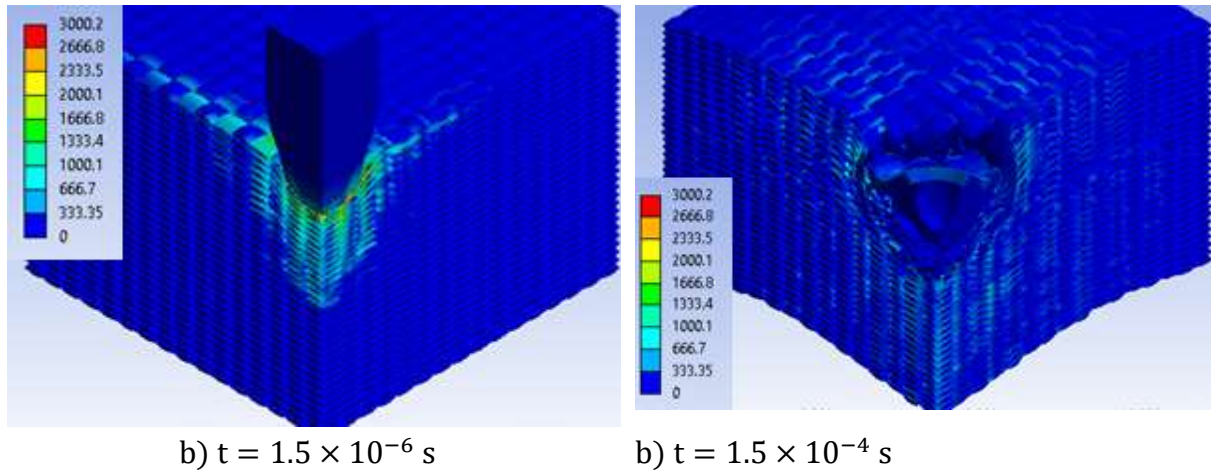


Figure 3.16. Distribution of von Mises stress (in MPa) for 32-layer fabric panel, variant 3, yield strength 3000 MPa

Figure 3.17 gives the von Mises stress distribution of the panel consisting of 32 fabric layers, variant 4, at time moment, $t = 7.5 \times 10^{-6} \text{ s}$ which is the first moment of the simulation and for the time moment $t = 1.5 \times 10^{-4} \text{ s}$, which represents the last moment of the simulation. The duration of the simulated impact between the 9 mm FMJ projectile and the target consisting of 32 layers of fabric is $t = 1.5 \times 10^{-4} \text{ s}$. First moment of impact, $t = 7.5 \times 10^{-6} \text{ s}$, records a stress distribution under the projectile in the direct impact zone, with wave propagation through the thickness of the first 16 layers (Figure 3.17a). The last 16 layers at this time moment, $t = 7.5 \times 10^{-6} \text{ s}$ are not stressed. The last time of the simulation records a stress value of 2720 MPa (meaning that, for a future trial, the time should be longer). The projectile, for this variant, does not penetrate the fabric, showing partial penetration (Figure 3.17b).

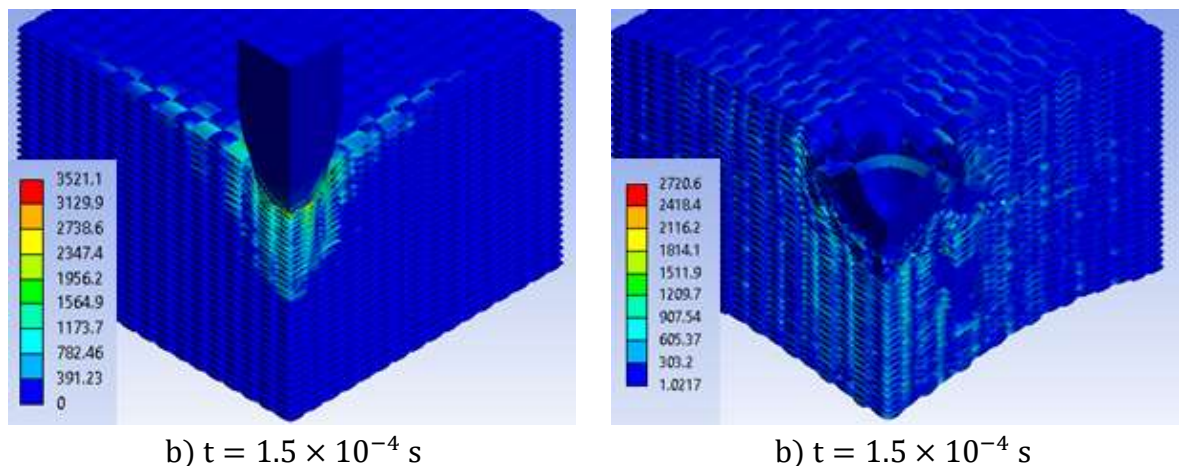


Figure 3.17. Distribution of von Mises stress (in MPa) for 32 fabric layer panel, variant 4, yield strength 3600 MPa

3.3.4. Conclusions on the Analysis of the Influence of the Constitutive Material Model for Aramid Yarns

This analysis aimed to evaluate the influence of material yield strengths on ballistic simulations, for different number of layered samples, keeping other material properties constant.

Panels made of 16 layers of fabric, modelled in the following variants will be discussed as follows:

- variant 1 (2000 MPa yield limit of the yarn) ran a mathematically correct simulation, but it is not realistic because it failed to meet validation criteria (number of broken layers and failure as appearance compared to the real one, obtained from laboratory testing),
- variant 2 (2500 MPa yield strength of the yarn) ran a mathematically correct simulation, realistic because it was able to satisfy validation criteria (number of broken layers and failure as appearance compared to the real one obtained from laboratory testing),
- variant 3 (3000 MPa yield strength of the yarn) ran a mathematically correct simulation, realistic because it was able to satisfy validation criteria (number of broken layers and failure as appearance compared to the real one obtained from laboratory testing),
- variant 4 (3600 MPa yield limit of the yarn) ran a mathematically correct simulation, but it is not realistic because it failed to meet validation criteria (number of broken layers and failure as appearance compared to the real one obtained from laboratory testing).

Panels consisting of 32 layers of fabric, modelled in the following variants will be discussed as follows:

- variant 1 (2000 MPa yield limit of the yarn) ran a mathematically correct simulation, but it is not realistic because it failed to meet validation criteria (number of broken layers and appearance compared to the real one obtained from laboratory testing),
- variant 2 (2500 MPa yield strength of the yarn) ran a mathematically correct simulation, realistic because it was able to satisfy validation criteria (number of broken layers and appearance compared to the real one obtained from laboratory testing),
- variant 3 (3000 MPa yield strength of the yarn) ran a mathematically correct, realistic simulation because it was able to satisfy validation criteria (number of broken layers and appearance compared to the real one obtained from laboratory testing)
- variant 4 (3600 MPa yield limit of the yarn) ran a mathematically correct simulation, but it is not realistic because it failed to meet validation criteria (number of broken layers and appearance compared to the real one obtained from laboratory testing).

The results indicate that the selection of the yield limit of the yarn material is crucial in ballistic simulations. Too low or too high a yield limit can compromise realistic simulation results. The 2500 MPa and 3000 MPa yield strength variants were found to provide accurate and realistic simulations suitable for ballistic protection system applications. This analysis provides valuable guidance for further development of ballistic simulations, with the specific aramid yarn material model.

3.4. Influence of Introducing Friction into the Impact Model Projectile-Target

3.4.1. Introduction

Friction between the material and the projectile can effectively "stop" or slow down the projectile. This is one of the mechanisms by which the protective system resists penetration. The combination of the strength of the fabric, its ability to deform or stretch and the frictional forces acting on the projectile, collectively, contribute to stop the projectile.

Friction has been shown to have a significant effect in determining the ballistic impact performance of fabrics. Much effort has been put into investigating how friction between yarns affects the ballistic impact response of fabrics in recent decades [Chu, 2014], [Ha-Ming, 2012]. However, the fundamental understanding of the mechanisms of how inter-yarn friction works in woven fabric panels has yet to be established and improved. It is extremely important to understand how friction affects the stress distribution and the magnitude of stress in yarns. This is necessary in determining yarn failure and energy absorption in a ballistic event.

3.4.2. Simulation Methodology for the Establishing Influence of Friction in the Impact Model

To study the influence of inter-yarn friction on the ballistic performance of a protective system, I used numerical simulation of the impact between a 9 mm FMJ projectile and a 24-layer laminated fabric (fabric size 50 mm × 25 mm), simulating two variants with different values of the friction coefficient (COF) and a simulation without inter-yarn friction and without projectile-yarn friction.

In this analysis, the model is modeled at mesoscale in Ansys, the software used for FE modeling. The model uses the Lagrangean formula to simulate the behavior of both the projectile and the 1/1 woven panel. Linear equation of state (EOS) is applied to describe the material response under different states or conditions.

The model integrates both projectile and 1/1 fabric panel geometries.

The behaviour of the yarn material is described using a bilinear hardening model. The failure criterion for the yarn is EPS (equivalent plastic strain at break). The failure criterion for the projectile jacket is Johnson Cook and for the projectile core is EPS, taken from literature [Forrestal, 2010], [Manes, 2014], [Johnson, 1985].

The cross section of the yarn can be realistically represented by a lenticular model and the wave path can be considered to be constructed of two lenticular arcs. The average width of the yarn cross-section in the model is 1.5 mm. The thickness of the fabric is 0.32 mm according to the manufacturer's catalogue [Catalog Teijin]. The geometry parameters for the generated yarn part and the fabric assembly are shown in Figure 3.18. The projectile is 9 mm FMJ with a diameter of 9 mm. The mass of the 9 mm FMJ projectile is 8.00 g.

Figure 3.18 shows the geometrical model used for the analysis of the influence of the friction coefficient values and Figure 3.20 shows the yarn discretization and Figure 3.19 discretization for the panel and projectile.

The initial conditions are:

$-v_0 = 420$ m/s, this is a value that characterizes the FB2 level of protection,

- the distance between the tip of the projectile and the first yarn is 0,03 mm (in order to shorten the time necessary to reach the panel).

Boundary conditions imply that each yarn has fixed lateral cross sections. The contact conditions take friction into account and the following variants were run:

- Variant 1:
 - contact with friction:
 - for yarn-yarn contact, the friction coefficient $COF=0.25$ and is considered constant,
 - for yarn-projectile contact, $COF=0.25$,
- Variant 2:
 - contact with friction:
 - for the yarn-yarn contact, the friction coefficient $COF=0.1$ is considered constant,
 - for yarn-projectile contact, $COF=0,1$
- Variant 3:
 - frictionless contact.

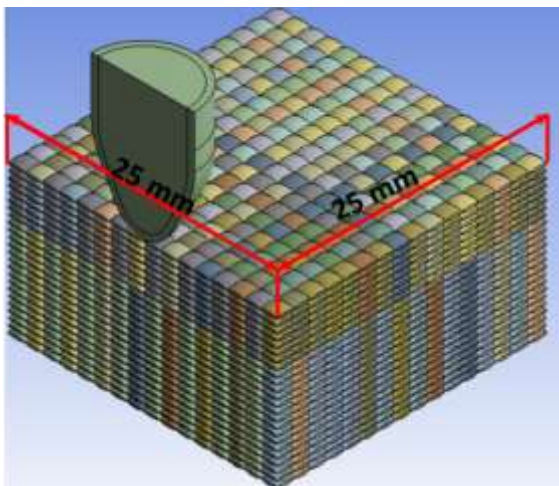


Figure 3.18. Geometric model used for the analysis of the influence of the friction coefficient values – main section

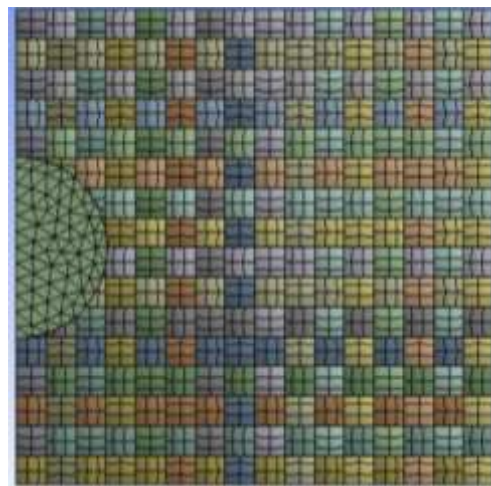


Figure 3.19. Panel and projectile discretisation (front view)

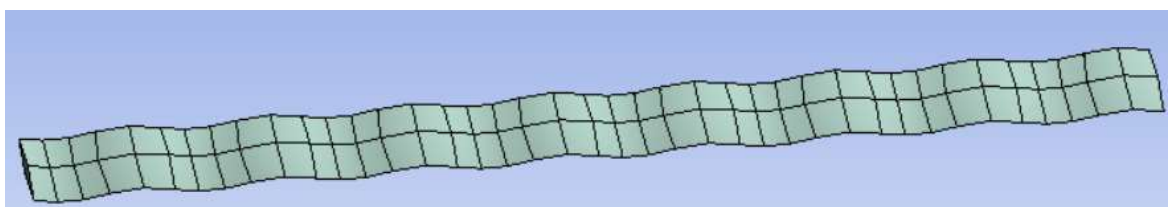


Figure 3.20. Yarn discretization (minimum element size 0.8 mm)

Table 3.4. Material properties of yarn (for analysis of the influence of friction coefficient values) [Yang, 2019]

Property	Valuation	Unit of measure
Density	1440	kg m ⁻³
Young modulus	90000	MPa
Poisson ratio	0,35	-
Bulk modulus	1×10 ¹¹	Pa
Shear modulus	3,33333×10 ¹⁰	Pa
Temperature	22	°C
Bilinear isotropic hardening model		
Yield limit	3000	MPa
Tangent modulus	1000	MPa
Temperature	22	°C
Maximum equivalent plastic strain, EPS	0,04	-

Table 3.5. Material properties for the projectile jacket (for analysis of the influence of friction coefficient values) [Peroni, 2012]

Property	Valuation	Unit of measure
Density	8300	kg m ⁻³
Young modulus	1,17×10 ⁵	MPa
Poisson ratio	0,34	-
Bulk modulus	1,2188×10 ¹¹	Pa
Shear modulus	4,3657×10 ¹⁰	Pa
Temperature	22	°C
Bilinear isotropic hardening model		
Yield limit	70	MPa
Tangent modulus	1150	MPa
Temperature	22	°C
Maximum equivalent plastic strain, EPS	1	-

Table 3.6. Material properties for the projectile core (for analysis of the influence of friction coefficient values) [Manes, 2014], [Forrestal, 2010], [Johnson, 1985]

Property	Valuation	Unit of measure
Density	11340	kg m ⁻³
Young modulus	16000	MPa
Poisson ratio	0,44	-
Bulk modulus	4,4444×10 ¹⁰	Pa
Shear modulus	5,5556×10 ¹⁰	Pa
Temperature	22	°C
Johnson Cook constitutive model		
Initial yield stress	24	MPa
Hardening constant	300	MPa
Hardening exponent	1	°C
Strain rate constant	0,1	-
Thermal softening exponent	1	
Melting temperature	760	K
Maximum equivalent plastic strain, EPS	0,75	

3.4.3. Analysis of Results on the Influence of Introducing Friction into the Ballistic Impact Model

When a projectile hit a fabric, it causes a transverse deflection in the main yarns and generates longitudinal stress waves that propagate in the fabric down the axis of the yarns. The transverse deflection continues until the stress at the point of impact reaches the breaking point.

Figure 3.21 gives the von Mises stress distribution of the first layer for four-time moments during the simulations of the simulated variant with the value of the friction coefficient of 0.25. First moment of impact, $t = 7.5 \times 10^{-6}$ s, has already recorded two

broken yarns, one in the warp direction and one in the weft direction, the von Mises stress is high on the unbroken central main yarn in the warp direction (Figure 3.21). At this first moment, the yarns under the projectile are compressed.

At the moment, $t = 1.5 \times 10^{-5}$ s, six broken main yarns are recorded, so, between the first moment of the simulation and the second moment four main yarns were broken. The von Mises stress value is 3016 MPa (Figure 3.21). The time moment, $t = 2.25 \times 10^{-5}$ s, shows a more pronounced destruction of the yarns in the impact zone, more fragments of the yarns were broken (Figure 3.69). The last moment of the simulation, $t = 1.5 \times 10^{-4}$ s, shows a rebound of the fabric after the projectile (Figure 3.21) is stopped.

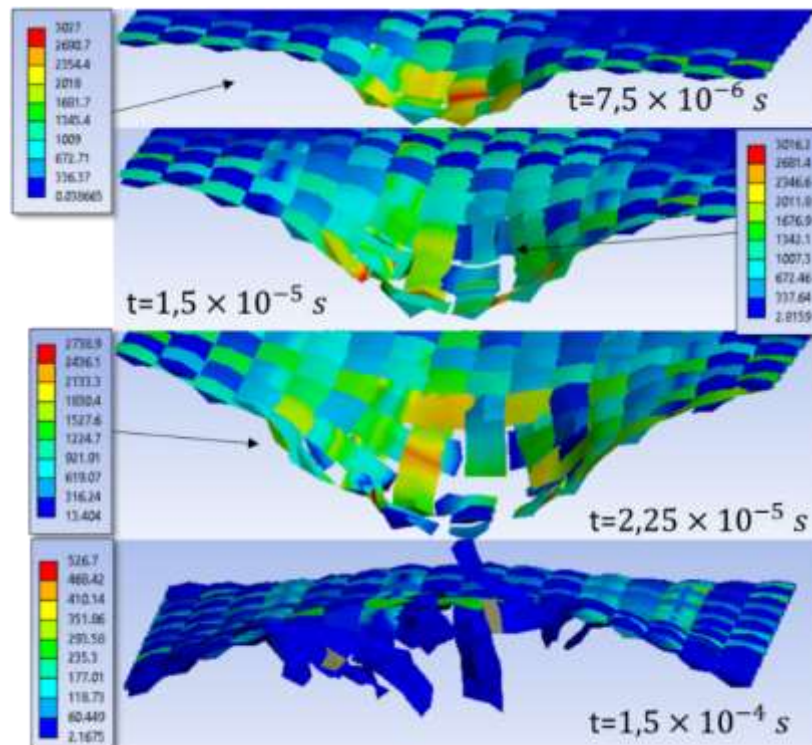


Figure 3.21. Distribution of von Mises stresses (in MPa), on layer 1, at four time moments for the 25 mm × 25 mm sample, $v_0=420$ m/s, COF = 0.25

Figure 3.22 shows the distribution of von Mises stress of the first layer for three time moments during the simulations, of the variant with a friction coefficient value of 0.1. At impact moment $t = 7.5 \times 10^{-6}$ s, two broken yarns are observed, one in the warp direction and one in the weft direction. At this first moment, the yarns under the projectile are compressed.

Moment of time, $t = 3 \times 10^{-5}$ s shows that the main yarns were broken. At this point, one may see how the projectile first rotates the secondary yarns next to the main yarns (Figure 3.22). At this moment in time, the secondary yarn in the direction of the weft shows an zone with stress concentrators in the area where it is twisted by the projectile penetration into the fabric, indicating that it is about to be broken in that zone. The last moment of the simulation, $t = 1.5 \times 10^{-4}$ s, shows a recovery of the layer, even if the projectile had already destroyed all layers of the fabric (Figure 3.22).

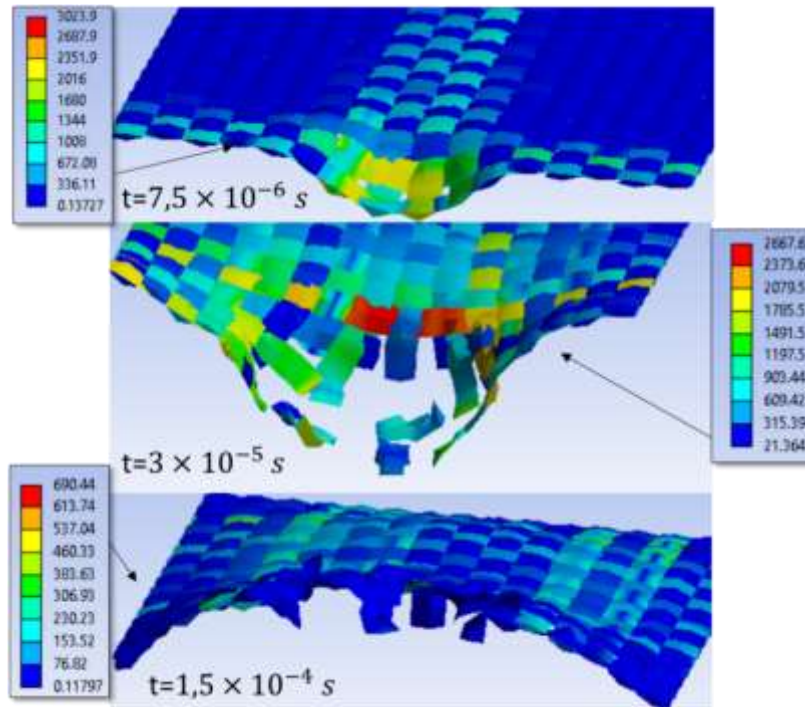


Figure 3.22. Distribution of von Mises stresses (in MPa) on layer 1 for four time moments, for the sample 50 mm × 25 mm sample, $v_0 = 420$ m/s, COF = 0.1

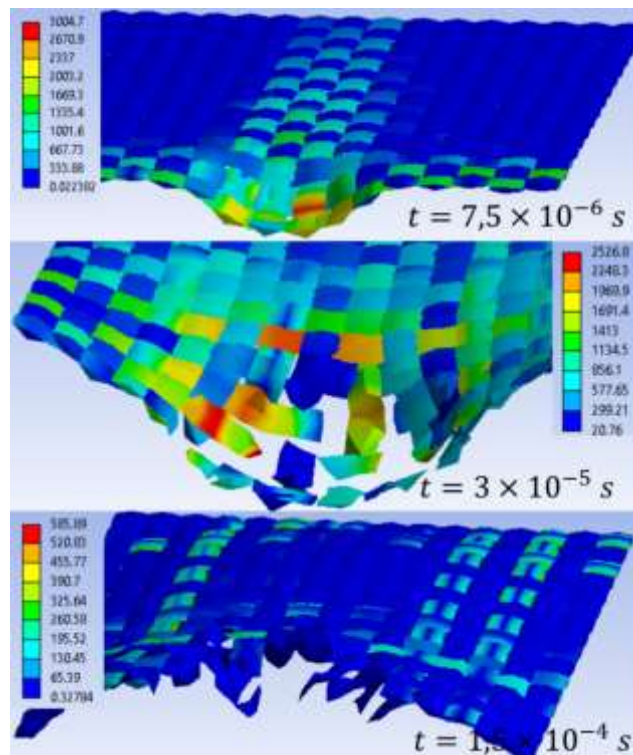


Figure 3.23. Distribution of von Mises stresses on layer 1 (in MPa), for four time moments for for the sample 50 mm × 25 mm sample, $v_0 = 420$ m/s, without friction

Figure 3.23 gives the distribution of the von Mises stress, of the first layer for three time moments during the simulations of the variant without friction between yarns. First

moment of impact, $t = 7.5 \times 10^{-6}$ s, presents three broken yarns, one in the warp direction and two in the weft direction, the von Mises stress is recorded on the unbroken central main yarn, in the warp direction (Figure 3.23). At this first moment, the yarns under the projectile are compressed. Time moment, $t = 3 \times 10^{-5}$ s, shows a more pronounced destruction of the main yarns, as well as the destruction of the secondary yarns next to the main yarns (Figure 3.23). The zones with stress concentrators are present on the yarns in the direction of the weft. The last moment of the simulation, $t = 1.5 \times 10^{-4}$ s, shows an elastic recovery of the layer after the projectile has been stopped and rebounded (Figure 3.23).

Figure 3.24 gives the von Mises stress distribution on yarns of the last layer for four time moments during the simulations of the variant with the value of the friction coefficient of 0.25. First moment of impact, $t = 7.5 \times 10^{-6}$ s, shows that the yarns of this layer are not stressed, the von Mises stress value being only 54 MPa (Figure 3.24).

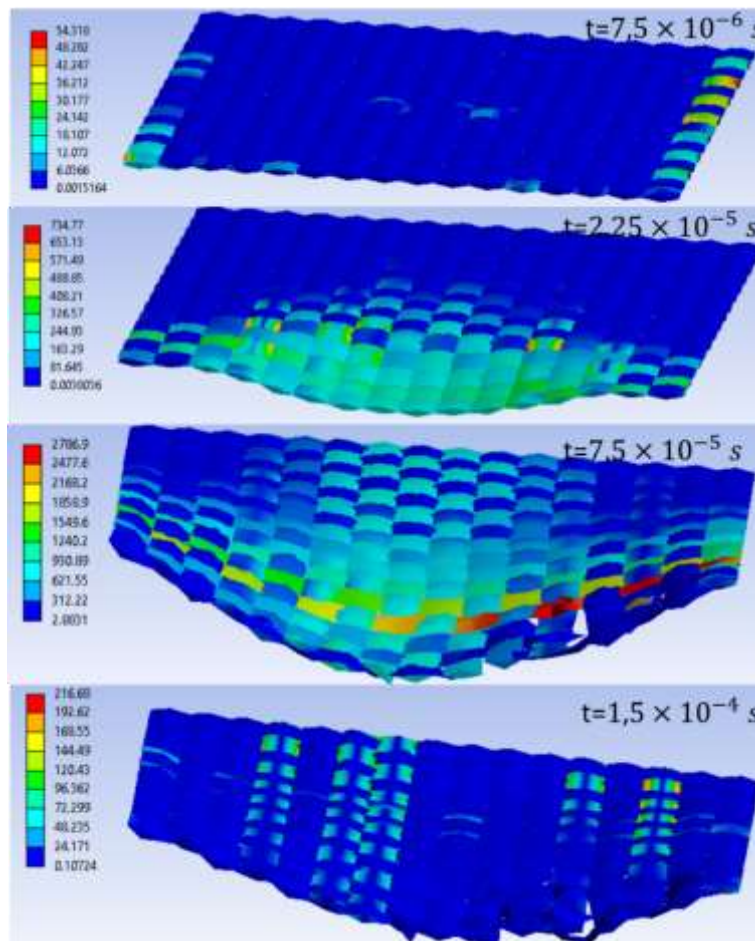


Figure 3.24. Distribution of von Mises stresses on layer 24, in MPa, for four time moments, for a sample of $50 \text{ mm} \times 25 \text{ mm}$, $v_0 = 420 \text{ m/s}$, $\text{COF} = 0.25$

At the time moment $t = 2.25 \times 10^{-5}$ s, the von Mises stress increases to 734 MPa, the secondary yarns in weft the direction are stressed to the fixed end zone (Figure 3.24). The stressed yarns in the warp direction are both main yarns and secondary yarns and they are not stressed the fixed ends of the yarns. At time moment, $t = 7.5 \times 10^{-5}$ s, a von Mises stress

value of 2786 MPa, is given recorded on a secondary yarn in the direction of the weft (Figure 3.24). Last moment of the simulation, $t = 1.5 \times 10^{-4}$ s, shows how the layer started to recover after the projectile rebounds, even though the main yarns are broken in the direction of the weft (Figure 3.24).

Figure 3.25 gives the von Mises stress distribution (in MPa) of the last layer, for three time moments during the simulations of the variant with the value of the friction coefficient of 0.1. First moment of the impact, $t = 7.5 \times 10^{-6}$ s, shows that the yarns of this 24 layer are not stressed, the von Mises stress value being 95 MPa (Figure 3.25).

Moment of time, $t = 7.5 \times 10^{-5}$ s, shows the breakage of the main yarns in the direction of the weft and the breakage of the secondary yarn next to these yarns (Figure 3.25). The secondary yarn in the weft direction shows zones with stress concentrators on the left side of the impact zone (in this image). The yarns are not symmetrically broken in the impact zone, the breakage occurs to the left of the impact zone (the main yarns and one secondary yarn are broken) and to the right of the impact zone (the main yarns in the weft direction are broken). The last moment of the simulation, $t = 1.5 \times 10^{-4}$ s, of this layer, shows the strong bending of the yarns due to the total penetration of the fabric (Figure 3.25).

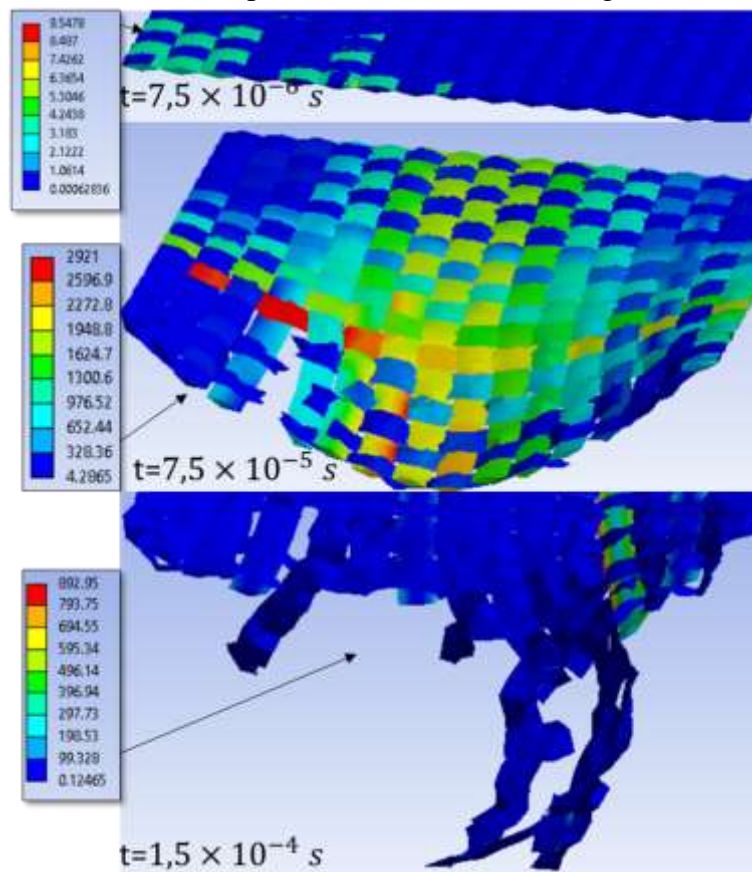


Figure 3.25. Distribution of von Mises stresses on layer 24 (in MPa), at four time moments, for the sample 50 mm × 25 mm, $v_0 = 420$ m/s, COF = 0.25

Figure 3.26 shows the von Mises stress distribution (in MPa), of the last layer for three time moments during the simulations of the variant without friction.

The first moment of impact, $t = 7.5 \times 10^{-6}$ s, shows that the yarns of this layer are not stressed, the von Mises stress value being 49.314 MPa (Figure 3.26). Moment of time, $t = 8,25 \times 10^{-5}$ s, shows the breakage of two main yarns in the weft direction, the third yarn is maximally stressed, indicating that it is about to be broken (Figure 3.26). The last moment of the simulation, records a stress value of 346 MPa, indicating that no more yarns will break (Figure 3.26).

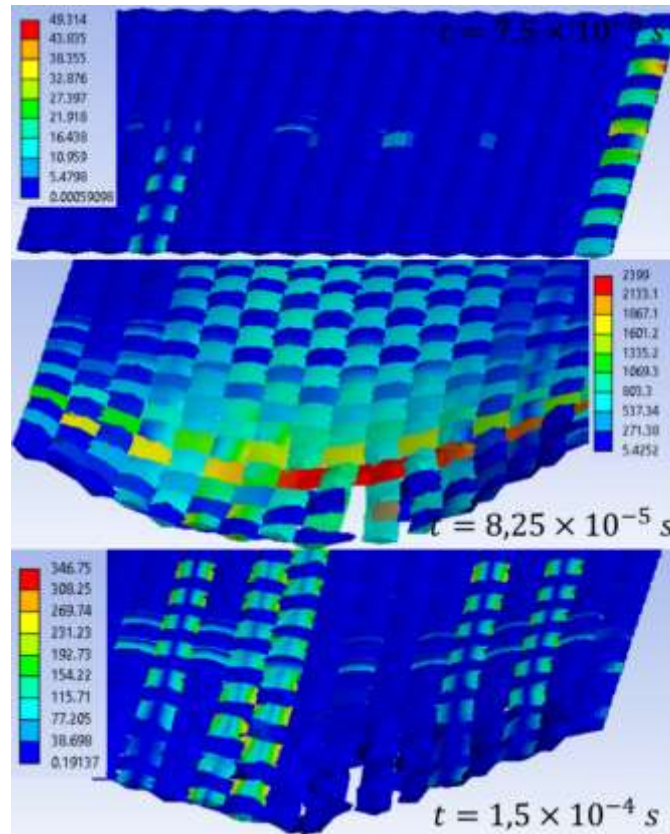


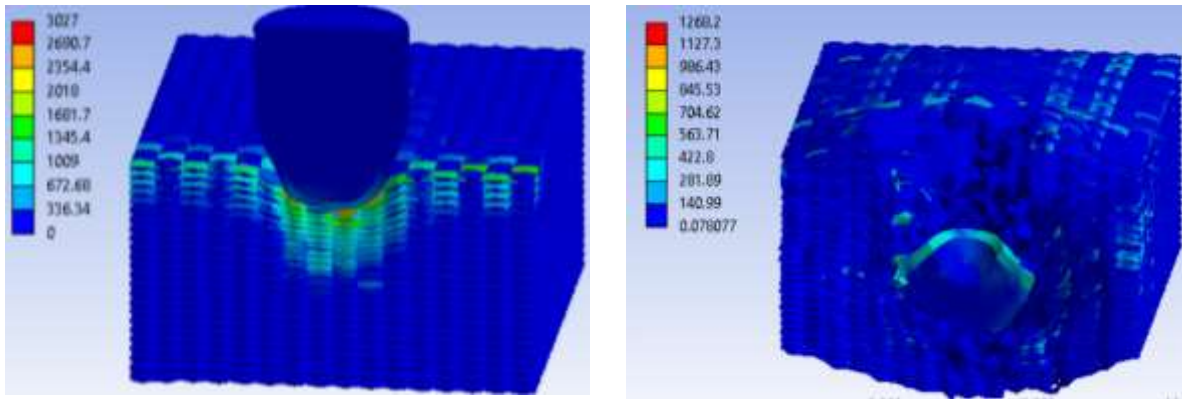
Figure 3.26. Distribution of von Mises stresses (in MPa) on layer 24, at four time moments for sample 50 mm × 25 mm sample, $v_0 = 420$ m/s without friction

3.4.4. Conclusions on the Influence of Friction Introduction in Ballistic Impact Simulation

Analysing the distribution of von Mises stresses over the whole panel, for the three analyzed cases, I observed that the variant with the value of the friction coefficient 0.1 shows a destruction/breakage of the 24 layers over a larger area, leading to the total penetration of the panel (Figure 3.27). This underlines the contribution of friction to absorb impact energy.

The variant with a friction coefficient value of 0.25 stops the projectile and bounces it, but the layers under the projectile are compressed and show broken yarns, even though the projectile has been stopped (Figure 3.28).

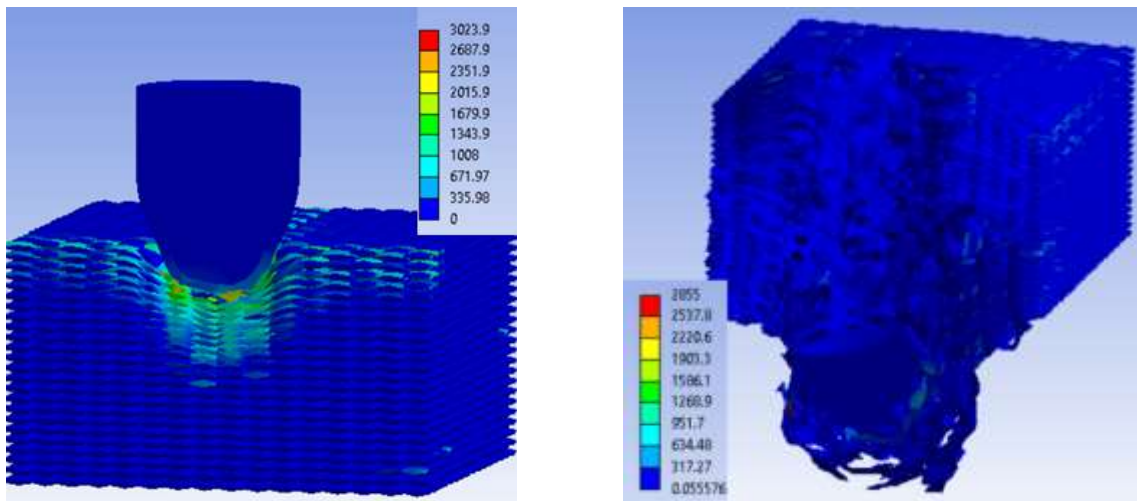
The variant without friction shows a partial penetration of the panel, but, again, the yarns are destroyed under the projectile (Figure 3.29).



a) $t = 7.5 \times 10^{-6} \text{ s}$

b) $t = 1.5 \times 10^{-5} \text{ s}$

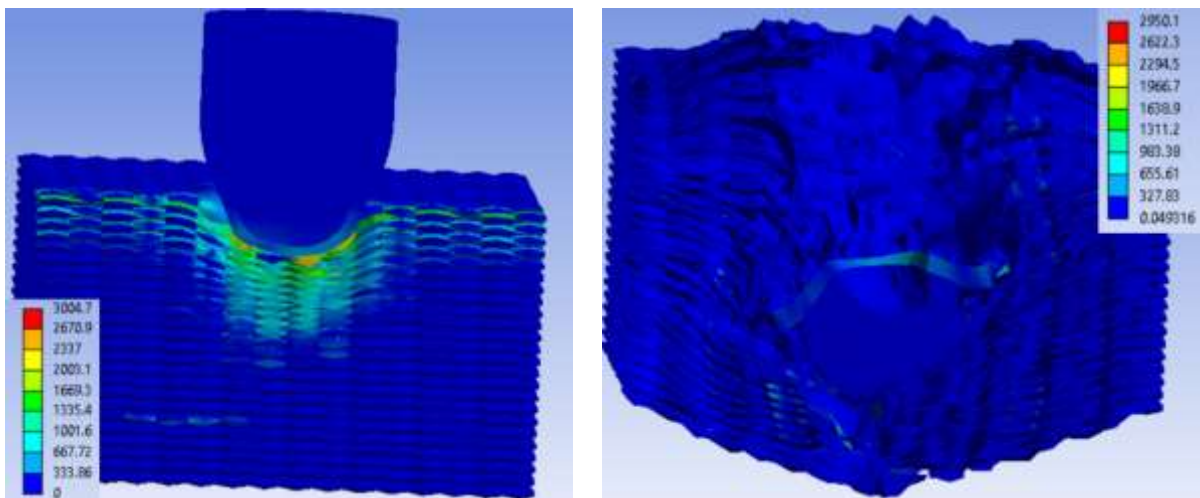
Figure 3.27. Von Mises stress distributions (in MPa) of the 24-layer panel at two time moments. Sample of $25 \text{ mm} \times 25 \text{ mm}$, $v_0 = 420 \text{ m/s}$, $\text{COF} = 0.25$



$t = 7,5 \times 10^{-6} \text{ s}$

$t = 1,5 \times 10^{-5} \text{ s}$

Figure 3.28. Von Mises stress distribution (in MPa) of the 24-layer panel, at two time moments. Sample of $25 \text{ mm} \times 25 \text{ mm}$, $v_0 = 420 \text{ m/s}$, $\text{COF} = 0.10$



$t = 7,5 \times 10^{-6} \text{ s}$

$t = 1,5 \times 10^{-5} \text{ s}$

Figure 3.29. Distribution of von Mises stress (in MPa) for the 24-layer Twaron CT736 panel, at two moments in time. Sample size $25 \text{ mm} \times 25 \text{ mm}$, $v_0 = 420 \text{ m/s}$, without friction

3.5. Influence of Sample Size in Numerical Simulation

3.5.1. Introduction

The aim of this analysis is to evaluate the behaviour of a fabric panel with a friction coefficient of 0.25, during impact with a projectile, and to understand how the sample sizes (50 mm × 50 mm and 50 mm × 25 mm) influences the results and the behaviour of the panel. The specific objectives respectively of this section are:

- assess the resistance of the fabric panel to projectile impact (the aim is to understand how the panel reacts to external force and whether it can stop or reduce the effects of impact in this specific configuration),
- observing the distributions of von Mises stress in yarns on different layers of the panel during impact and assessing the damage of the yarns and projectile, including the number of broken yarns and how they evolve over time,
- analysis can identify areas of the panel that are more susceptible to damage during impact.

3.5.2. Methodology to Simulate the Influence of Sample Size in Numerical Simulation

The initial conditions used for these simulations are:

- $v_0 = 420$ m/s, this is a value that characterises the FB3 level of protection given in [EN 1063:1999], [EN 1522:2004], [EN 1523:2004]
- the distance between the tip of the projectile and the first yarn is 0,03 mm.
Boundary conditions imply that each yarn has fixed lateral cross sections. Contact conditions take friction into account:
 - for yarn-yarn contact, the friction coefficient is set for COF=0.25 and is considered constant,
 - for yarn-projectile contact, COF=0.25, also constant.

The model uses the Lagrangean formula to simulate the behaviour of both the projectile and the 1/1 woven panel [Ansys, 2021].

The linear equation of state (EOS) is applied to describe the response of the material under different states or conditions. Linear EOS involves a linear relationship between pressure, density and other variables in the model [Ansys, 2021].

The model incorporates both projectile geometry and 1/1 woven panel geometry. The geometry plays an important role in determining how the projectile interacts with the panel and is a key aspect of numerical simulations.

The material behaviour of the yarn is described using a bilinear hardening model, which suggests a material response characterized by two distinct linear regions.

The yield criterion for the yarn is EPS. The yield criterion for the projectile jacket is Johnson Cook and for the projectile core is EPS [Manes, 2014], [Forrestal, 2010], [Johnson, 1985].

The Johnson-Cook model is specifically used for the behaviour of the projectile material, under high strain rates.

The boundary conditions were set so that the numerical model reflects the characteristics of the actual experimental system.

The projectile was assigned an initial linear velocity of $v_0 = 420$ m/s (on vertical direction in this simulation). The numerical model of the 9 mm FMJ projectile was shown in Figure 3.6. Since a plane of symmetry was used in the analysed models (Figure 3.30 and 3.31), the angular velocity of the projectile being neglected. Discretizations of the two model (panel and projectile) are given in Figures 3.22-3.25.

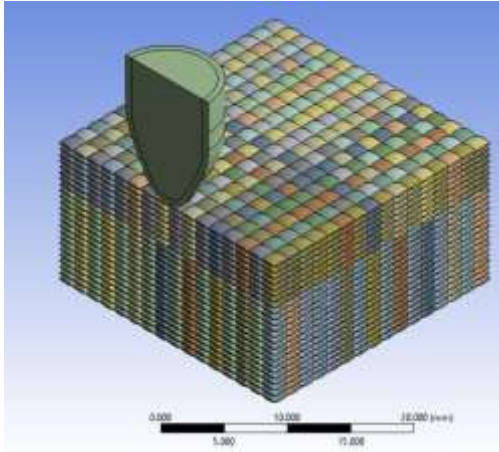


Figure 3.30. Geometry of the sample 50 mm \times 25 mm

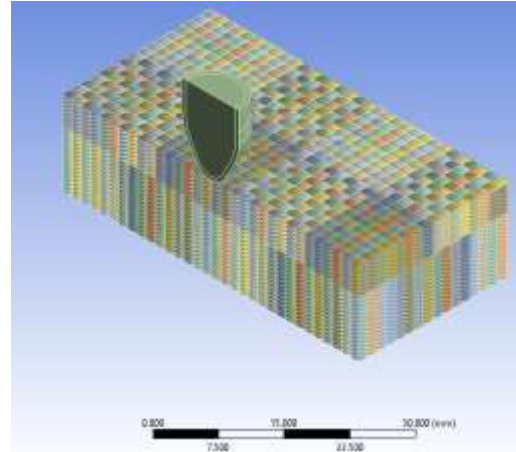


Figure 3.31. Geometry of the sample 50 mm \times 50 mm

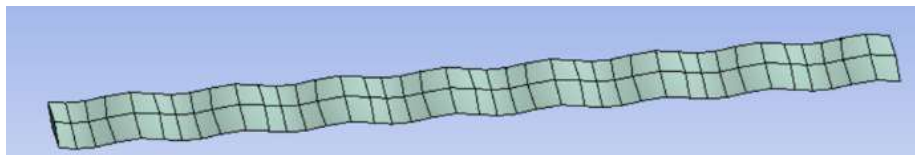


Figure 3.22. Yarn discretisation for sample size 50 mm \times 25 mm

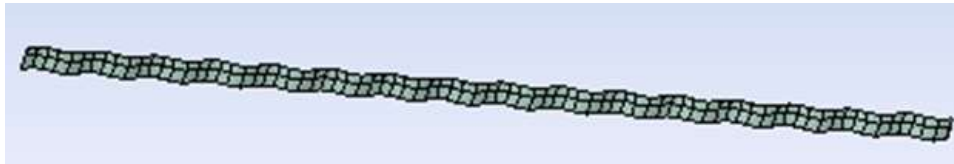


Figure 3.23. Yarn discretisation for sample size 50 mm \times 50 mm

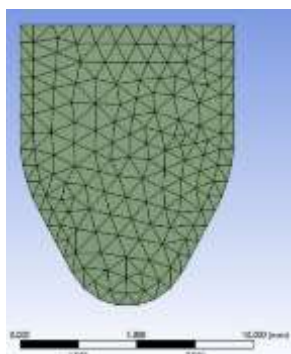


Figure 3.24. Projectile discretisation for the sample size 50 mm \times 25 mm

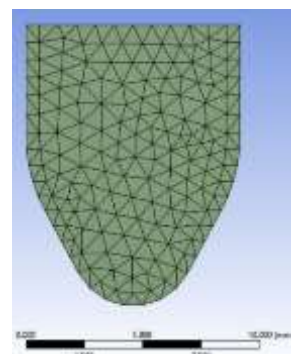


Figure 3.25. Projectile discretization for the sample size 50 mm \times 50 mm

The values of the parameters for the projectile characteristics are given in Table 3.4 and Table 3.5. The values of the yarn material parameters are given in Table 3.6.

3.5.3. Analysis of the Results on the Influence of Sample Size in the Numerical Simulation

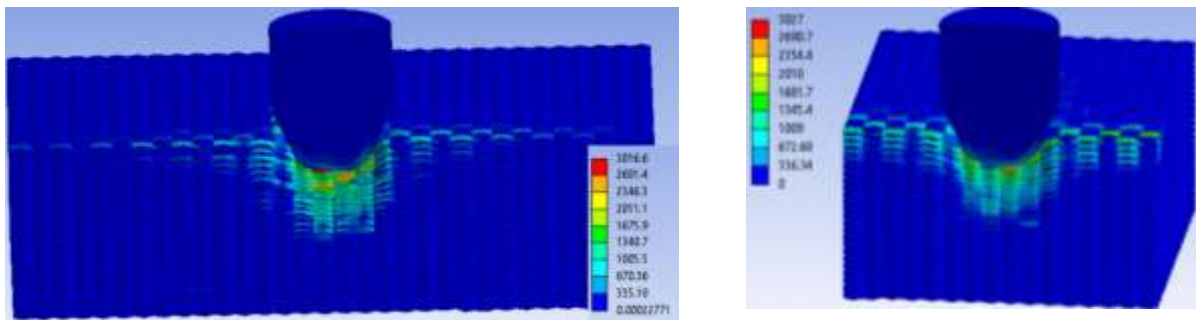
Analysing Figure 3.36, I observe that the stress distribution in the panel, under the projectile, in the impact zone, has a propagation of stress waves through the thickness, in both analysed cases. Case 2, with sample size of 50mm x 25 mm, additionally shows a propagation of stress waves along the yarn length on the first layers.

The last moment of the simulation, $t = 1.5 \times 10^{-4}$ s shows that the projectile is stopped in both the analysed variants, only that the layers remaining under the projectile are broken/destroyed. The jacket and core of the projectile, in variant 2 are destroyed and deformed, in the case of variant 1, the projectile is only deformed and changes its impact angle during impact. In the variant 2, the projectile does not change its impact angle (Figure 3.38).

The projectile in variant 2 with sample size 50 mm \times 25 mm shows cracking (fragmentation) of the jacket, process that was also noticed in actual tests.

Figure 3.37 gives the von Mises stress distribution for a main yarn of layer 1, at three moments in time, for the 50 mm \times 50 mm sample, $v_0 = 420$ m/s, friction coefficient = 0.25.

The time moment $t = 7.5 \times 10^{-6}$ s shows a maximum stress value of 2230 MPa, and this maximum value is plotted as an upward pointing peak and indicates the red area in Figure 3.37 at this time moment. This peak represents the maximum stress recorded on the yarn at that time and serves as an indicator of the maximum stress sustained by the material during impact at this time. For this moment in time, there are two more areas of maximum values on the graph, represented by two jumps (peaks) upwards, with a stress value between 1500-1750 MPa.



a) Sample 50 mm \times 50 mm

b) Sample 50 mm \times 25 mm

Figure 3.36. Distribution of von Mises stress (in MPa) of the 24-layer panel, at time moment, $t = 1.5 \times 10^{-4}$ s, $v_0 = 420$ m/s, COF = 0,25

Moment of time $t = 3 \times 10^{-5}$ s, shows an zone (micro-volume) of stress concentrators of the periphery of the impact zone on the left side, plotted with an upward pointing peak, reaching a maximum stress of 2848 MPa. I noticed that at this moment in time, the graph presents a higher yarn stress in the left side of the central zone, with a stress between 1700-2000 MPa and in the right side of the central zone, the yarn is not so stressed, the given values are being 1000-1300 MPa (Figure 3.37).

The last moment of time of this yarn, $t = 1.5 \times 10^{-4}$ s, shows that the yarn is not stressed, the von Mises stress value being 244 MPa (Figure 3.37), under the yield limit of the material model, introduced in simulation.

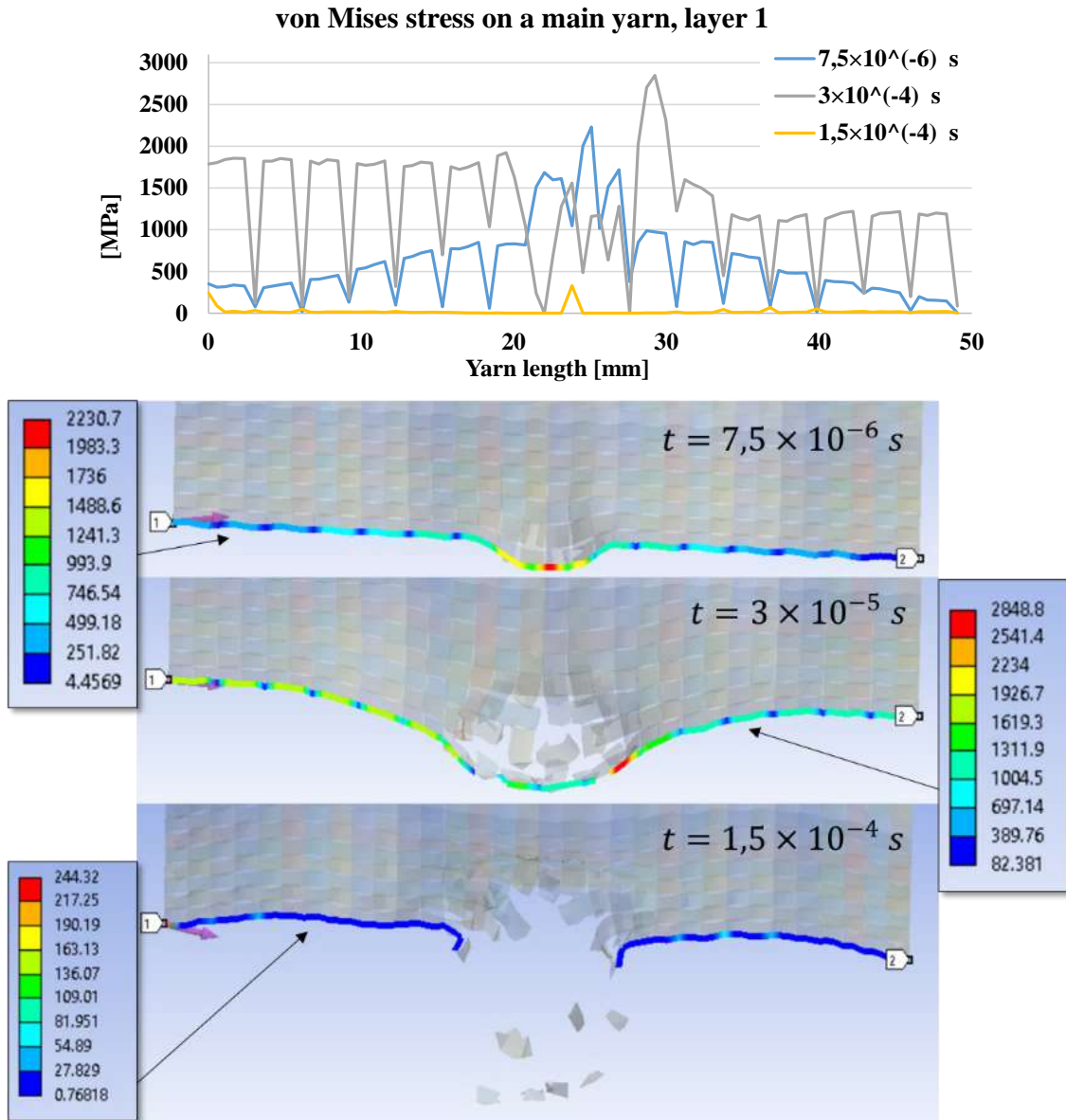


Figure 3.37. Distribution of von Mises stress (in MPa) for a main yarn, at three moments in time, for sample 50 mm × 50 mm, layer 1, $v_0=420$ m/s, COF=0.25

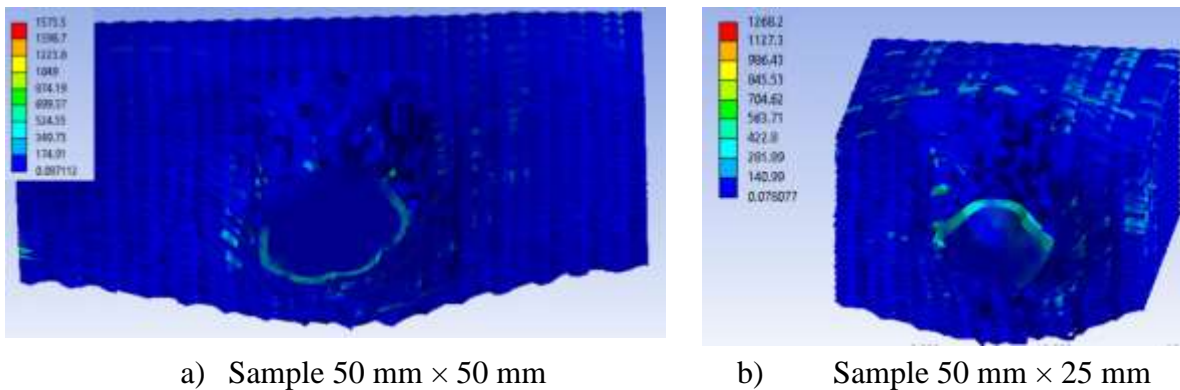


Figure 3.38. Distribution of von Mises stress (in MPa) of the 24-layer Twaron CT736 panel, at time moment, $t = 7.5 \times 10^{-6}$ s, $v_0 = 420$ m/s, COF = 0.25

Figure 3.39 gives the von Mises stress distribution for a main yarn of layer 24 at four time moments for the sample $50 \text{ mm} \times 50 \text{ mm}$, $v_0 = 420 \text{ m/s}$, the value of the friction coefficient being 0.25.

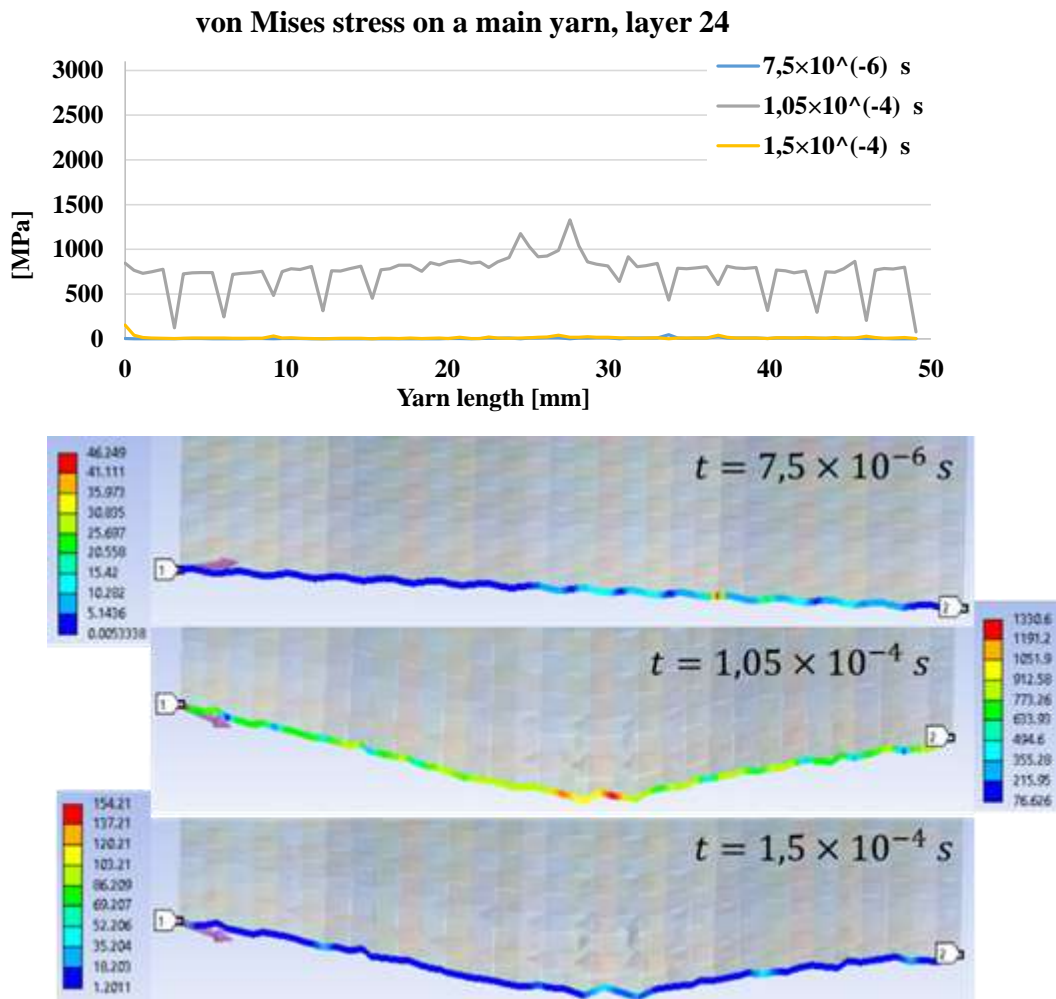


Figure 3.39. Distribution of von Mises stress (in MPa) for a main yarn at three moments in time. Sample of $50 \text{ mm} \times 50 \text{ mm}$, layer 24, $v_0 = 420 \text{ m/s}$, $\text{COF} = 0,25$

Layer 24 (the last layer), between the initial moment, $t = 7,5 \times 10^{-6} \text{ s}$, and the final, $t = 1,5 \times 10^{-4} \text{ s}$, is stressed at maximum 1330 MPa, value under the yield limit considered for the constitutive material model of the yarn. Thus, this yarn is not broken during the impact. Moment of time, $t = 1,05 \times 10^{-4} \text{ s}$, records a maximum stress value of 1330 MPa, the main yarn under analysis is stressed in the central area (Figure 3.39).

Figure 3.40 gives the von Mises stress distribution for a main yarn of layer 1, at four moments in time, for the $50 \text{ mm} \times 25 \text{ mm}$ sample at, $v_0 = 420 \text{ m/s}$, the value of the friction coefficient being 0.25. The maximum stress recorded at the first time of the simulation, $t = 7,5 \times 10^{-6} \text{ s}$, for this yarn is 2654 MPa. The moment $t = 1,5 \times 10^{-5} \text{ s}$, records the highest von Mises stress value of the simulated. When the voltage drops to zero, the yarn is broken. The values recorded on the yarn in the peripheral zone are between 1000-1500 MPa, for the first three time moments analysed. The last time moment registers a stress value of 102 MPa, which is lower than the yield limit. Thus the yarn strain and stress are in the elastic domain.

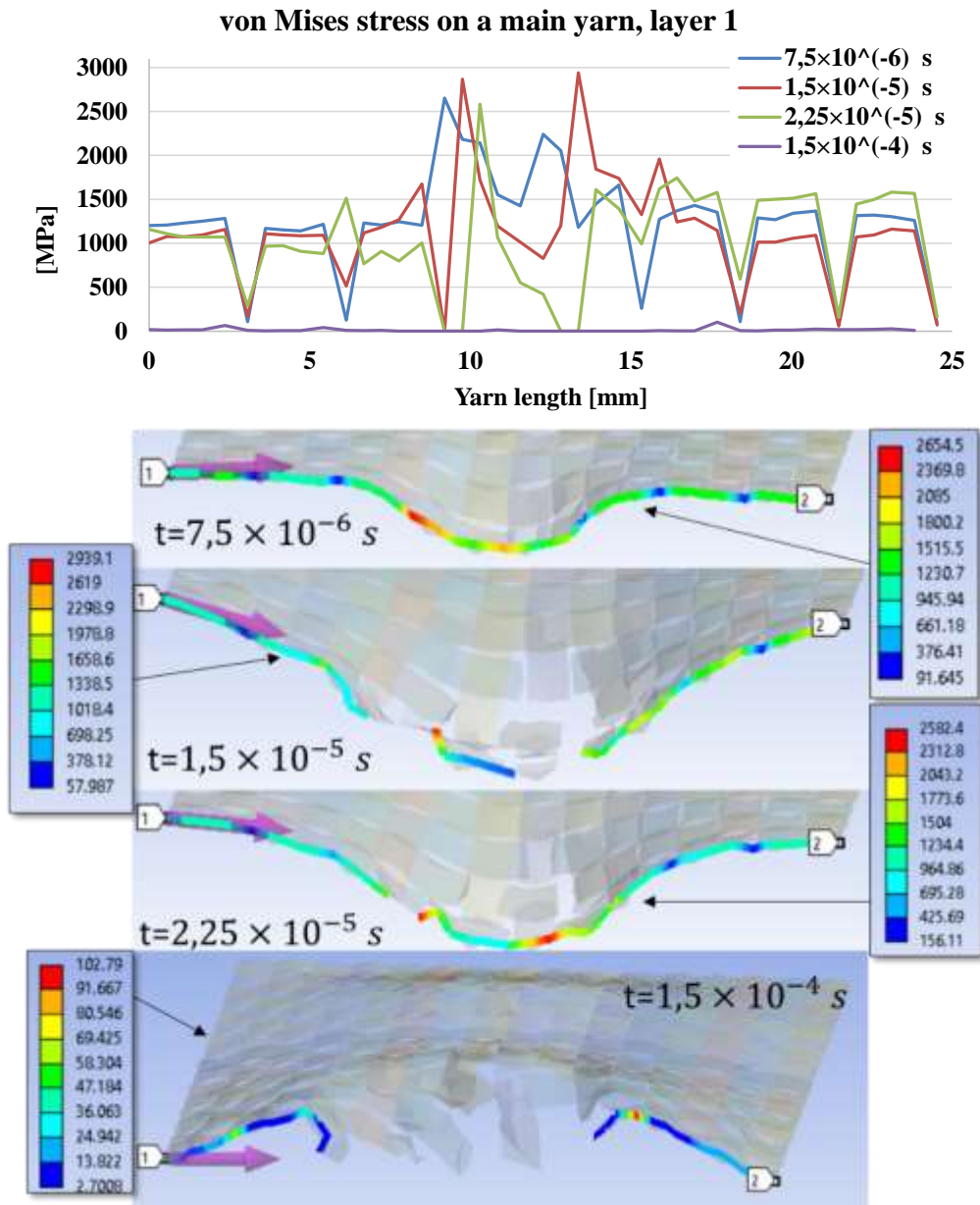


Figure 3.40. Distributions of von Mises stress (in MPa) on the main yarn on layer 1, at four time moments, sample $25 \text{ mm} \times 25 \text{ mm}$, $v_0 = 420 \text{ m/s}$, $\text{COF} = 0,25$

Figure 3.41 gives the von Mises stress distribution for a main yarn of layer 24 at four moments in time, for the $50 \text{ mm} \times 25 \text{ mm}$ sample, $v_0 = 420 \text{ m/s}$, the value of the friction coefficient being 0.25. Of the simulation moments analysed, the maximum stress is recorded at time moment $t = 8.25 \times 10^{-5} \text{ s}$, with a value of 1573 MPa. The first time of the simulation, $t = 7.5 \times 10^{-6} \text{ s}$ records a stress value of 50 MPa, which shows that this layer at the first time of the simulation, was not stressed enough to undergo plastic strain.

The last moment of the simulation, $t = 1.5 \times 10^{-4} \text{ s}$, records a von Mises stress value of 63 MPa, which shows that this layer is longer stressed in the impact process at this end moment and the impact process could be considered as completed (Figure 3.41).

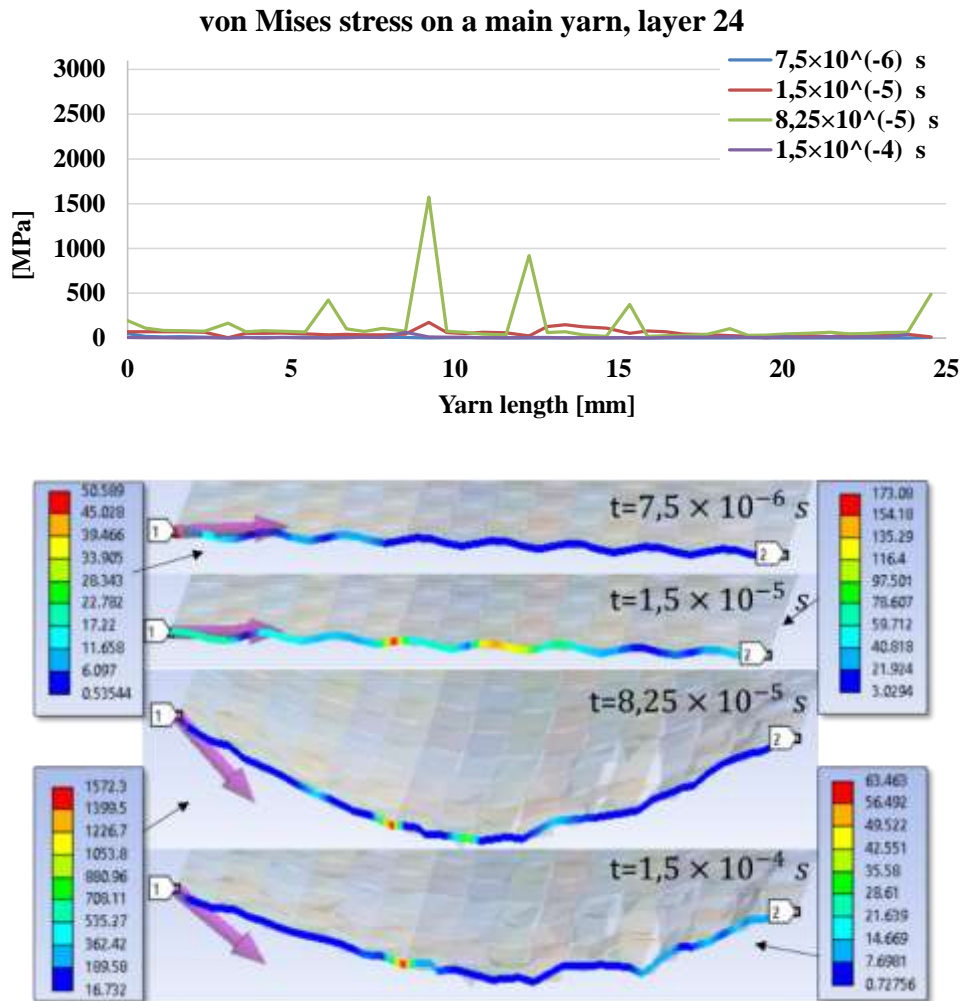


Figure 3.41. Distributions of von Mises stress (in MPa) on the main yarn on layer 24, at four moments in time, for sample 25 mm × 25 mm, $v_0 = 420$ m/s, COF = 0.25

3.6. Model Validation

Validation of the simulated model is an important step in ballistic protection research and development, in order to ensure that the simulation provides plausible and realistic results. The validation of the simulated model is achieved here through two important criteria:

- number of broken layers, as compared to actual panels,
- quality appearance of the panel and projectile after impact, and any other important characteristics. The qualitative aspect is important to ensure that the simulation correctly reproduces the ballistic process and that the results are plausible.

Figure 3.42 shows the number of layers broken from the simulated sample and from a real panel. On the real sample, fire C broke 20 layers of 32-layer panel and fire B broke 15 layers. The difference in broken layers in practice is logical because after the first shot, the material in the area close to this shot is weakened. The simulations obtained a result close to that of fire C (simulated panel also with 32 layers, but with a yield strength of 3000 MPa), with 19 broken layers on the simulation (virtual panel) and 20 broken layers on the real panel (simulation may be considered realistic). For fire B on the real sample, 15 layers were broken,

the simulation closest to that real value, when using the yield limit of 2500 MPa, when 14 layers were broken.

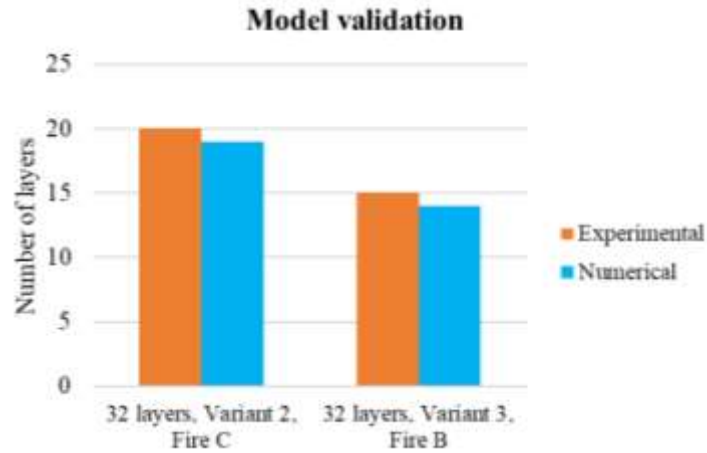


Figure 3.42. Validation of the simulated numerical model with 32 layers by the criterion of number of broken layers (Variant 2 - yarn yield limit is 2500 MPa, Variant 3 – yarn yield limit is 3000 MPa)

Figure 3.43 shows the comparison between the qualitative appearance of layer 19 (fire C) of the experimental sample consisting of 32 layers of Twaron CT736 fabric and 9 mm FMJ projectile, after impact, and the numerical simulation for 32 layers, simulated variant 2, with yield strength 2500 MPa (Figure 3.43b), for the same yarn

Significantly, the numerical simulation succeeds in accurately presenting the qualitative appearance of the experimental sample (Figure 3.43a), including the presence of the projectile (already stopped). This indicates that the simulated model has the ability to correctly reproduce the material behaviour and its interaction with the projectile under these impact conditions and it could be used to evaluate other panels with materials similar and designs.

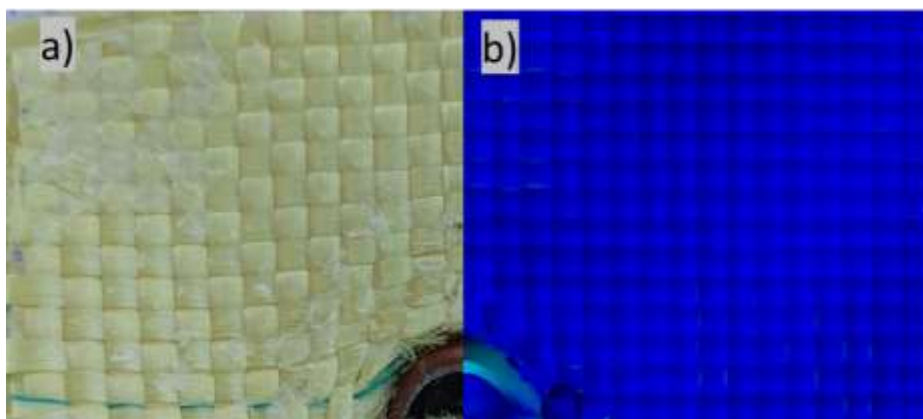


Figure 3.43. Qualitative aspect, analysed for validation: a) layer 19 (focus C) of the experimental sample consisting of 32 Twaron CT736 layers, b) numerical simulation, variant 2, for the same panel as number of layers

3.7. Final Conclusions

Conclusions on of the influence of the constitutive material model for aramid yarns in ballistic simulations

The impact simulation between the 16-layer panel with 2000 MPa yarn yield limit and the 9 mm FMJ projectile, as well as the impact simulation between the 16-layer panel with 3600 MPa yarn yield limit and the 9 mm FMJ projectile are mathematically correct, but these cannot be considered realistic due to failure to meet the validation criteria (in terms of number of broken layers and qualitative aspect, as compared to the results obtained from laboratory tests).

The impact simulation between the 16-layer panel with 2500 MPa yarn yield limit and the 9 mm FMJ projectile and the impact simulation between the 16-layer panel with 3000 MPa yarn yield limit and the 9 mm FMJ projectile are mathematically correct because they meet the validation criteria (in terms of number of broken layers and qualitative aspect, as compared to the results obtained from laboratory tests).

The impact simulation between the 32-layer panel with 2000 MPa yarn yield limit and the 9 mm FMJ projectile as well as the impact simulation between the 32-layer panel with 3600 MPa yarn yield limit and the 9 mm FMJ projectile are mathematically correct but these cannot be considered realistic due to failure to meet the validation criteria (in terms of number of broken layers and qualitative aspect, as compared to the results obtained from laboratory tests).

The impact simulation between the 32-layer panel with 2500 MPa yarn yield limit and the 9 mm FMJ projectile and the impact simulation between the 32-layer panel with 3000 MPa yarn yield strength and the 9 mm FMJ projectile are mathematically correct because it meet the validation criteria (in terms of number of broken layers and qualitative aspect, as compared the results obtained from laboratory tests).

Conclusions on the influence of introducing friction in the impact model

In variant with $COF=0.25$, the last layer starts to recover after the projectile bounces back, but shows broken main yarns in the direction of the bending.

In the version with $COF= 0.1$, the last layer has a strong bending due to total penetration of the fabric and the yarns are broken.

In the version without friction between the yarns and between yarns and projectile, the last layer also shows broken yarns, even after the projectile has stopped and rebounded.

In general, the coefficient of friction significantly affects the behavior and integrity of the fabric during impact, determining whether the projectile is stopped or rebounded, especially for thinner panels, as well as the degree of damage to the yarns. The variant with a higher coefficient of friction ($COF=0.25$) seems to provide a better ability to stop the projectile but may still lead to damage to the fabric, both on main and secondary yarns.

Conclusions on the influence of sample size in numerical simulation

Simulation results can help to design and develop more effective protection systems in terms of performance and destructiveness. This can be crucial in the military to ensure target resistance capability or to minimize collateral damage in military operations.

Simulations allow researchers and engineers to better understand how projectiles and protective systems behave in different situations and how they can be optimized for different use scenarios.

The sample size of 50 mm × 50 mm is more relevant to obtain realistic results. It provides a realistic insight into the behaviour of the projectile under impact and fragmentation conditions and shows that the simulations are able to accurately portray the effects on the projectile structure and target, here with layers.

In variant 1, with a sample size of 50 mm × 50 mm, the wires are destroyed in the impact area with partial penetration of the panel. Here, the projectile is only deformed and changes its original shape. This suggests a less dramatic deformation of the projectile and a change in its parameters (especially velocity), but with partial penetration of the target.

In variant 2, sample size 50 mm × 25 mm, the yarns are broken near the impact zone, too and the projectile jacket fragments. There is also partial penetration and the non-broken yarns under the projectile are only compressed. This indicates a more significant destruction and fragmentation of the projectile and a more pronounced influence on the target.

The results indicate that variant 2 shows more severe projectile destruction and fragmentation, with extensive influences on the target and underlying layers. The sample size seems to be important to obtain meaningful data on the projectile behaviour under ballistic conditions by simulation.

Chapter 4. Selected Fabrics for Ballistic Protection Systems and the Test Campaign

4.1. Introduction

Experimental testing is used on ballistic protection systems at every stage of the product life cycle, from the creation of ballistic impact resistant materials and systems to end-of-life testing of the ballistic protection system, after it has been used. In order to maintain the performance to be delivered over the lifetime of the product, protective systems must be built with a tolerance that can cover all performance requirements. In order to ensure that performance, they are checked during the lifetime of the protection systems, appropriate validation of a new protection system before it is launched on the market is required, as well as continuous evaluation of the product once it has been implemented.

The optimal materials must be selected before any ballistic impact-resistant protection system can be developed.

The manufacturer and/or user of the protective system may then specify appropriate levels of ballistic performance and design validation testing is then required to achieve these levels. Design validation testing provides a reliable baseline of data that can be compared to subsequent tests, such as batch quality testing or performance deterioration tracking for deployed protective systems. A wide range of ballistics tests can be included in design validation testing programmes. Surface density, flexibility, moisture resistance, thickness, hardness and other non-ballistics tests can be used at this stage to ensure that the requirements of the secondary auxiliary system meet the specific requirements of the intended user. In order to confirm that the personal protective equipment is robust and will perform as intended in the standards over its typical lifetime, validation should also involve testing it after exposure to various environmental extremes.

4.2. Sample Procedures for Ballistics Testing: a National Institute of Justice (Ballistic Resistance, NIJ Standard-0101.06)

According to NIJ standards, the panel must be positioned on the backing material in such a way as to ensure that the point of impact, projected through the panel, is at least 106 mm away from the surface of the backing material (ballistic plastiline).

The target panels must be held firmly in contact with the plasticine, which is commonly used as a backing material in ballistics tests (usually grade Rome #1). This ensures consistent and accurate impact measurement.

Figure 5.1 shows how the panels tested for this research study are mounted. The panels have dimensions of 400 mm x 400 mm and are fastened to the backing material with straps.

The test conditions that have been met for ballistic panel testing are those given in the NIJ Standard [NIJ -0101.06].

By maintaining consistent environmental conditions, test results can be accurately compared and analysed. This helps to ensure that any observed changes in the ballistic performance of the protection system are primarily attributable to the variables tested, rather than external environmental factors. These standardised conditions facilitate accurate and

reliable assessment of the performances of the protective system, under different test scenarios.



Figure 5.1. Mounting procedure of the tested panels

In preparation for testing the designed protection systems, the equipment and setup must follow specific instructions to ensure consistent and accurate results. Based on the information provided, the key points for range configuration are as following:

The ballistic protection panel shall be mounted at a distance of $5.0 \text{ m} \pm 1.0 \text{ m}$ from the edge of the fire barrel pipe (Figure 5.2).

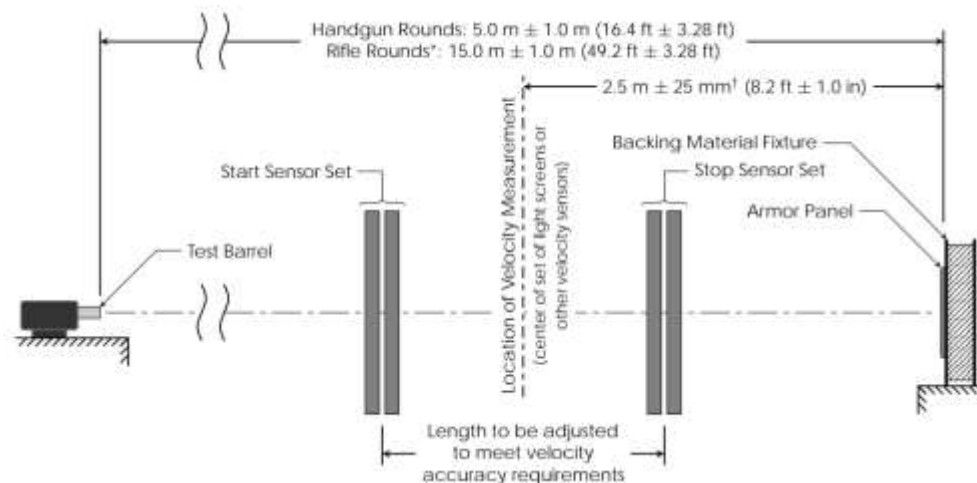


Figure 5.2. Test configuration [NIJ Standard-0101.06]

The objective of this study is to test and examine the impact of the projectile on ballistic protection systems made of two types of fabric from Teijin Limited:

- samples made by layering Twaron CT736 fabric,
- samples made by layering Twaron SRM509 fabric and Twaron CT736 fabric.

4.3. Methodology of Ballistic Impact Experiments

Several samples for personal protective systems with different number of layers of Twaron CT 736 CMP fabric and samples of protective systems made with different number of layers of two types of fabrics, Twaron SRM509509 and Twaron CT 736, were tested.

According to NIJ 0101.04/2004 [NIJ Standard-0101.06], STANAG 2920 [STANAG], STP/M 40202-99 and SMT 4003.5-2003 the ballistic resistance of the protective systems to the action of a 9 mm FMJ (Full Metal Jacket) projectile was carried out, the projectile moving at a speed of 400 to 440 m/s.

The test campaign aimed to determine the behaviour of the samples of protective systems to the impact of a 9 mm FMJ projectile. The test campaign was carried out at the CBRN Defence and Ecology Scientific Research Center in Bucharest.

The experiments were conducted in accordance with operating protocols and authorised working instructions, and the weapons and ammunition required for testing were stored in specially constructed and controlled warehouses.

According to NIJ standard], the trace in the plasticine used in ballistics experiments was measured to an accuracy of ± 0.1 mm using a depth gauge. In order to prevent any residue of plasticine on the measurement area, the screwdriver was cleaned after each measurement.

4.4. How to Attach the Ballistic Panels

Ballistic panels can be composed of a single type of material or several types of material combined. How these materials are arranged and how many layers of each type are used can significantly affect the ballistic performance of the package. Sometimes manufacturers may include an additional layer of non-ballistic material in the structure of the ballistic package for the sole purpose of improving protection against impact trauma. In addition, there are also composites that use two or more types of ballistic materials or blanks to achieve superior performance.

4.5. Fabrics Used for the Protective Panels

Teijin Limited supplied Twaron CT736 plain (1/1) fabric with the same characteristic, of 410 g/m^2 as Twaron CT736 and Twaron SRM509 with basket or twill architecture. These two fabrics are used more for helmets. What I used is a Twaron CT736 fabric with a PVB phenolic coating also Tables 4.1 and 4.2 presents the characteristics of the two selected fabrics (or prepegs).

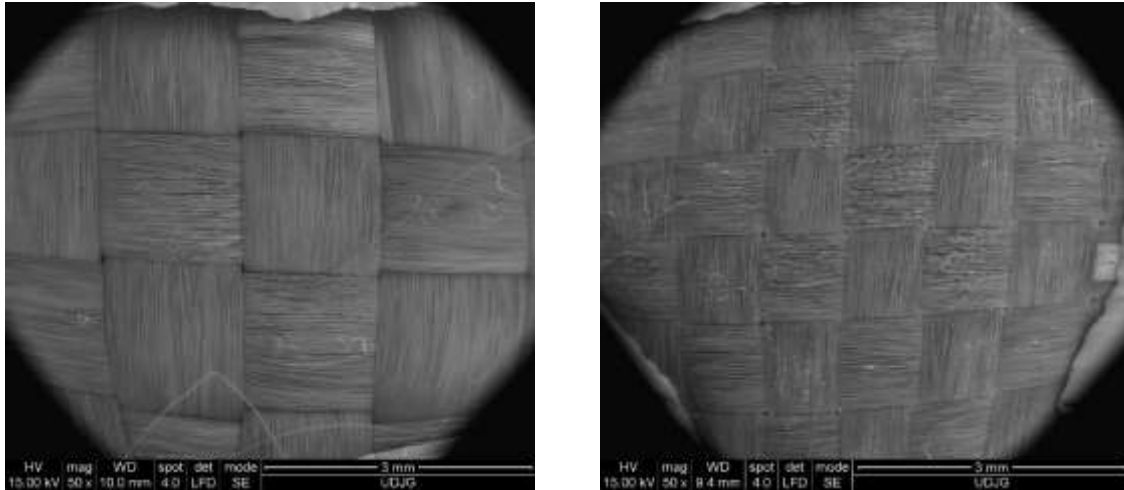
Table 4.1. Twaron CT736 fabric characteristics [teijin catalogue]

Linear density [dtex _{nom}]	Twaron- Type	Set [per 10 cm]		Areal Density [g/m ²]	Thickness [mm]	Minimum Breaking Strength [N/5 cm × 1000]	
		Warp	Weft			Warp	Weft
1680f1000	2000	127	127	410	0,62	15.5	16.60

Table 4.2. Twaron SRM509 fabric characteristics [teijin catalogue].

Main application	Linear density [dtex] _{nom}	Twaron- Type	Total weight [g/m ²]	Construction
Stab-proof vests	930f1000	2040	430	CT 709 woven Twaron fabric + silicon carbide coating

Teijin provides several fabrics for personal protection systems (Figure 4.1).



Twaron CT736

Twaron SRM509

Figure 4.1. Fabrics provided by Teijin

4.6. The Process of Making Samples of Individual Ballistic Protective Armour

In accordance with NIJ standard [NIJ 0101.06], the ballistic vest prototype was made using a template created to scale (Figure 4.4). These layers were cut by hand, using two special scissors for aramid fibres. This vest prototype was not tested yet as a system. Only find panel as square shape tested.



Figura 4.4. Assembling the vest prototype

The size of the panel is 400 mm × 400 mm. According to the NIJ Standard 0101.06 [NIJ 0101.06] the size of the test panel is 500 mm × 500 mm. This size of 400 mm × 400 mm was chosen due to lack of resources.



Figura 4.5. Sample preparation

The 16-layer and 24-layer Twaron CT736 fabric panels were constructed with the layers sewn into the corners with Twaron yarns (Figure 4.6). The 32-layer Twaron CT736 fabric panel was constructed from two 14-layer panels sewn at the corners and fastened with textile shells. The 32-layer Twaron CT736 fabric panel was constructed from two 16-layer panels sewn at the corners and fastened with textile shells. The 42-layer Twaron CT736 fabric panel was constructed of four panels, three 8-layer panels and one 18-layer panel that had the layers sewn into the corners and fastened with fabric shells (Figure 4.6).



a) Sewn panels forming the 42-layer Twaron CT736 fabric panel



b) 42-layer panel fastened with textile shells

Figure 4.6. Construction of the 42-layer Twaron CT736 fabric panel

The panel consisting of 16 combined layers of Twaron SRM509 and Twaron CT736 fabric was constructed from a single panel with the layers sewn into the corners, 8 layers of Twaron SRM509 fabric, which were layered first, and 8 layers of Twaron CT736 fabric.

The panel consisting of 24 combined layers of Twaron SRM509 and Twaron CT736 fabric was constructed from a single panel with the layers sewn into the corners, 12 layers of Twaron SRM509 fabric, that were layered first, and 12 layers of Twaron CT736 fabric.

The panel made of 28 combined layers of Twaron SRM509 and Twaron CT736 fabric was constructed of two panels with the layers sewn in the corners and fastened with textile shells. The first panel consists of 7 layers of Twaron SRM509 fabric, which were layered first, and 7 layers of Twaron CT736 fabric. The second panel consists of 7 layers of Twaron SRM509 fabric, which have been layered first and 7 layers of Twaron CT736 fabric.



Figure 4.7. How the Twaron CT736 fabric layers panel is attached



Figure 4.8. How to fasten the Twaron SRM509+ Twaron CT736 combined fabric layers panel

The panel consisting of 32 combined layers of Twaron SRM509 and Twaron CT736 fabric was constructed of two panels with the layers sewn in the corners and fastened with textile shells. The first panel consists of 8 layers of Twaron SRM509 fabric, which were layered first, and 8 layers of Twaron CT 736 fabric. The second panel consists of 8 layers of Twaron SRM509 fabric, which have been laminated first and 8 layers of Twaron CT 736 fabric.

The 40-layer combined Twaron SRM509 and Twaron CT736 fabric panel was constructed from three panels with the layers sewn in the corners and fastened with textile shells. The first panel consists of 12 layers of Twaron SRM509 fabric, which were layered first, and 12 layers of Twaron CT736 fabric. The second panel consists of 4 layers of Twaron SRM509 fabric, which have been arranged first and 4 layers of Twaron CT736 fabric. The third panel consists of 4 layers of Twaron SRM509 fabric, which have been laminated first and 4 layers of Twaron CT736 fabric.

The systems of panel architecture are given in Tables 4.3, 4.4, 4.5 and 4.6.

Table 4.3. Thickness of Twaron CT736 fabric layers panels

Panel	Order and number of layers of material	Thickness of each material [mm]	Total thickness [mm]
42 Twaron CT736	8 layers CT736	4.31	22.07
	8 layers CT736	4.29	
	8 layers CT736	4.30	
	18 layers CT736	9.17	
32 Twaron CT736	16 layers CT736	8.61	17.2
	16 layers CT736	8.59	
28 Twaron CT736	14 layers CT736	7.30	15.24
	14 layers CT736	7.32	
24 Twaron CT736	24 layers CT736	12.85	12.85
16 Twaron CT736	16 layers CT736	8.60	8.60

Table 4.4. Weight of Twaron CT736 fabric layers panels

Panel	Order and number of layers of material	Weight of material layers [g]	Total weight [g]
42 Twaron CT736	8 layers CT736	600	3122
	8 layers CT736	595	
	8 layers CT736	600	
	18 layers CT736	1327	
32 Twaron CT736	16 layers CT736	1202	2421
	16 layers CT736	1219	
28 Twaron CT736	14 layers CT736	1042	2090
	14 layers CT736	1048	
24 Twaron CT736	24 layers CT736	1780	1780
16 Twaron CT736	16 layers CT736	1205	1205

Table 4.5. Thickness of Twaron SRM509 and Twaron CT736 combined fabric layers panels

Panel	Order and number of layers	Thickness of each material [mm]	Total thickness [mm]
40 Twaron SRM509 + Twaron CT736	12 layers SRM509	4.60	18.29
	12 layers CT736	6.15	
	4 layers SRM509	1.70	
	4 layers CT736	2.08	
	4 layers SRM509	1.67	
	4 layers CT736	2.09	
32 Twaron SRM509 + Twaron CT736	8 layers SRM509	3.14	14.79
	8 layers CT736	4.1	
	8 layers SRM509	3.35	
	8 layers CT736	4.2	
28 Twaron SRM509 + Twaron CT736	7 layers SRM509	2.74	12.28
	7 layers CT736	3.15	
	7 layers SRM509	2.76	
	7 layers CT736	3.63	
24 Twaron SRM509 + Twaron CT736	12 layers SRM509	4.85	11.35
	12 layers CT736	6.5	
16 Twaron SRM509 + Twaron CT736	8 layers SRM509	3.20	7.35
	8 layers CT736	4.15	

Table 4.6. Weight of Twaron SRM509 and Twaron CT736 combined fabric layers panels

Panel	Order and number of layers	Weight of layers [g]	Total weight [g]
40 Twaron SRM509 + Twaron CT736	12 layers SRM509	863	2936
	12 layers CT736	883	
	4 layers SRM509	285	
	4 layers CT736	303	
	4 layers SRM509	300	
32 Twaron SRM509 + Twaron CT736	4 layers CT736	302	2363
	8 layers SRM509	576	
	8 layers CT736	603	
	8 layers SRM509	578	
28 Twaron SRM509 + Twaron CT736	8 layers CT736	606	2026
	7 layers SRM509	500	
	7 layers CT736	515	
	7 layers SRM509	501	
24 Twaron SRM509 + Twaron CT736	7 layers CT736	510	1747
	12 layers SRM509	857	
16 Twaron SRM509 + Twaron CT736	12 layers CT736	890	1179
	8 layers SRM509	579	
	8 layers CT736	600	

Chapter 5. Experimental Data for the Front Panels of a Vest with Protection Level IIA

5.1. Back Face Signature Analysis and Assessment of the Ability of Protective Systems to stop the Projectile

5.1.1. Introduction

The back face signature (BFS) is a measurement used in ballistic protection system testing to assess the performance of ballistic materials, when subjected to ballistic impact [Oliveira, 2019], [Yang, 2019] [Jiang, 2022] [Saleem, 2022], [Mudzi, 2022], [Yang, 2017], [Kumar, 2023]. Back face signature refers to the depth of deformation or indentation that occurs in the backing material (ballistic plastiline Rome #1). This depth is an indicator of the amount of energy transferred to the protective system and can help determine the ability of the individual protective system to stop or mitigate the effects of a projectile impact on the carrier's body.

5.1.2. The Back Face Signature Analysis (BFS)

The recorded values for the trace depth for the Twaron CT736 CMP and Twaron SRM509 plain weave layered samples, are given in Table 5.1. These measurements were made according to "Ballistic Resistance of Body Armor, NIJ Standard-0101.06, U.S. Department of Justice Office of Justice Programs National Institute of Justice, 2008 [NIJ 0101.06].

Figure 5.1 shows images of the shape of the backing material, following the impact of the panel with 32 layers of CT736 fabric and 16 layers of Twaron CT736 fabric, respectively (BFS).

Table 5.1. Values obtained for back face signature according to NIJ standard - 0101.06

Sample	Fires		
	A	B	C
	BFS [mm]		
16 layers Twaron CT736 fabric	TP	TP	TP
24 layers Twaron CT736 fabric	TP	TP	23
28 layers Twaron CT736 fabric	TP	25	28
32 layers Twaron CT736 fabric	14	17	16
42 layers Twaron CT736 fabric	9	4	5
16 combined layers of Twaron SRM509509 fabric and Twaron CT736 fabric	TP	TP	TP
24 combined layers of Twaron SRM509509 fabric and Twaron CT736 fabric	TP	TP	TP
28 combined layers of Twaron SRM509509 fabric and Twaron CT736 fabric	TP	TP	TP
32 combined layers of Twaron SRM509509 fabric and Twaron CT736 fabric	TP	TP	TP
42 combined layers of Twaron SRM509509 fabric and Twaron CT736 fabric	14	17	TP

TP - total penetration

To determine whether the personal protective panel will provide sufficient protection, the back face deformation (BFD) measured on the back side of a tested panel must be examined.

The standard requirements outlined in Section 7.8.8 of [NIJ 0101.06] state that either all measured BFS depths resulting must be 44 mm or less, or there must be a 95% confidence level that 80% of all measured BFS depths are 44 mm (or less if there are BFS depths exceeding this threshold). The BFS depth must not be greater than 50 mm.



a) 32 layers of Twaron CT736 fabric



b) 16 layers of Twaron CT736 fabric

Figure 5.1. Front view of the backing material after impacting the panels with 3 hits

5.1.3. The Back Face Signature Analysis by 3D Scanning

The 3D registration or measurement of the back face signature in the ballistic plastiline (noted with BFS in NIJ Standard - 0101.06) was performed with the Handyscan 3D scanner.



Figure 5.2. Measurements HandyScan 3D scanner

This helps to make an assessment based on several parameters and to compare the resulting indentations from several types of panels and projectiles. These additional parameters can participate in differentiating the response of the panel to successive hits or to different materials or projectiles and, of course, it has high precision.

During scanning, various reflective marks were placed on the surface of the deformed support material for easy detection and modelling of the indentation deformation (Figure 5.3). Such scanning methods not only provide an accurate result and measurement in a short time, but also facilitate visual depth comparison for different panel targets. Using Autodesk Inventor [Autodesk, Inc. 2021] and importing the high precision scans, I was able to virtually re-build the indentation and to calculate their volumes and base section areas (Table 5.2), the trace depth measurement created in the backing material, and the volume of the holes created by the full penetration of the panel.

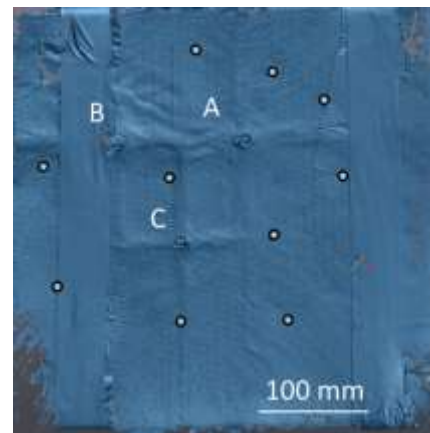
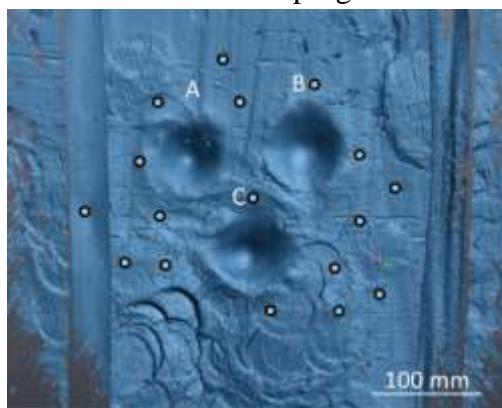
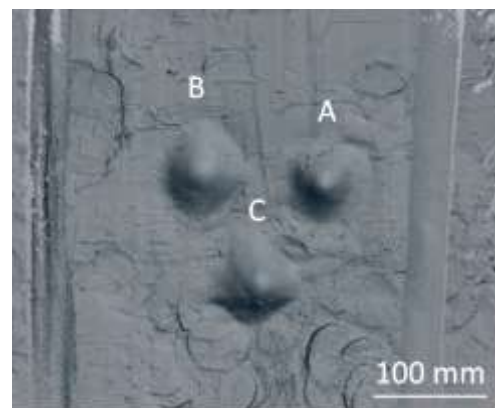


Figure 5.3. Positioning reflective signs on

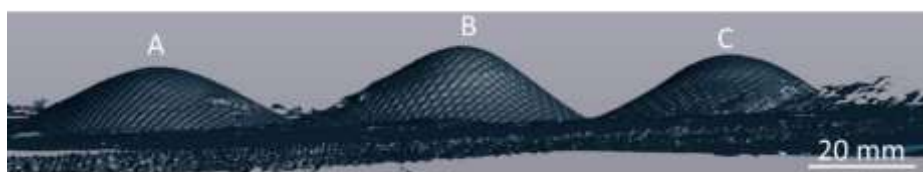
Figure 5.4 shows the 3D view of the ballistic plastiline after impacting the panels obtained from the VXelements program.



a) front view of the backing material after striking the panel with three projectiles



b) rear view of the backing material surface (virtual surface considered to be zero thickness)



c) indentations detail in backing material as zero thickness surface

Figure 5.4. 3D view of the plastiline after impacting the 32-layer Twaron CT736 panel

Table 5.2 shows the values for the back face signature volume in the support material.

Table 5.2. Values for back face signature volume in the support material

Test	Volume [mm] ³
24 layers Twaron CT736 fabric - Fire C	26076
28 layers Twaron CT736 fabric - Fire B	23428
28 layers Twaron CT736 fabric - Fire C	27459
32 layers Twaron CT736 fabric - Fire A	17472
32 layers Twaron CT736 fabric - Fire B	19872
32 layers Twaron CT736 fabric - Fire C	12134
42 layers Twaron CT736 fabric - Fire A	3555
42 layers Twaron CT736 fabric - Fire B	10534
42 layers Twaron CT736 fabric - Fire C	1554
40 combined layers of Twaron SRM509509 fabric and Twaron CT736 fabric - Fire A	9411
40 combined layers of Twaron SRM509509 fabric and Twaron CT736 fabric - Fire B	13566

Figures 5.5 show 3D views (front view, back view), how to measure the back face signature and a vertical section through the backing material in a plane containing the greatest back face signature (and also referred as BFS), with the surface of the indentation sectioned by a plane containing the undeformed surface of the backing material, for the 32-layer Twaron CT 736, Fire A fabric panel.

Table 5.3 presents values of BFS measured by two methods: by the help of Shuble and form 3D scans.

Table 5.3. Back face signature (BFS) values in the backing material

Test	Back face signature - measured with a shubler [mm]	Back face signature - 3D scanning [mm]
24 layers Twaron CT736 fabric	23	21.051
28 layers Twaron CT736 fabric - Fire B	25	24.003
28 layers Twaron CT736 fabric - Fire C	18	18.115
32 layers Twaron CT736 fabric - Fire A	17	16.000
32 layers Twaron CT736 fabric - Fire B	16	14.060
32 layers Twaron CT736 fabric - Fire C	14	13.000
42 layers Twaron CT736 fabric - Fire A	5	4.669
42 layers Twaron CT736 fabric - Fire B	9	8
42 layers Twaron CT736 fabric - Fire C	4	3.214
40 combined layers of Twaron SRM509 fabric and Twaron CT736 fabric - Fire A	14	12.354
40 combined layers of Twaron SRM509 fabric and Twaron CT736 fabric - Fire B	17	15.394

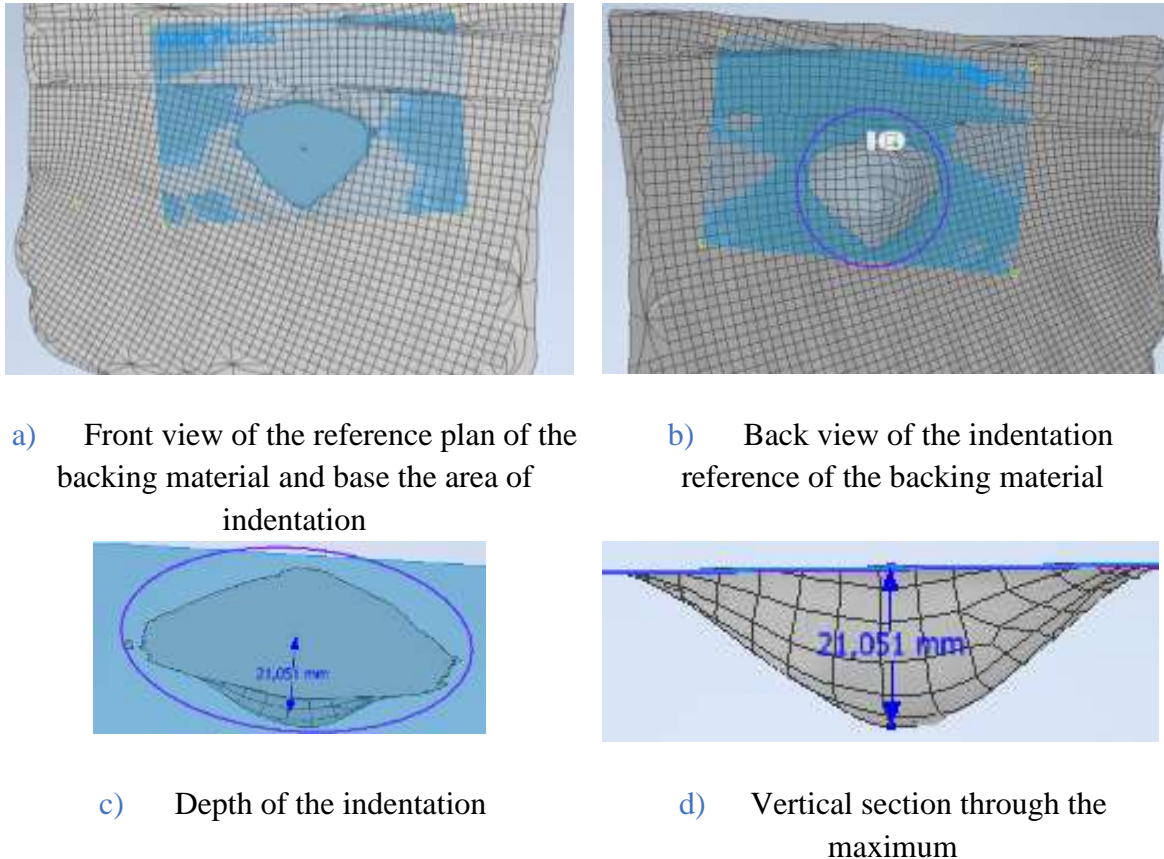


Figure 5.5. 3D view of the indentation surface delineated by a plane containing the undeformed plastiline surface, indentation for the Twaron CT 736 24-layer panel, fire B

5.2. Factors Influencing the Performance of Ballistic Material in High Impact Scenarios

5.2.1. Introduction

The aspects to be taken into account for improving ballistic protection are:

- material properties,
- adding more layers in different arrangements, during ballistic panel production

[Oberg, 2015], [Yang, 2017], [Joo, 2008] (which has a relatively negative effect due to total weight increased and on target flexibility [Karahan, 2008], [Liu, 2018]).

Parameters that influence ballistic impact performance [Abteu, 2019] are fiber type [Karahan, 2015], yarn properties, material properties, fabric structure, projectile geometry, mass and velocity, surface density of ballistic panel, target size, number of layers, layering sequence of panel layers [Ralph, 2023], [Porwal, 2005], textile constructions such as woven/woven fabrics and 2D/3D fabrics [Briscoe, 1992], [Karahan, 2008], [Othman, 2013], [Mishra, 2013], [Bajya, 2021], friction between projectile-yarn, yarn-yarn and even fibre-fibre [Maithani, 2023], [Zhou, 2022], [Chu, 2014], [Chu, Y., Chen, X., Wang, 2014], [Ha-Minh, 2012].

During the ballistic impact event, the target provides resistance to penetration/puncture by the projectile itself. The incident kinetic energy of the projectile

would be absorbed by the target through various damage and energy absorption mechanisms (Figure 5.6).

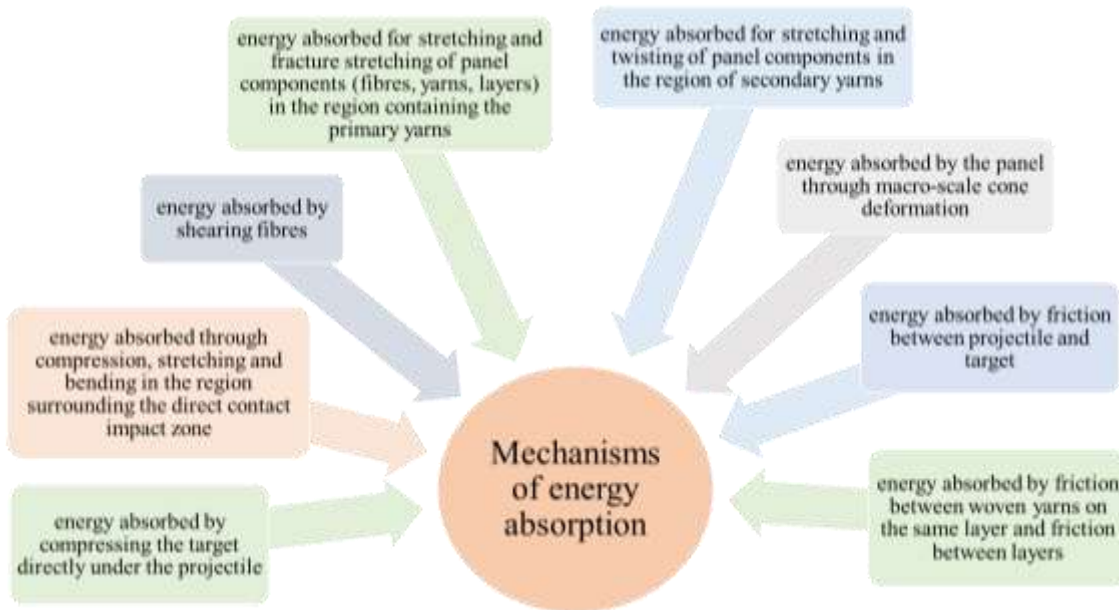


Figure 5.6. Energy absorption mechanisms [Pandya, 2014].

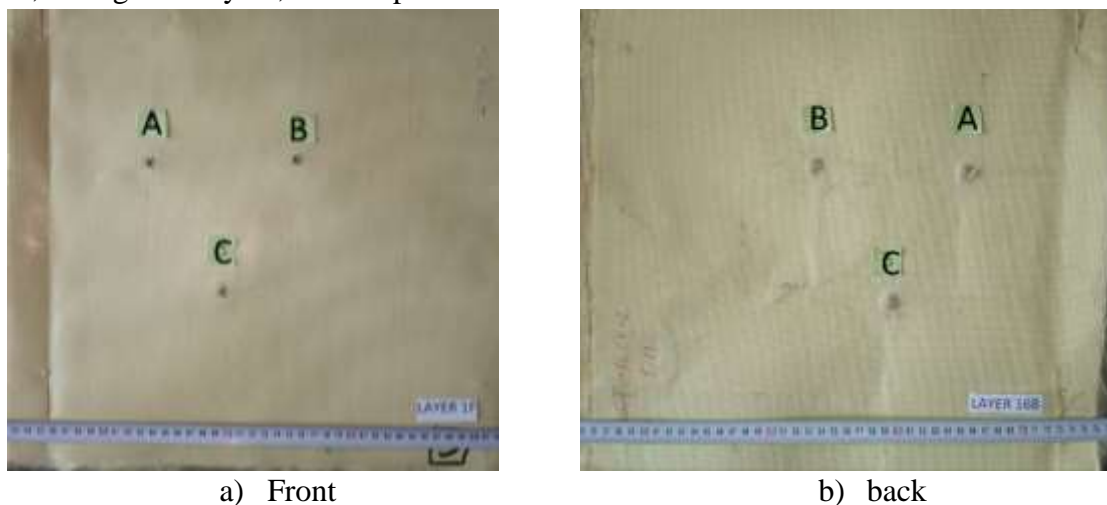
5.2.2. Macro Photo Analysis of the Tested Panels

Analysis of macro photographs of the impact of Twaron CT736 laminated fabric panels with a 9 mm FMJ projectile and the impact of Twaron SRM509 and Twaron CT736 laminated fabric panels involves a detailed examination of the images to gather information about impact dynamics and material failure. It is possible to identify the number of failed layers and the intensity of projectile or/and fragmentation.

5.2.2.1. Analysis of the Three Fires on Twaron CT736 Fabric Panels

Three-fire analysis of the 16-layer Twaron CT736 panel

Figure 5.7 shows images of the panel consisting of 16 layers of Twaron CT 736 fabric, arranged in layers, after impact.



a) Front

b) back

Figure 5.7. Panel made of 16 layers of Twaron CT 736 fabric, after being tested (the order of fires is A, B and C)

Analisis of the A-fire of Twaron CT736 16-layer panel

Layer 1 shows two broken yarns, one in the direction of the weft and one in the direction of the warp (Figure 5.8) and five partially broken yarns, the fibres that were not broken are pushed to the side. Layer 8 shows a similar breakage as layer 7, only two yarns are completely broken and the polymer coating (PVB) cracks and some of the fragments peeled off the fabric coating stick to the destroyed area of the previous layer. Layer 16 has two broken yarns, one in the direction of the warp and one in the direction of the weft, and four yarns that have only part of the fibres broken. The fibres that were not broken from the partially broken yarns are pushed to the side.

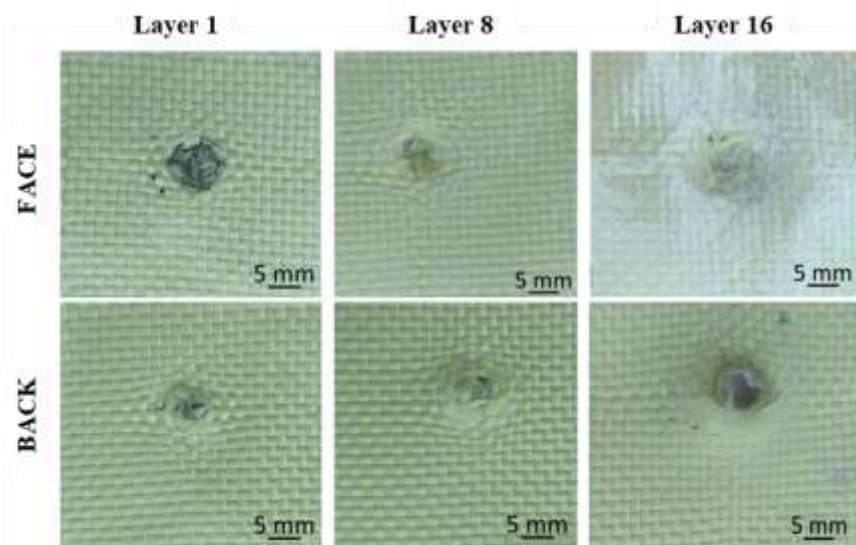


Figure 5.8. Details of fire A of the 16-layer fabric panel Twaron CT 736

B-fire analysis of Twaron CT736 16-layer panel

Layer 1 (Figure 5.9) has one completely broken yarn and four partially broken yarns. The fibres that have not been broken are pushed to the side. The polymer coating (PVB) is peeled off and jumps in and around the impact area (Figure 5.36). Layer 8 has no completely broken yarns, shows four partially broken yarns, the fibres that were not broken are pushed to the side. Layer 16 has two completely broken yarns and the yarns that are pushed to the side have broken fibres.

C-fire analysis of Twaron CT736 16-layer panel

Layer 1 (Figure 5.10) shows the complete breakage of a single yarn and five partially broken yarns. The main yarns that were not broken are pushed to the side. The polymer coating (PVB) is detached only aramid the impact area, where the yarns are broken and twisted. Layer 8 has two completely broken main yarns, shear breakage and two partially broken main yarns. The fibres of the partially broken yarns that have not been broken are pushed to the side. Layer 16 has two completely broken yarns and one yarn two partially broken yarns; this yarn breakage is due to the stretching of the yarns.

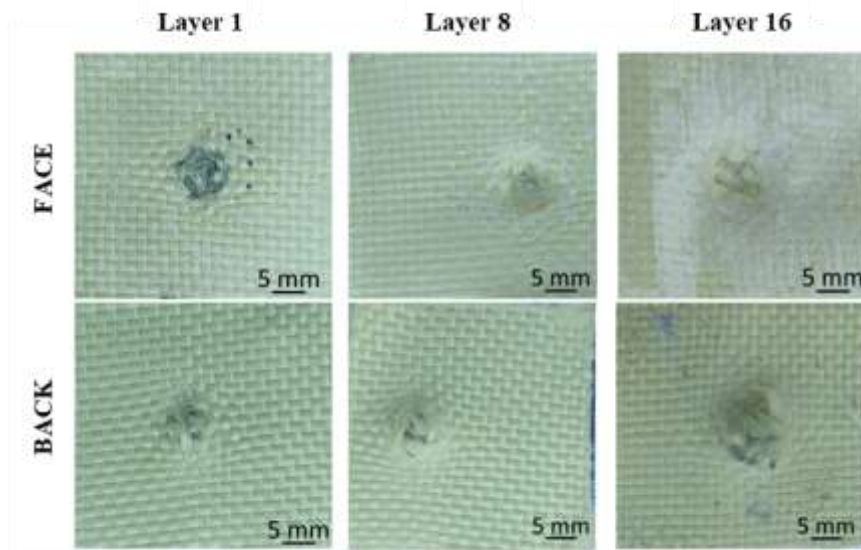


Figure 5.9. Details of fire B of the 16-layer Twaron CT 736 fabric panel, total penetration

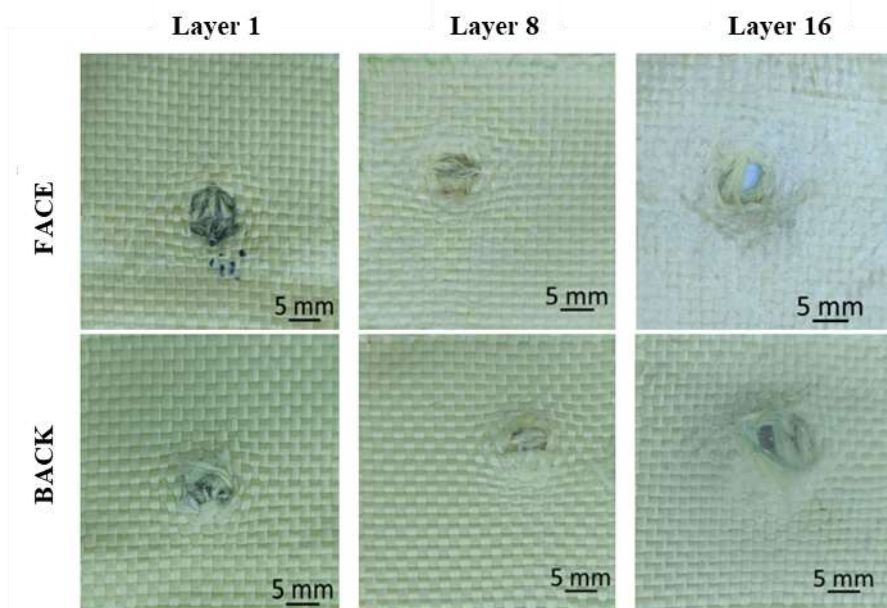


Figure 5.10. Details of the fire C, on the 16-layer Twaron CT 736 fabric panel, total penetration

Analysis of the 32-layer Twaron CT736 panel after being tested

The impact of the projectile of 9 mm FMJ on the panel made of 32 layers of Twaron CT736 fabric, in which three projectiles were fired, with projectiles at different velocities, provides a detailed insight into the behaviour of this layered material (Figure 5.11).

Fire B, with an initial velocity of 413.86 m/s, produced a partial penetration in the Twaron CT736 fabric panel. Fire A, with an initial velocity of 428.07 m/s, produced a similar partial penetration in the panel. Fire C, with an initial velocity of 422.39 m/s, generated a partial penetration into the Twaron CT736 fabric.

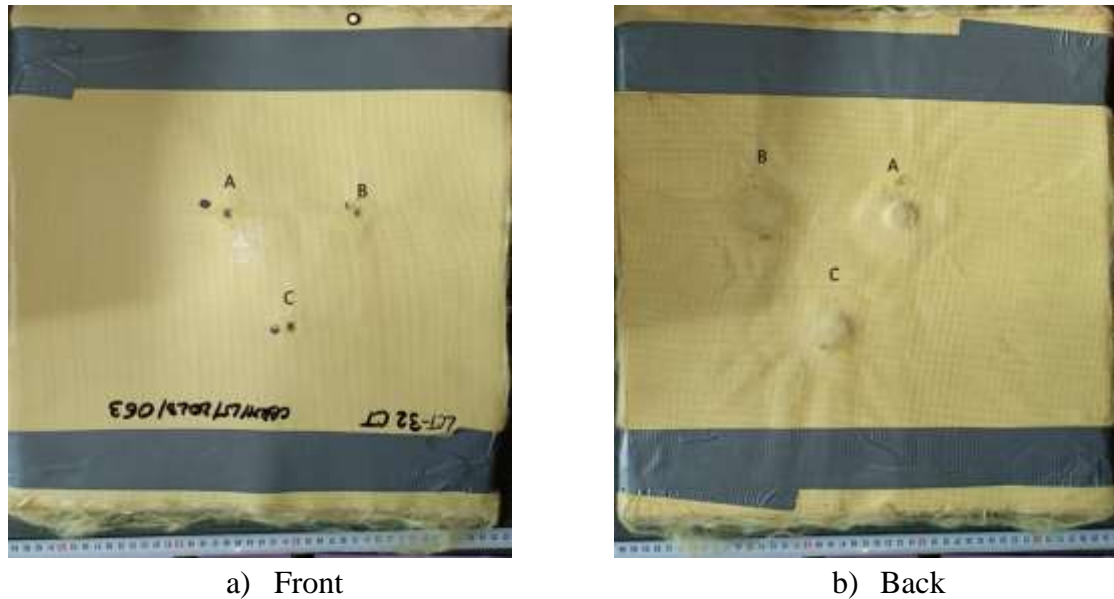


Figure 5.11. Twaron CT 736 32-layer fabric panel after being tested all fires producing partial penetration

Analysis of the fire A, on the 32-layer Twaron CT736 panel

Layer 1 (Figure 5.12) shows four partially broken yarns, the fibres that were not broken are pushed to the side. The polymer coating (PVB) is detached from the impact area and the area around the impact area. Layer 16 has one totally broken yarn and one partially broken yarn. The other main yarns are pushed to the side and have some broken fibres. The polymer coating (PVB) behaves similarly to that of layer 15. On the last layers, the polymer coating (PVB), cracks but does not peel off from the fabric coating.

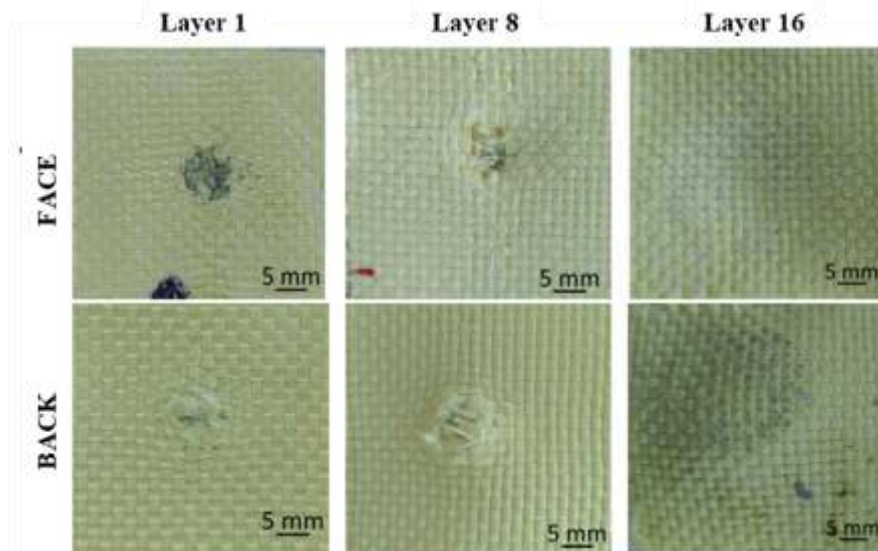


Figure 5.12. Details of fire A of the 32-layer Twaron CT 736 fabric panel

Analysis of the B- fire upon the 32-layer Twaron CT736 panel

Layer 1 (Figure 5.13) has one totally broken yarn and three partially broken yarns. The other main yarns have broken fibres. The polymer coating (PVB) is detached and jumps in the impact area and in the area around the destroyed area. Layer 16 shows eight stretched

and compressed yarns due to the impact force of the projectile. This phenomenon of stretched and compressed yarns highlights the complexity of the interaction between the projectile and the layered material. On the last 2 layers it can be seen how the polymer coating (PVB) cracks even though the projectile was stopped on layer 15. The layer deformation in the projectile direction is smaller than measure BFS.

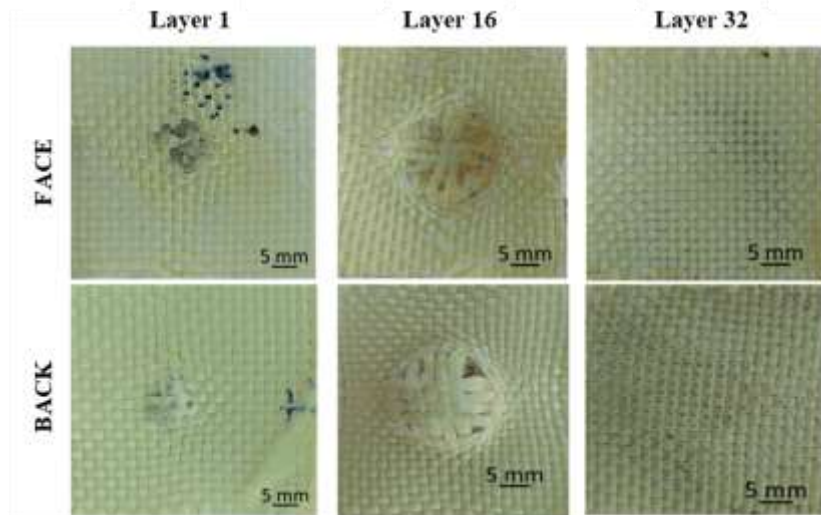


Figure 5.13. Details of fire B of the 32-layer Twaron CT 736 fabric panel (partial penetration)

Analysis of the C- fire on the 32-layer Twaron CT736 panel

Layer 1 (Figure 5.14) has the polymer coating (PVB) stripped from the fabric coating in and around the impact zone. This layer has four partially broken yarns and the other main yarns are pushed to the side showing several broken fibres.

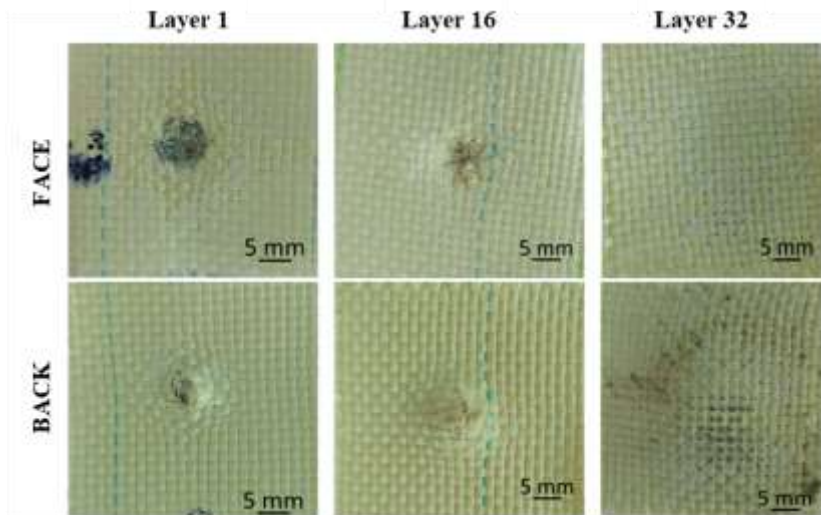


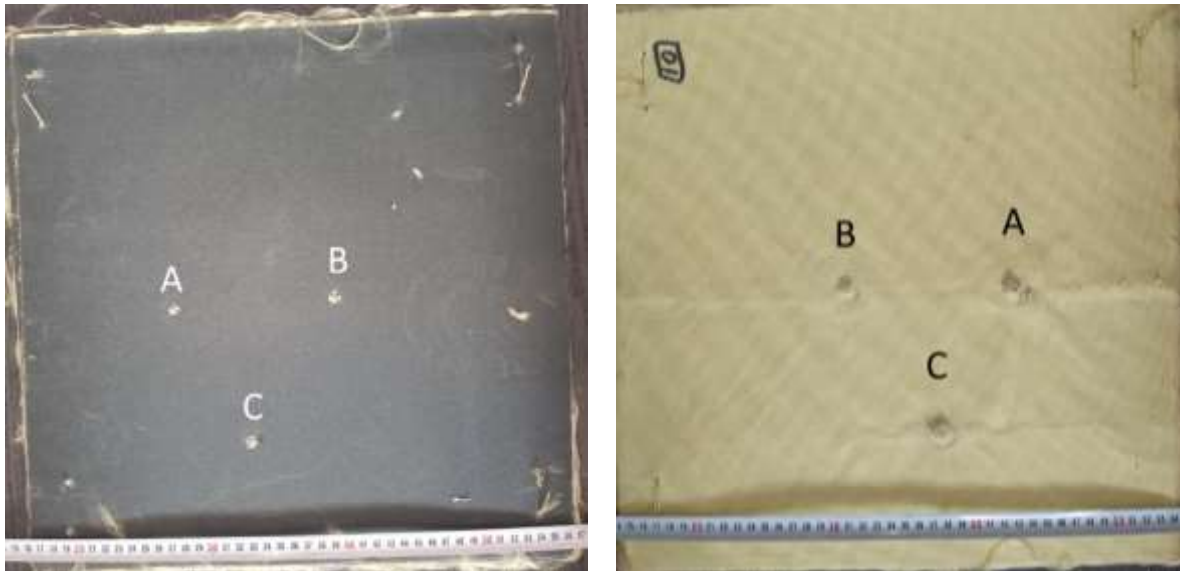
Figure 5.14. Details of the C-fire of the 32-layer Twaron CT 736 fabric panel (partial penetration)

Layer 16 (Figure 5.14) shows two totally broken yarns and two partially broken yarns. The polymer coating (PVB) shows cracking and delamination in and around the impact areas. The last layers, layers 31 and layer 32 show cracking of the PVB polymer coating due to the impact force of the projectile even though the projectile, was stopped on layer 20.

5.2.2.2 Analysis of the Three Fires on Combined Panels Twaron SRM509 Fabric and Twaron CT736 Fabric

Analysis of the three fires of the combined 16-layer panel with Twaron SRM509 fabric and Twaron CT736 fabric

The impact of the 9 mm FMJ projectile on the composed panel made of 16 layers of Twaron SRM509 fabric and 16 layers of Twaron CT736 fabric, subjected to three fires at different velocities, reveals distinct material reactions to different levels of kinetic energy (Figure 5.15). Fire A, with an initial velocity of 412.33 m/s, generated an impact that resulted in complete penetration of the panel. Fire B, with an initial velocity of 415.67 m/s, with increased the level of kinetic energy, transferred into the panel. This resulted in a similar total penetration as fire A. Fire C, with the highest initial velocity of 427.12 m/s, exerted maximum kinetic energy on the panel. The result was a total penetration similar to the other two fires. The conclusion is this panel does not offer protection against this threat (9 mm FMJ).



a) Front view

b) Back view

Figure 5.15. Hybrid panel with 16 layers of Twaron SRM509 fabric and 16 layers of Twaron CT736 fabric

Analysis of the 16-layer combined Twaron SRM509 and Twaron CT fabric panel - Fire A

Layer 1 (Figure 5.16) has eleven broken yarns, six in warp direction and five in the weft direction. The silicon carbide coating is only detached from the broken ends of the yarns and shows slight delamination aramid the impact area.

Layer 8 (made of SRM509 fabric, Figure 5.16) shows a larger area of destruction as compared to the other layers, even though the number of broken yarns did not increase. The weave layer shows twelve broken yarns, six in the warp direction and six in the weft direction. The silicon carbide coating is detached from the impact area and from the area around the impact, the broken fragments remained attached to the previous layer.

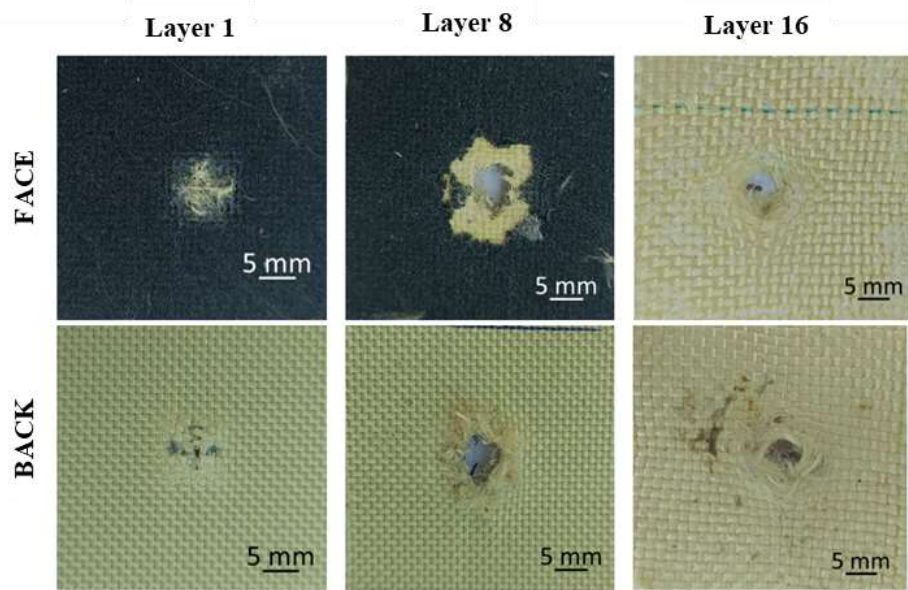


Figure 5.16. Fire A on the 16-layer combined Twaron SRM509 and Twaron CT 736 fabric panel

Layer 16, made of Twaron CT736, has four partially broken yarns. The other main yarns and the fibres not broken from the partially broken yarns are pushed to the side. The polymer coating (PVB) cracks and peels away from and around the impact area.

Analysis of the 16-layer combined Twaron SRM509 and Twaron CT fabric panel – Fire B

Layer 1 (Figure 5.17) has twelve broken yarns, six in the direction of the warp and six in the direction of the weft. The silicon carbide coating is detached and jumps out of the impact zone.

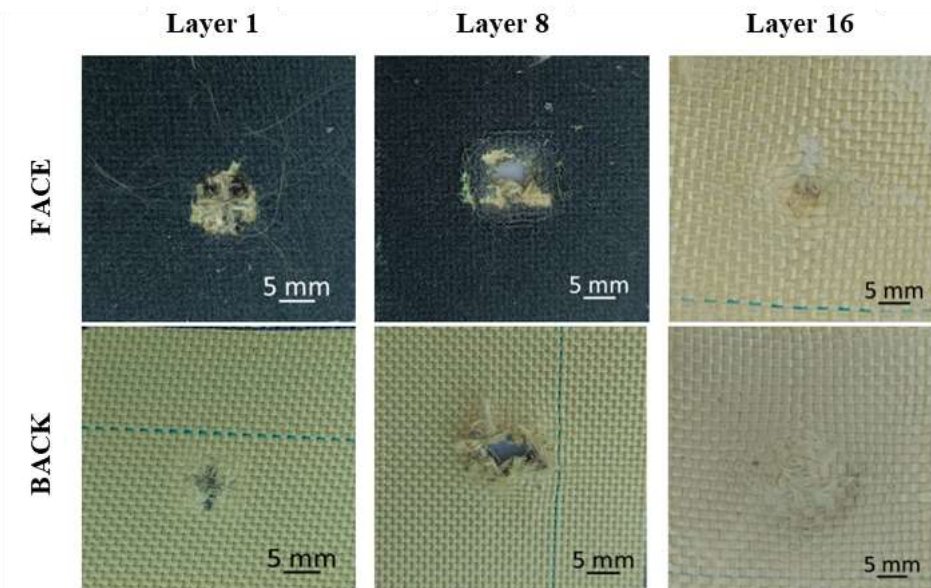


Figure 5.17. Fire B of the panel with 16 combined layers of Twaron SRM509 fabric and Twaron CT 736 fabric

Layer 8 shows a larger area of yarn destruction and a larger area of delamination and breakage of the silicon carbide coating. Some of the broken fragments remained trapped by the previous layer. The fabric coating shows eleven broken yarns, six in one direction and five in the other direction. Layer 16, which is the last layer, shows no total broken yarns. The polymer (PVB) PVB coating, is cracking and fragments are detaching from the impact area and around this area over a larger portion compared to the previous layers.

Analysis of the 16-layer combined Twaron SRM509 and Twaron CT736 fabric panel - Fire C

Layer 1 (Figure 5.18) has thirteen completely broken yarns, six in one direction and six in the other. The silicon carbide coating is detached from the broken ends of the yarns and shows slight delamination around the impact area.

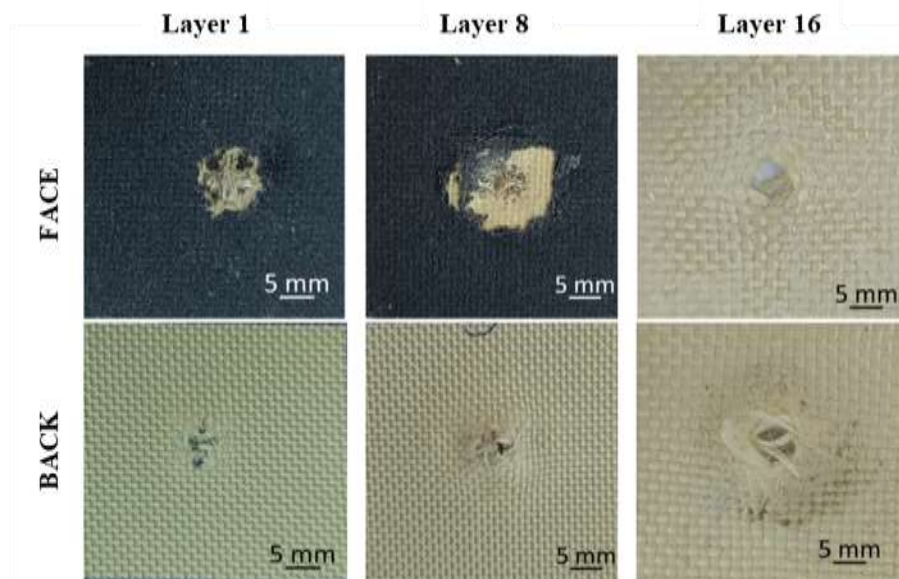


Figure 5.18. C-fire of the 16-layer panel combined Twaron SRM509 fabric and Twaron CT736 fabric

Layer 8 (Figure 5.18) shows nine total broken yarns, five in one direction and four in the other. There is also some sideways pushing of the yarns that were not broken hit not so evident as for the panel made only Twaron CT736. The silicon carbide coating is detached from the fabric coating, the broken fragments remained attached to the previous layer.

Layer 16 (Figure 5.18) does not show totally broken yarns, it shows partially broken yarns. The polymer coating (PVB) cracks are detached from the broken ends of the yarns and fragments a layer are detached from area around the impact as compared to the previous layer.

Analysis of the 40-layer combined Twaron SRM509 and Twaron CT736 panel - Fire A

Layer 1 (Figure 5.19) has twelve total broken yarns. The silicon carbide coating, applied on the first layer exfoliates on impact with the projectile, both in and around the impact area. On layer 6 of the panel, it can be seen that, in and around the impact area, the silicon carbide coating is detached from the fabric and wrinkled/folded. Layer 23 has four

completely broken yarns and four partially broken yarns. The polymer coating (PVB) is detached from the destroyed area and shows cracks in the area around the direct impact.

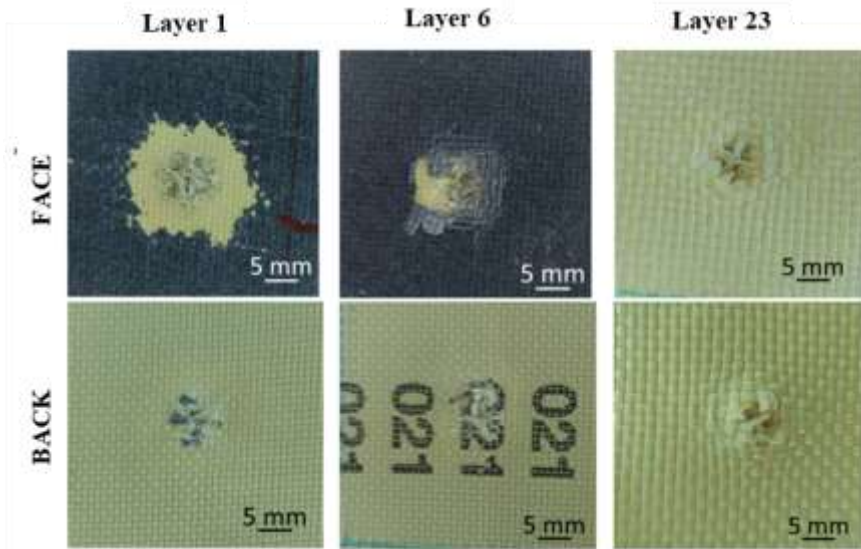


Figure 5.19. Fire A of the 40-layer combined Twaron SRM509 and Twaron CT 736 fabric panel

Analysis of the 40-layer combined Twaron SRM509 and Twaron CT 73 panel - Fire B

As the projectile advances through the panel, the destructive effect is amplified and affects the next layers to a greater extent. Due to the kinetic energy transferred by the projectile to the material, the projectile generates a propagation of damage across the depth and width of the structure. This process can be observed by the breaking, stretching or delamination of yarns, cracks or deformations present in the layers affected by the impact.

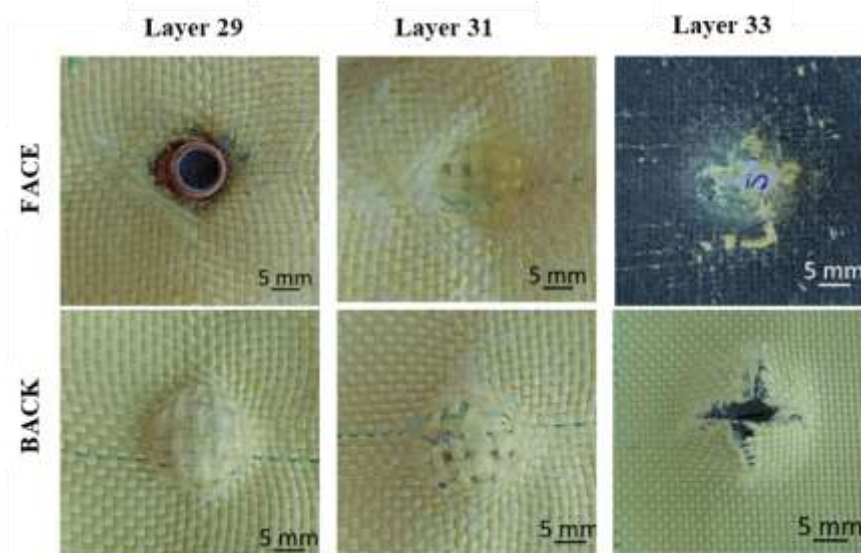


Figure 5.20. The hybrid panel fire B on with 40 combined layers of Twaron SRM509 fabric and Twaron CT736 fabric

The projectile stops on layer 29 hit pressure and deformation of the projectile were so high that Layer 29 and 30 were "stitched" by the projectile and these layers were not

detached from the projectile in order to keep their shape. Layer 29 and layer 30 (Figure 5.20) remained trapped by the projectile. The polymer coating (PVB) on layer 29 is detached over a larger area, only a few fragments remain. The yarns on layer 30 show yarns elongation of the fabric, suggesting that when being stopped the projectile is forced to lateral space and it pressed so hard the fabrics that yarns are "sticked" to the projectile jacket. This elongation is the result of the temporary deformation of the yarns under the pressure of the projectile moving at high velocity. These strong forces cause the yarns to stretch and bend without breaking them. The elongation of the yarns may indicate the ability of the material to momentarily absorb the high stresses generated during the impact.

Layer 31 (Figure 5.20) shows elongation of the yarns under the projectile, indicating that this layer contributed to the projectile stopping. The elongation of the yarns can be interpreted as a reaction to the forces and pressures exerted by the projectile during impact. This phenomenon indicates that layer 31 was able to absorb and redistribute the impact energy in a way that contributed to slowing or stopping the projectile.

The next 4 layers (including layer 33, in Figure 5.20) show broken yarns, meaning that these layers failed to absorb a significant part of the impact energy exerted on the material. This observation indicates that these layers did not have the ability to effectively dissipate or redistribute the energy of the projectile. Although the previous layers were able to stop or slow down the projectile's progress, these four subsequent layers could not perform the same energy absorbing function, resulting in the breakage of the yarns. Thus, this combined panel would not be recommended for an actual panel and neither the material SRM509.

Analysis of the 40-layer combined Twaron SRM509 and Twaron CT 736 panel - Fire C

Layer 1 shows 13 (Figure 5.21) completely broken yarns, six yarns in one direction and seven yarns in the other direction. The silicon carbide coating applied to this layer is detached from the impact area and from the area around the impact zone. This delamination is generated by the powerful impact of the projectile.

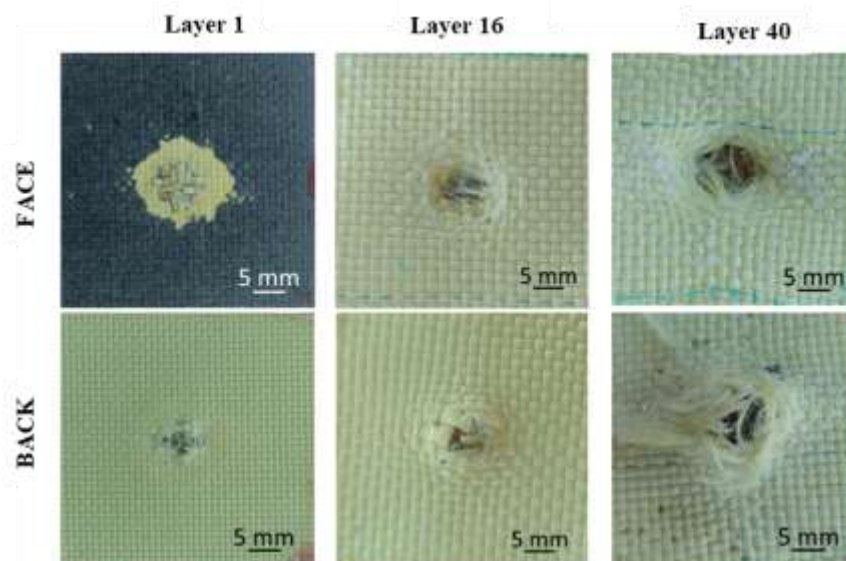


Figure 5.21. C-fire of the 40-layer combined Twaron SRM509 and Twaron CT 736 panel

Layer 16 shows two totally broken yarns and one partially broken yarn in the perpendicular direction. These yarns are broken by shearing with combined stretching. The polymer coating (PVB) is detached from the area of destruction and fragments are also detached and jumping to the area around the destroyed area on the attached.

I observe that the destruction of the next 4 layers, which are made of Twaron CT736 material, behaves similarly to the previous layers as the projectile advances and the destruction of the layers is more pronounced as compared to the panel made of only Twaron CT736.

5.2.3. Analysis of the Mechanism of Panel Failure on Impact Using SEM Images

5.2.3.1. Introduction

This subchapter discusses and explains how Twaron fabrics are destroyed at a multiple scales. This material is used in various protective systems, whose main requirement is a high level of penetration resistance against high kinetic energy projectiles. The high mass efficiency (i.e. mass normalised performance) of these materials makes them particularly suitable for use in applications, such as protective clothing.

5.2.3.2. Multiscale Material Analysis for Protection Systems

Continuous fibre reinforced polymer-matrix composites or fabrics under investigation are quite complex materials [Grujicic, 2016]. This complexity is given by:

- microstructure/hierarchical architecture/at different length scales,
- their mechanical response is often quite non-linear and depends on velocity, time, temperature, pressure,
- are associated with a multitude of complex phenomena/processes (e.g. filament twisting/buckling, interfilament friction, slippage and splitting).

A detailed examination of the intrinsic composition of this class of materials typically reveals the existence of eight well-defined microstructural length scales [Grujicic, 2016]. Schematics and explanations of these length scales, starting from the finest length scale (i.e., at the molecular chain level), are provided in Figure 5.22.

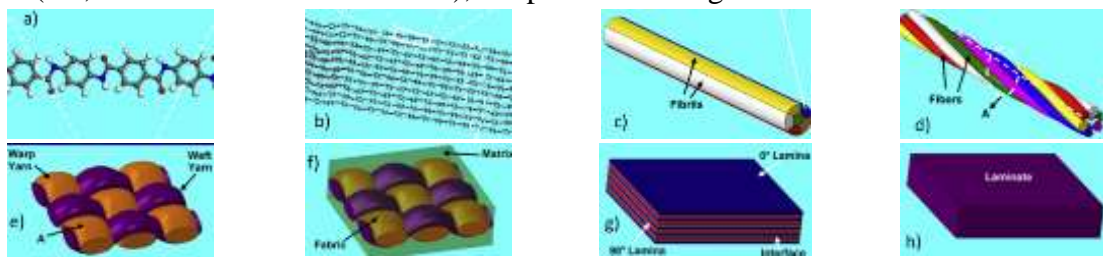


Figura 5.22. Simple schematic of material microstructure/architecture, at different length scales [Grujicic, 2016].

5.2.3.3. Structure and Morphology of Aramid Fibres

At the molecular chain length scale, the chemical structure and conformation of the individual molecules that constitute the chain of aramid fibers are analyzed using

atomic/molecular/process modeling tools [Grujicic, 2011b,c]. The material is modeled as a collection of constituent particles (atoms or ions) interacting via valence (chemical) and non-valence (physical) forces. The purpose of modelling materials at this scale is to identify the most likely molecular conformations present in fibrils. This greatly reduces the computational cost spent at fibril scale and make understandable the behaviour of the fibre.

Fibrils are smaller bundles of molecular chains, in which the chain molecules are tightly bound in a perfect or nearly perfect crystalline phase. Material at this length scale (as well as the fibril length scale) can contain a variety of microstructural and topological defects and chemical impurities that can significantly alter its properties (Grujicic et al., 2011b,c). Material at this scale is treated as a collection of discrete interacting/bonded particles and analyzed using classical atomic/molecular modeling tools/procedures. The information obtained at this scale is then passed to the fibre length scale, where it is used as input to a homogenisation procedure to determine the mechanical properties of the material at the fibre level.

To obtain high performance fibres, the following approach has to be taken into account in order to meet the requirements:

- highly oriented, but relatively low molecular weight, rigid chain and rod-like polymer, such as an aramid (lyotropic) or liquid crystal (thermotropic) polymer. It can then be spun into fibre and given a high molecular weight by drawing and/or annealing processes; aramid spinning is as an example of this approach,
- a long-chain, very high molecular weight, flexible, randomly bonded polymer such as very high molecular weight polyethylene (HMPE) [Tam, 2006].

When an aramid fibre is subjected to tensile load, its typical failure mode is generally dominated by fibrillation and stretching. [Tam, 2006].

5.2.3.4. Failure Analysis of the Tested Panels Based on SEM Images

In order to explain in a unified framework the damage observed with the scanning electron microscope, Figure 5.23 and Figure 5.24 show synthetically, characteristic failure mechanisms of ballistic impact on fabric panels.

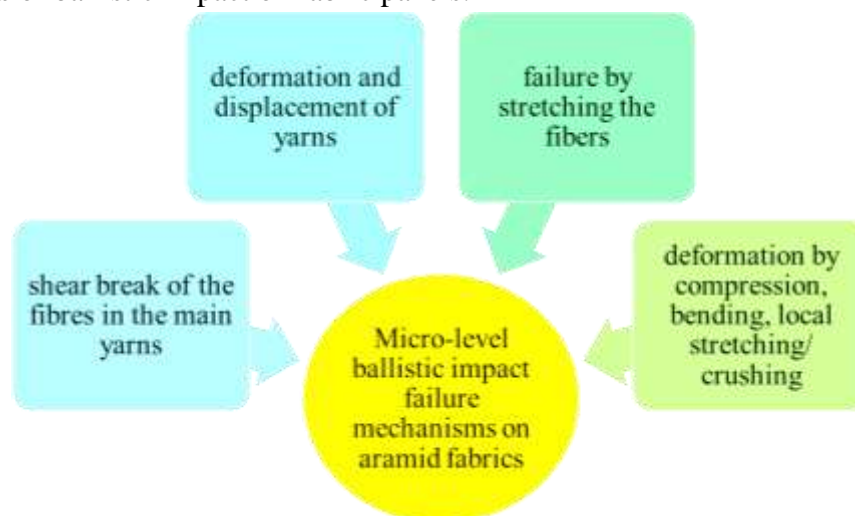


Figure 5.23. Micro-level failure mechanisms at ballistic impact on aramid fabrics

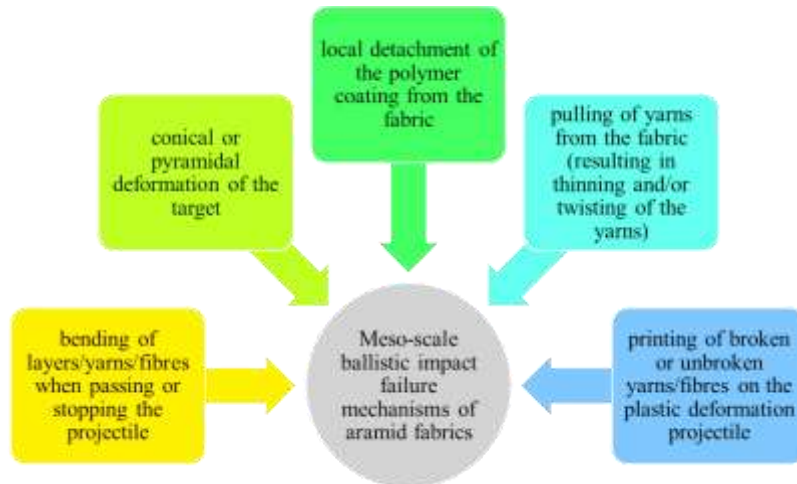


Figure 5.24. Meso-scale failure mechanisms at ballistic impact on aramid fabrics

I performed microscopic examinations of the damaged samples, using scanning electron microscopy (SEM). Figure 5.25 a and b show the penetration results of the front side of the first layer of the panel consisting of 32 layers of Twaron CT736 fabric. It was noted on Figure 5.25 a) with letter A and letter B the yarns that have completely broken and with letter a, b and c pieces/fragments from the polymer coating. In Figure 5.23 b) a detail is given to see the mode of fibre breakage which is fibrillated.

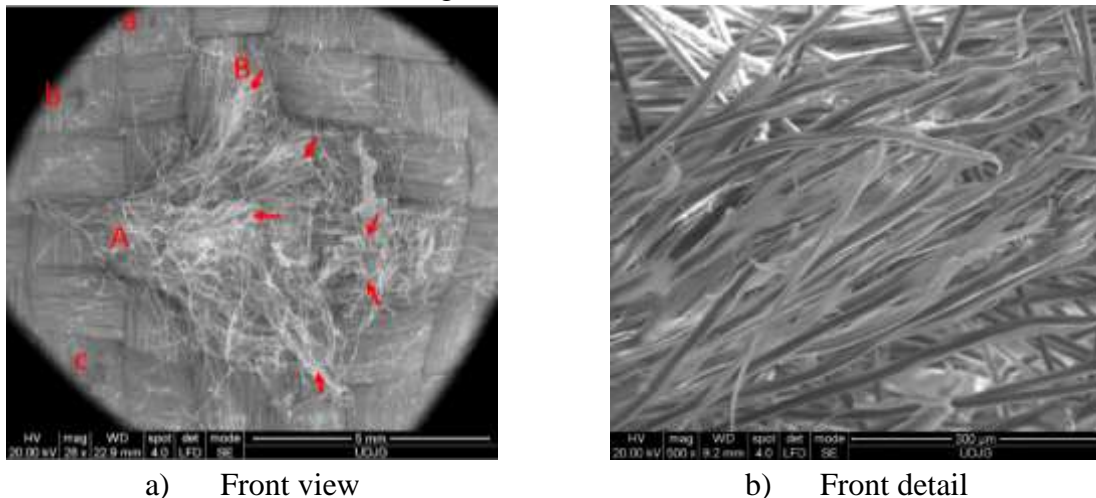
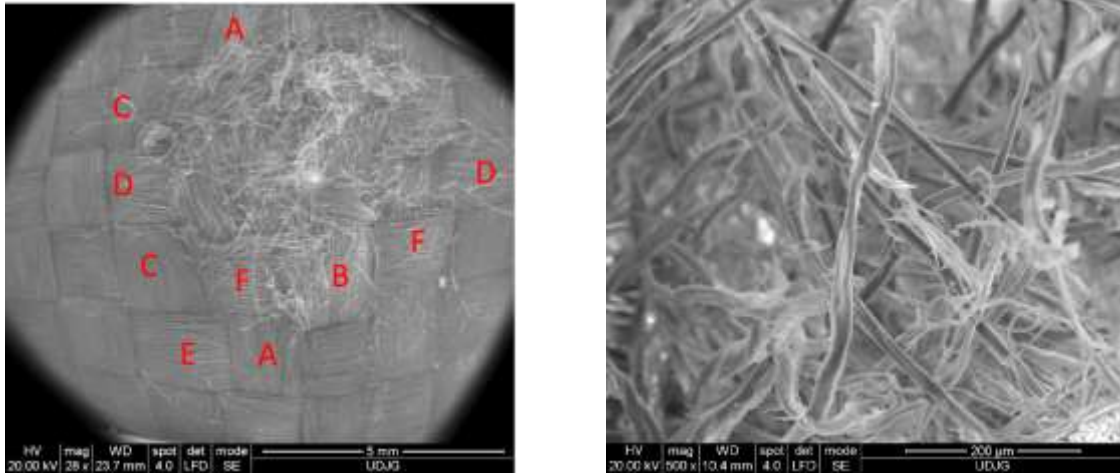


Figure 5.25. Front view - Twaron CT736 32-layer panel, layer 1, yarn failure mode.

Figure 5.26 a and b show the back view of the destruction of the first layer of the panel consisting of 32 layers of Twaron CT736 fabric. In Figure 5.26a, with letter D and letter B the yarns that have been completely broken are coded and with letter A and C, partially broken yarns, with E and F, yarns pushed to the side with the presence of some broken fibres. In Figure 5.26b a detail is given to see the mode of fibre breakage, which is of fibrillated type.

Figure 5.23b and Figure 5.26b show a fibrillated type of fiber breakage, breakage due to tensile stress, as their highly ordered fiber structure leads to a fibrillated type of breakage, in which the fibers break along axial lines, revealing their internal fibril structure

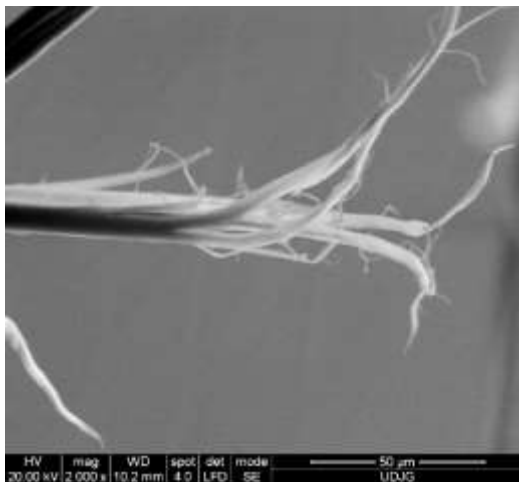
in the outer layer. This unique behaviour is a result of the molecular arrangement of the fibre and contributes to the exceptional mechanical properties of aramid fibres.



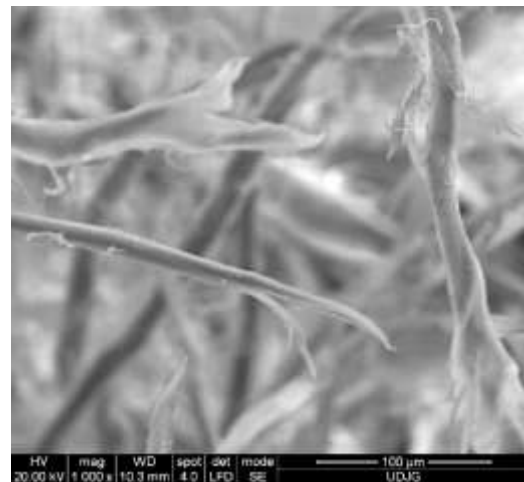
a) back

b) rear detail

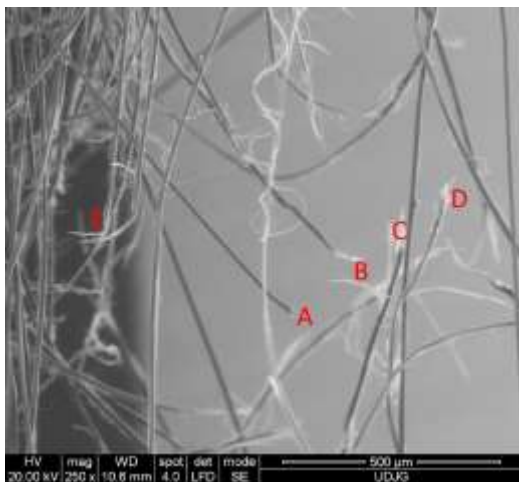
Figure 5.26. Back of layer 1 from the Twaron CT736 32-layer panel's modes of fibre failure



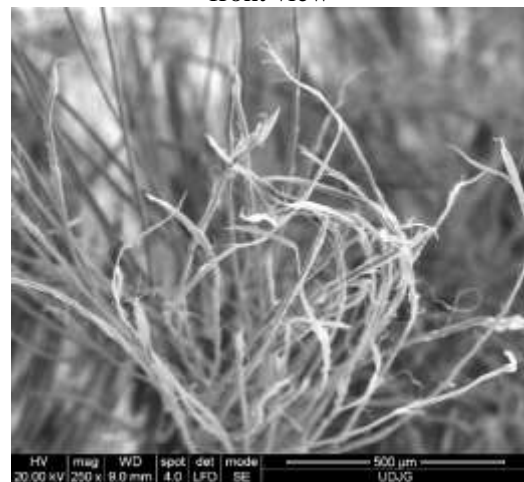
a) 32 layers Twaron CT736, fire B, layer 2, front view



b) 32 layers Twaron CT736, fire B, layer 1, front view



c) 32 layers Twaron CT736, fire B, layer 2, front view



d) 32 layers Twaron CT736, fire B, layer 13, front view

Figure 5.27. Fibrillation of aramid fibres, after ballistic impact test

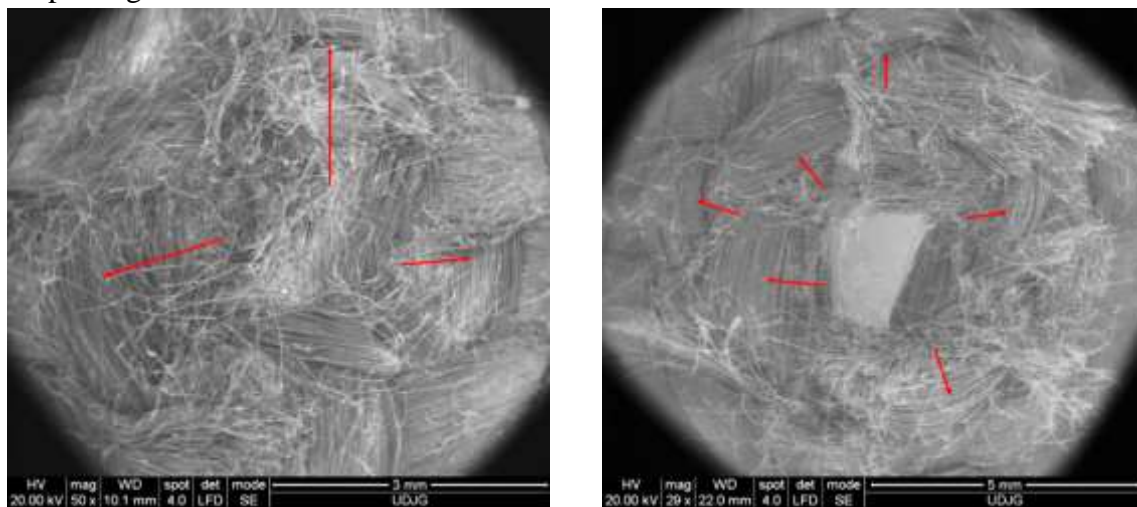
Figure 5.27a presents a fibre from a main yarn (i.e. from a yarn directly broken by the projectile and it can be seen that the stress caused the fibrils to detach from each other and then they are successively broken by stretching. Some ends of the fibrils are twisted and with large local stretch strain. All these indicates a stretch rupture. In detail from layer 1 of the 32-layer panel (Figure 5.27b), three fibres are seen to have been failed by different mechanisms, the top yarn is broken by shearing and crushing, the almost vertical right-hand yarn is twisted, stretched, with some fibrils broken, and the bottom fibre is fibrillated in the zone of breakage and other fibres are broken by stretching. On the left side, beyond the fibrillation, the fibre is locally gargled, also due to stretching stress.

In Figure 5.27c presents broken fibres at the edge of the penetration orifice. Looking at the micro level, it is difficult to imagine what happens on a larger scale, but studying the failure mechanisms at the fibre level makes it possible to select the appropriate fibres for a given application. A - sheared fibre (it is observed that the fibre diameter is not modified), B - several fibrils in a fibre have been stretched a lot and have broken one by one, C - fibre broken by stretching with locally thinned end, typical for polymers and a little further on a local twist is seen, D - fibre is broken by shearing, E - two fibres broken by stretching and fibrillation is observed.

What was observed in Figure 5.27c on layer 2 can also be seen on the broken fibres on layer 13 (Figure 5.27d); braking by sketching of the fibres.

Figure 5.28 shows SEM micrographs of the failed surface of distinct samples, after ballistic testing. Figure 5.28a shows that there was displacement to the side of the fibres during the impact. This is probably due to the lower friction between the projectile and the target. As a result, the portion of the fibres hit by the projectile was smaller and consequently there was less energy absorption by the panel.

In Figure 5.28b, it can be seen that there was fibrillation along the axis of the aramid fibres due to the existence of a gradient of properties inherent to the manufacturing process. This mechanism due to the fibre stretching and breaking of smaller fibril process is known as 'peeling'.



a) Layer 1, back

b) Layer 2, back

Figure 5.28. SEM photographs of the failed surface of layer 1 and 2, after ballistic test of Twaron CT736 fabric panel (9 FMJ, $v_0 = 428,07$ m/s).

Figure 5.29 and 5.30 show that some fibres exhibit longitudinal striations on the axial direction. This is the initial appearance under high tensile stress. Such longitudinal striations may develop more pronounced to form axial fissure, with increasing strain, as shown in Figure 5.31- 5.32, also named fibrillation (as the fibre become visible as a brinch of smaller fibres-fibrile). In some situations, axial fissure proliferates in many fibrils. Such destruction morphologies was the dominant mode of failure of Twaron fibers under impact, which was commonly observed around the perforated hole on the impacted panel.

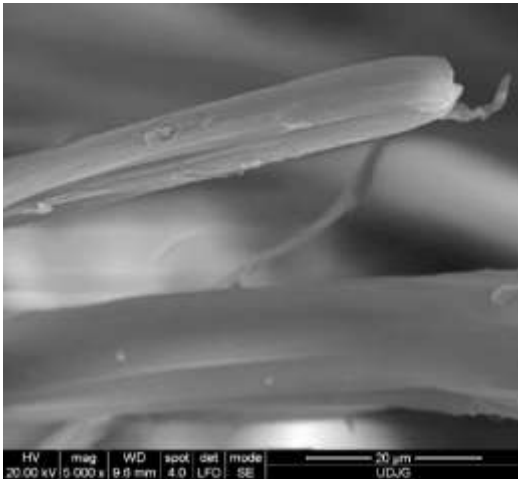


Figure 5.29. Longitudinal split (fibrillation) on a fibre, Twaron SRM509 fabric, layer 2, front view

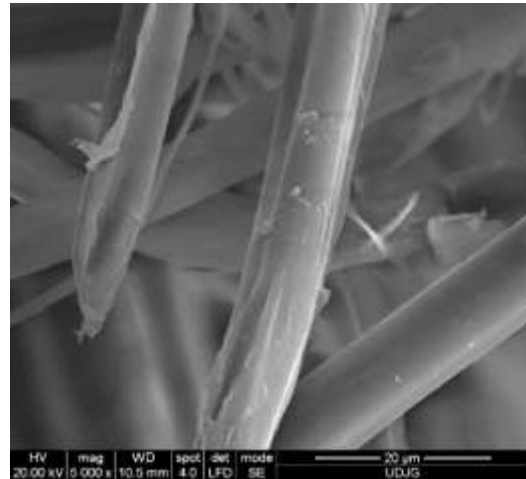


Figure 5.30. Longitudinal split on a fibre surface, Twaron SRM509 fabric, layer 2, front view

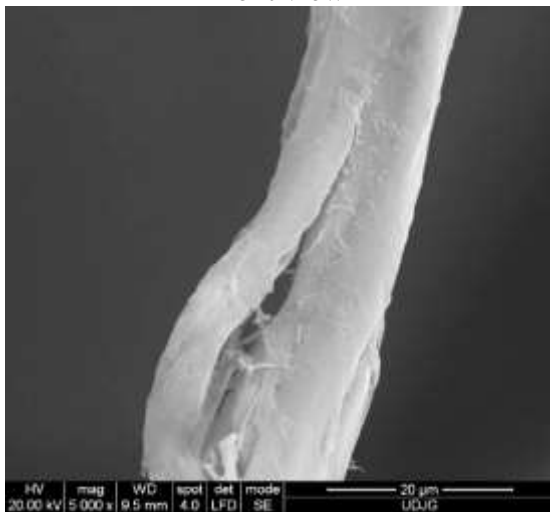


Figure 5.31. Axial split (fibrillation), on a fibre of Twaron CT736 fabric, layer 14, front view

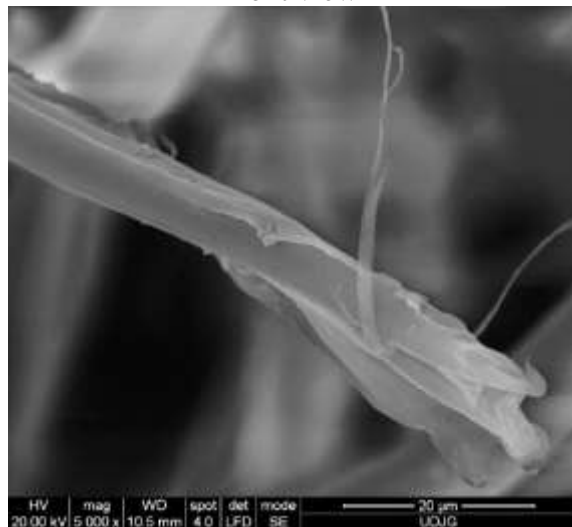


Figure 5.32. Axial fissure, Twaron SRM509 fabric, layer 1, front view

5.3. Final conclusions on the test campaign

The panels that showed partial penetration (all three shots partially penetrated the panel) are

- the panel with of 32 layers of Twaron CT 736 fabric;
- the panel with of 42 layers of Twaron CT 736 fabric.

The diagrams in Figures 5.33-5.34 show BFS values that support the use of CT736 material to make panels that are tested to current Level IIA standards. Thus, the proposed study proves useful for preliminary evaluation of this type of woven semi-finished material for ballistic vests.

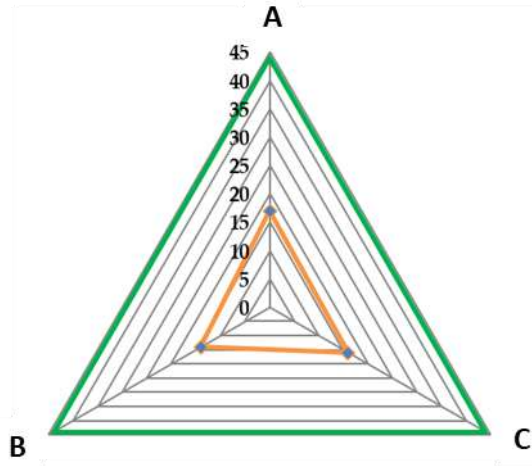


Figure 5.33. BFS values for the 32-layer Twaron CT736 fabric panel

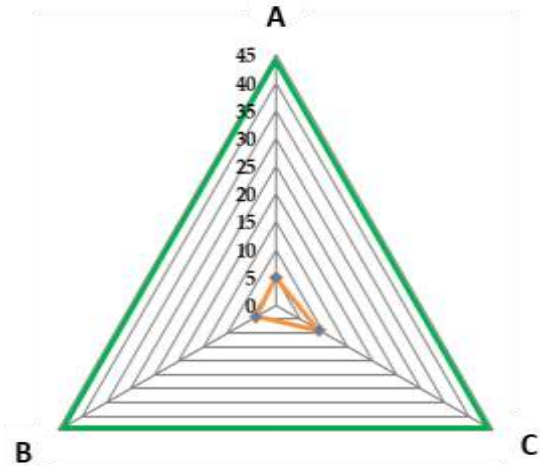


Figure 5.34. BFS values for the 42-layer Twaron CT736 fabric panel

The 16-layer Twaron CT736 fabric panel has full penetration for all three fires. The 16-layer combined Twaron SRM509 and Twaron CT736 fabric panel has also full penetration for all three fires. The mode of yarn breakage is different, the Twaron CT736 fabric yarns are pushed sideways by the projectile and are broken one, two, maximum three yarns per layer (shows a stretch break), Twaron SRM509 fabric shows no sideways pushed yarns, all yarns are totally broken, up to 13, 14 yarns broken (Figure 5.35 and Figure 5.36).



Figure 5.35. Detail of layer 1 (Twaron CT736 fabric), Fire A, of the 16-layer Twaron CT736 fabric panel, front view



Figure 5.36. Detail of layer 1 (Twaron SRM509), Fire A, of the 16-layer combined Twaron SRM509 panel, back view

The final layer of the 16-layer Twaron SRM509 and Twaron CT736 combined panel is made of Twaron CT736 fabric. I observed that, in this case the last layer of the two 16-layer panels of Twaron CT736 fabric and the 16 combined layers of Twaron SRM509 fabric and CT736 fabric, which behave similarly, are pulled the main yarns of the fabric by the projectile (Figure 5.37 and Figure 5.38).

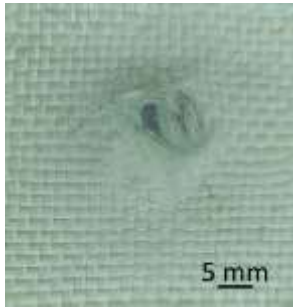


Figure 5.37. Detail of layer 16, fire C, of the 16-layer Twaron CT736 fabric panel, back view

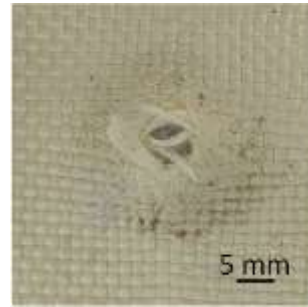


Figure 5.38. Detail of layer 16 (Twaron CT736 fabric), Fire C, of the 16-layer hybrid panel, back view

The 32-layer Twaron CT736 fabric panel has partial penetration for all three fires. The 32-layer Twaron SRM509 hybrid fabric panel with Twaron CT736 fabric has full penetration for all three fires. The yarn count of the first layer of the hybrid fabric panel shows a much higher number of broken yarns as compared to layer 1 of the Twaron CT736 fabric panel, which has four partially broken yarns, the fibres that have not been broken are pushed to the side (Figure 5.39 and Figure 5.40). Layer 1 of the Twaron CT736 fabric panel shows yarns pushed to the side, indicating that the yarns are more flexible. Layer 1 of the hybrid fabric panel has no yarns pushed to the side, they are broken.



Figure 5.39. Detail of layer 1 (Twaron CT fabric), Fire A, of the 32-layer Twaron CT736 fabric panel, back view



Figure 5.40. Detail of layer 1 (Twaron SRM509 fabric), Fire A, of the 32-layer hybrid panel, back view

The mode of yarn failure on the last layer of the 32-layer combined Twaron SRM509 fabric and Twaron CT736 fabric panel is similar, the main yarns are pulled by the projectile, but as the the projectile is slopping, it is forced to floten and the improve in last layers when the projectile is sloppinds is greats the deformation area is larger (Figure 5.41).

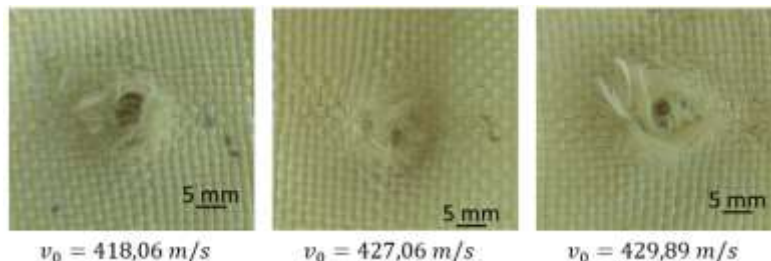


Figure 5.41. Front view of the last layer of the 32-layer combined Twaron SRM509 and Twaron CT736 fabric panel for all three fires

The yarns are pushed to the side when the impact velocity is lower, as the velocity increases, the yarns are broken. At lower impact velocities, the material resists the impact

forces and the yarns are pushed sideways, causing local deformation, as the impact velocity increases, the forces become more intense and may exceed the ability of the material to resist (Figure 5.42). The higher the impact velocity, the higher the stress and strain levels generated by the impact. This leads to yarns breaking instead of just being pushed sideways or locally deformed. The pressure generated by the impact at high velocity causes higher stresses in the material structure. Because of this intense projectile pressure and the high level of kinetic energy, the material breaks and allows the wires to break.

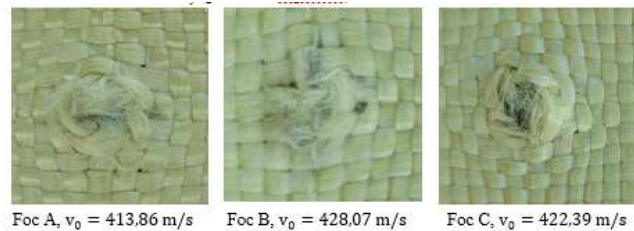


Figure 5.42. Back view of the first layer of the 32-layer Twaron CT736 fabric panel, for all three fires

The panel with 42 combined layers of Twaron SRM509 fabric and Twaron CT736 fabric behaves differently, the projectile is stopped on layer 29 (Twaron CT736 fabric), layer 29 and layer 30 attached by the projectile (Figure 5.43). This suggests that these layers were able to absorb and distribute the impact pressure, but suffered significant deformation. Layer 29 and layer 30 are Twaron CT736 fabric and show compression and stretching of the main yarns. Layer 32, which is also of Twaron CT736 fabric, is broken, even showing significant destruction, with a higher yarn count. The next 4 layers, which are Twaron SRM509 fabric are broken, showing a larger area of yarn destruction/breakage caused by compression of the previous plies. This indicates how the previous layers influenced the behaviour of the subsequent ones and led to a distribution of mechanical loading. Layer 37 is not broken, this layer and the next three are made of Twaron CT736 fabric. The silicon carbide coating did not allow the yarns to stretch, resulting in the breakage of the layers under the projectile.

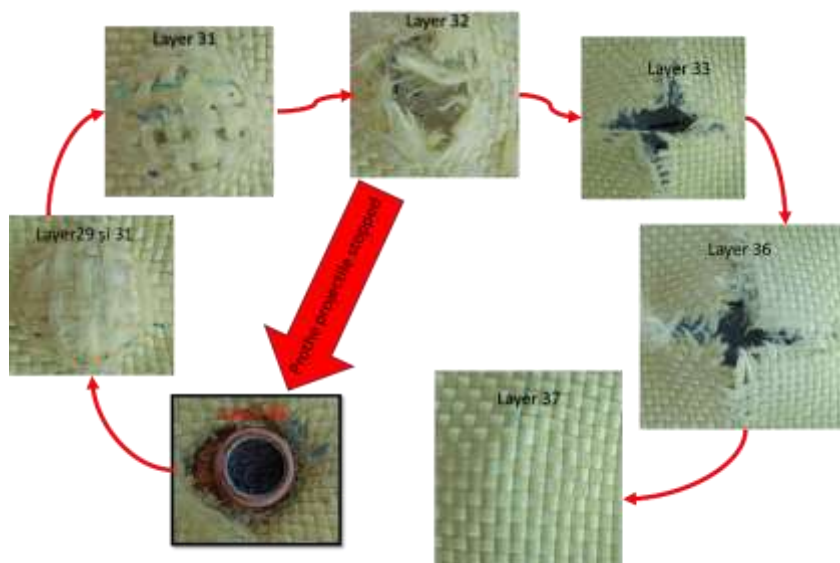


Figure 5.43. Twaron SRM509 and Twaron CT736 40-layer hybrid panel failure mode

Chapter 6

FINAL CONCLUSIONS ON NUMERICAL AND EXPERIMENTAL RESULTS

6.1. Importance of the Research Topic

Protection against high velocity projectiles is one of the critical requirements for various structural components. High velocity impact can lead to penetration/perforation of the target by the projectile. Ballistic impact is a high velocity impact caused by a propulsion source, generally of low mass and high velocity. Protection against ballistic impact charges is a critical issue in the design of ballistic armour, shock absorbers and in the development of high-quality aerospace, marine, automotive and civil structures. In recent years, extensive research has been conducted on the ballistic impact performance of polymeric composites. Various parameters, such as mass, shape and size, projectile velocity and geometry and mechanical properties of the target, influence the ballistic impact performance of composite structures.

Based on the phenomenon of energy transfer between projectile and target, energy dissipation and failure mechanisms, the impact is classified into three categories: low velocity impact, high velocity impact and very high velocity impact.

The reason for this classification is that the energy transfer between the projectile and the target, the energy dissipation and the failure mechanisms in the target undergo drastic changes as the velocity of the projectile changes. An impact event is considered to be a low-velocity impact if the contact duration of the impact is longer than the time period of the lowest vibration mode of the structure. On the other hand, in a high velocity or ballistic impact, the contact duration of the impact is much shorter than the time period of the lowest vibration mode of the structure. Very high velocity impact involves projectiles travelling at extremely high velocities, so that the target materials behave like fluids.

Protection against high-velocity projectiles is one of the critical requirements. Extensive research is being carried out on the ballistic impact behaviour of polymeric composites. In many aerospace and defence applications, composite structures can be subjected to localised projectile impact. Such impacts could lead to indentation, partial penetration or perforation of the composite target, depending on the projectile mass, velocity and shape. To ensure the safety of composite structures against penetration/perforation by high velocity projectiles, a clear and complete understanding of the penetration and perforation process in composites is essential. Protection against ballistic impact loads is a critical issue in the design of ballistic armour, shock absorbers and in the development of high-quality aerospace, marine, automotive and civil structures. Events of impact loading on aerospace and defence structures include bird strikes, hail, fugitive debris impact, small and medium caliber bullets and blast fragments.

The main objective of this thesis entitled "Numerical and Experimental Study for Ballistic Protection Systems with Aramid fibre fabrics", is to improve the ballistic impact resistance of personal protection systems.

The specific objectives are as follows:

- a) analysis of the impact effectiveness of a particular type of high-performance fabric,
- b) investigating hybrid armour design strategy using coated high-performance fabrics,
- c) the use of 3D scanning for measuring the print depth in the backing material for a single projectile (level IIA) tests on protective panels,
- d) development of a meso-level (yarn-level) numerical model that validates the experimental tests and may be useful within a range of variable parameters, such as number of fabric layers, projectile type and impact velocity.

6.2. Final Conclusions of the Thesis

Table 6.1 gives the ballistic test results for the personal protection samples, impacted by the 9 mm Full Metal Jacket (FMJ) projectile studied in this paper.

Back Face Signature (BFS), also called Back Face Deformation (BFD), is a measure of how much the material of the personal protective system deforms when struck by a ballistic threat (in this case a 9mm FMJ projectile). It is a key measure in assessing the safety of the protective system because it determines the level of blunt trauma or injury a wearer may suffer, even if the projectile is stopped from penetrating the protective system. A shallower rear face depth indicates a lower risk of injury because it means that less force is transmitted through the armour to the wearer's body on impact.

The depth BFS in the backing material is usually measured in millimetres and is an essential parameter in body armour testing and certification. Essentially, while ballistic performance assesses the armor's ability to stop projectiles and prevent penetration, the back face signature measures the extent to which the armor reduces impact on the wearer's body. Reducing the back face signature is important to minimize trauma or injury even when the armour successfully stops a projectile. Both aspects are important in the design and evaluation of soft armour panels to ensure that they provide protection against ballistic threats, but also provide a level of comfort and safety for the wearer by limiting energy transfer to the body on impact. The results obtained for the BFS in the backing material for the two Twaron CT736 fabric panels is given in Table 6.1.

One widely used standard is that of the US National Institute of Justice (NIJ). Since its first introduction in 2000, it has been applied by many countries around the world. In this standard, performance requirements and test method for the protection of the human body against ballistic impact are listed. The backing material used is Roma 1 plasticine, also called ballistic plasteline.

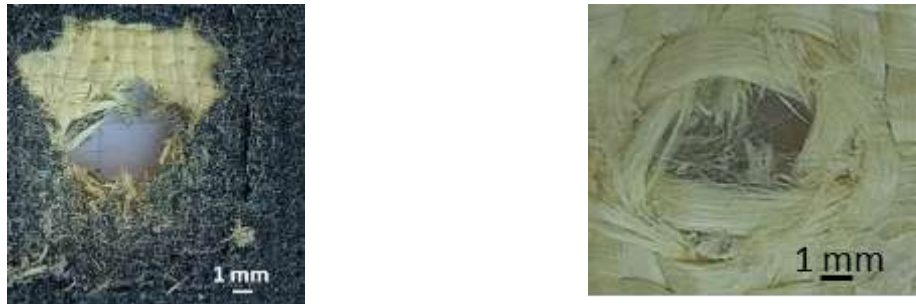
Tabel 6.1. Summary of ballistic test results for panels impacted by the 9 mm Full Metal Jacket (FMJ) projectile

Panel	Fire	Speed [m/s]	Back face signature (BFS) [mm]	Volume of the back face signature [mm] ³
16 layers Twaron CT736 fabric	A	410.26	PT	-
	B	414.45	PT	-
	C	422.98	PT	-
24 layers Twaron CT736 fabric	A	422.97	PT	-
	B	424.41	PT	-
	C	415.03	23	26076
28 layers Twaron CT736 fabric	A	425.55	PT	-
	B	417.46	25	23428
	C	408.51	28	27459
32 layers Twaron CT736 fabric	A	413.86	14	17472
	B	428.07	17	19872
	C	422.39	16	12134
42 layers Twaron CT736 fabric	A	426.93	9	3555
	B	410.51	4	10534
	C	417.46	5	1554
16 combined layers of Twaron SRM509 and Twaron CT736	A	412.33	PT	-
	B	415.67	PT	-
	C	427.12	PT	-
24 combined layers of Twaron SRM509 and Twaron CT736	A	434.07	PT	-
	B	422.78	PT	--
	C	411.01	PT	-
28 combined layers of Twaron SRM509 and Twaron CT736	A	429.93	PT	-
	B	417.51	PT	-
	C	413.91	PT	-
32 combined layers of Twaron SRM509 and Twaron CT736	A	418.06	PT	-
	B	427.94	PT	-
	C	429.89	PT	-
42 combined layers of Twaron SRM509 and Twaron CT736	A	411.45	14	9411
	B	416.08	17	13566
	C	421.76	PT	-

The 16-layer, 24-layer, 28-layer and 32-layer hybrid panels show full penetration for all three fires.

The failure mode of Twaron SRM509 yarns is different from that of Twaron CT736 yarns. The Twaron CT736 fabric yarns during impact are pushed to the side, not completely broken, some of the fibres are broken, whereas in the Twaron SRM509 fabric layer, the yarns are completely broken, not pushed to the side during impact (Figure 6.1).

Fibre failure is similar for all tests in Twaron CT736 layered panel and differentiation was more useful using macro detail photos of the fibres on each layer, as well as on hybrid samples.



a) Hybrid panel, 24 layers

b) 24 layers of Twaron CT736 fabric

Figure 6.1. Difference in appearance between Twaron SRM509 and Twaron CT736 hybrid panels and Twaron CT736 panel

The 40-layer hybrid panel shows two partial penetration shots, one projectile stopped on layer 29 and one projectile is trapped in layers 29 to 31 (Figure 6.2). Main yarns play an important role in preventing projectile breakage or penetration of the material layer. They contribute to the deformation and energy absorption of the projectile, thus reducing the risk of injury caused by the fire. The quality and strength of the main yarns are important characteristics for the performance of the material in terms of ballistic protection.

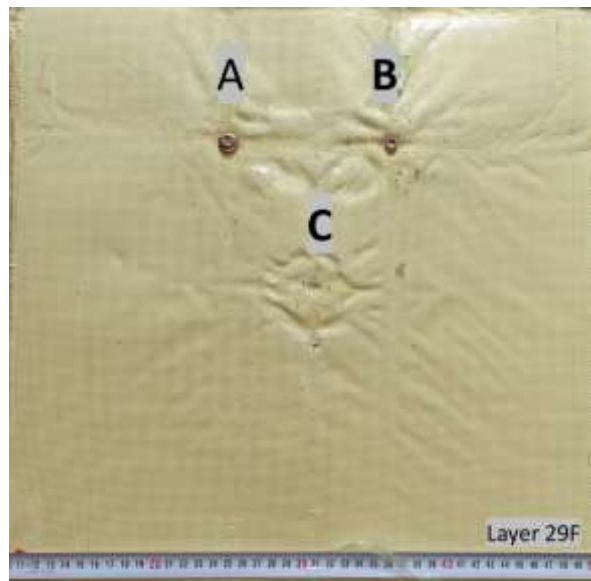


Figure 6.2. 42-layer hybrid panel, layer 29, front

Samples made of Twaron CT736 laminated fabric showed different results. One panel had full penetration, the 16-layer panel, one panel showed 2 shots with full penetration, the 24-layer panel, one panel showed one shot with full penetration, the 28-layer panel and two shots showed partial penetration, the 32-layer panel and the 42-layer panel showed partial penetration, with a different number of destroyed layers.

The fabric layers of the two types of tested panels, a hybrid of Twaron SRM509 and Twaron CT736 combined fabrics and Twaron CT736 fabric plies, show different results in terms of how the yarns were destroyed when the projectile was stopped. In the case of the hybrid panel, even if the projectile was stopped, the following layers were broken/failed. The silicon carbide coating applied to the fabric does not allow for the yarns being elastic, to stretch, as is the case with Twaron CT736 fabric panels.

Energy dissipated and absorbed during ballistic impact are key factors in assessing the effectiveness of a protective material. The main yarns in the fabric play an important role in distributing and absorbing this energy (Figure 6.3), helping to prevent penetration of the projectile and protecting people or objects behind the protective systems (using 3D profilometry I have highlighted the role of the main yarns in absorbing the kinetic energy of the projectile). Figure 6.3 shows how the main yarns were stressed to prevent the material layers from breaking.

By warping and stretching, the main yarns convert the projectile's kinetic energy into mechanical energy and heat, thus reducing the projectile's power and velocity.

Shear and tensile failure models demonstrate the importance of understanding how stresses act on these materials. The development of manufacturing and design techniques that take these patterns into account can help to increase the performance of materials in impact protection design.

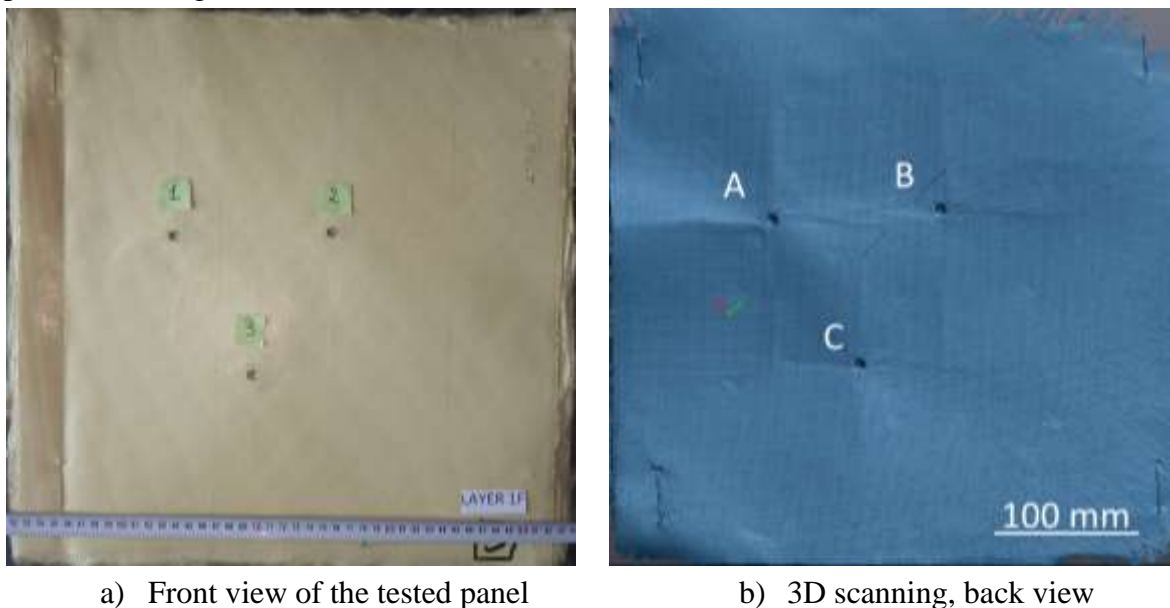


Figure 6.3. Role of the main yarns in the ballistic impact process of the 16-layer panel with three, 9 mm FMJ projectiles

The different responses, depending on the depth of layering, highlight the importance of layer configuration in composite design. This can affect how impact energies are dispersed and absorbed, ultimately having a significant impact on material performance.

The velocity of the 9 mm FMJ projectile influences how the yarns, polymer coating (PVB) and silicon carbide coating are failure. Depending on the impact velocity, some yarns

may be completely or partially broken, while others may be significantly deformed or pushed to the side. The silicon carbide and PVB resin substrates show delamination from the fabric in the impact area. Poor adhesion between the substrates and the fabric can lead to debonding and the formation of fragments that can affect the structure of the material.

This observation underlines the fact that the choice of appropriate design of ballistic panels plays a key role in achieving the desired performance in impact protection. Twaron CT736 fabric has demonstrated excellent properties in terms of strength and ability to absorb impact energy, which has allowed this portion of the panel to remain intact and prevent yarn breakage. This is particularly important in the context of ballistic threat protection, where each component of the panel contributes to the overall effectiveness of the protection provided.

It should also be outlined that this result reflects not only the qualities of the used materials, but also the design and structure of the ballistic panel. The optimal combination of different layers, depending on their individual properties, can provide effective protection against various types of threats.

The conclusion here is that without laboratory testing one cannot assess the quality and protection of a panel, no matter how good the materials for other protections are. This is very important.

One conclusion is that the hybridization did not give in this case the expected results, although the abrasive coating gives good stabbing and puncture results, considering the results obtained by the colleague [Totolici,2023] in stabbing and puncture tests.

Another conclusion of my study is that the more realistic fabric model is, more helpful in developing, virtual solutions, which can then be “translated” into practice, at lower cost and most likely with better results.

6.3. Personal Contributions

Through the investigations I have carried out and presented in this paper, and by using a synergistic approach of the subject, which focuses on the comparative analysis of data obtained from simulation and those from real experiments, I have generated multiple original contributions in the field of interest.

The main contributions of this thesis can be summarised as follows:

1. systematic and critical analysis of relevant documentation for theoretical and experimental investigation,
2. systematisation of a rich bibliographic material, focusing on the characteristics of ballistic materials and their performance (this bibliographic material covers a wide range of information on the use of ballistic materials over time in the production of personal ballistic protection equipment, ballistic research methods),
3. designing a meso-level numerical model (from yarns woven exactly as in the real fabric) and analysing the simulations from the perspective of the influence of important parameters for a realistic simulation, validation and use of the model to limit the test campaign, which is very expensive:

- a. influence of some parameters of the material constitutive model, the breaking limit, at break of the aramid yarns, considering $\sigma_r = 2000 \text{ MPa}$, $\sigma_r = 2500 \text{ MPa}$, $\sigma_r = 3000 \text{ MPa}$, $\sigma_r = 3600 \text{ MPa}$,
 - b. the influence of introducing friction in the projectile-target impact model,
 - c. influence of sample size in numerical simulation,
4. model validation from a qualitative point of view and the number of failed layers as a validation criterion;
5. design a 3D footprint analysis methodology in the backing material and introduce two other parameters that reflect the behaviour of the designed panel: the volume of the footprint in the backing material and the area of the footprint relative to the initial surface of the backing material; these can be useful in the evaluation and ranking of some materials for ballistic protection panels,
6. analysis and interpretation of the experimental data, related to the back face signature (BFS). Other researchers investigating the influence of the number of layers, have observed that an increase in the number of layers leads to a higher energy absorption, to a certain extent, even up to the projectile stopping. However, when the number of layers exceeds a certain point, adding layers only leads to an increase in the mass of the protective system, compromising the ratio of impact resistance to the mass of the protective system,
7. a detailed macro- and micro-scale study of the failure processes in the tested ballistic panels (they are useful in comparing impact response with existing panels or data presented in the literature). This contributes to improving the performance of ballistic protection systems. As for the failure mechanism study, it should be said that, at the micro level, the fibre failure is similar for all tests and that differentiation was more useful using macro detail photographs of the shots on each layer.

Given the time constraints and limited financial resources available to me for this study, I have chosen to carry out the research on a limited number of samples, while attempting to outline possibilities for future optimisation in terms of the number of layers required for the specific targeted level of protection.

6.4. Research Perspectives Opened up by This Work

In the sphere of personal protection systems against ballistic impact, there is a continuous and dynamic competition between the penetrator and the ballistic protection design. The aim of this competition is to develop personal protection systems that are as versatile as possible and capable of dealing with multiple threats. Research areas in this field include:

- development and evaluation of new composite and/or hybrid materials based on high-strength fibres,
- evaluation of the obtained solutions on the basis of criteria related to the flexibility of mobile protective equipment, specific mass and manoeuvrability,

- simulation of impact processes at different levels, from the macro level to the meso level, in order to effectively exploit material properties and architecture,
- expanding the application of ballistic protection solutions in civil industries with impact risks, such as aerospace, energy, heavy industry, automotive and others.

This work may evolve in the following directions:

- development and testing of rigid protection systems for military personnel equipment, such as helicopter protection systems or light armoured vehicle protection systems. These protection systems could be made of semi-fabricated parts containing aramid fibres or combinations with metal or ceramic plates, with the advantage of a specific lower mass of the aramid fibre semi-fabricated parts.
- production and testing of personal protective vest samples made of Twaron CT736 material, complying with all current standards. This paper provides experimental results for panels of 16, 24, 28, 38 and 42 layers of Twaron CT736 fabric and hybrid panels of 16, 24, 28, 38 and 42 layers of Twaron SRM509 fabric and Twaron CT736 fabric, but the investigation of panels with an intermediate number of layers between 28 and 32 can help to reduce the mass of the product without compromising the safety in use of the protective system.
- extending the application of aramid fibre-based semi-finished products and their combinations with other materials for other fields of activity, where there is a risk of impact, such as the aeronautical industry or technological systems characterised by high working parameters, in particular velocity and load.

List of the author's scientific works

Articles in indexed/published journals or conference volumes indexed by Web of Science (WoS), visible in the database

1. Ojoc, G.G.; **Chiper Titire, L.**; Munteniță, C.; Pîrvu, C.; Sandu, S.; Deleanu, L. (2023) Ballistic Response of a Glass Fiber Composite for Two Levels of Threat. *Polymers*, 15, 1039. <https://doi.org/10.3390/polym15041039>, (IF=5,0)
2. Totolici Rusu V., Ojoc G. G., Cristea G. C., **Titire Chiper L.**, Botan M., Muntenita C., Deleanu L. (2022) Characteristics of Stab-resistance Panels Made of Twaron Aramid Fabrics, *Materiale Plastice (Mater. Plast.)*, Volume 59/4, 144-154, <https://doi.org/10.37358/MP.22.4.5633>, (IF=0,782)
3. **Titire, L. C.**, Musteata, A. E., CIOROMILA, A., Cristea, G. C., Ojoc, G. G., & Deleanu, L. (2021). Characterization of Blend PA6+ EPDM (60/40) by Tensile Tests. *Materiale Plastice*, 58(3), 51-63, <https://doi.org/10.37358/MP.21.3.5503>, WOS:000756838300001, (IF=0,782)
4. Georgescu, C.; Deleanu, L., **Chiper Titire, L.**, Ceoromila, A.C. (2021) Tribology of Polymer Blends PBT + PTFE. *Materials*, 14, 997. <https://doi.org/10.3390/ma14040997C>, WOS:000624122100001, (IF=3,4)

Articles in indexed journals or international conferences in BDI accepted by the specialized CNATDCU committee

1. **Chiper Titire, L.**, Ojoc, G., Popescu, C. & Deleanu, L. (3923). Simulation of an Impact on an Aramid Fabric Panel by A .357 Projectile. International conference KNOWLEDGE-BASED ORGANIZATION, 29(3) 1-9. <https://doi.org/10.2478/kbo-2023-0068>
2. Ojoc, G. G., Deleanu, L., **Titire, L. C.**, Munteniță, C., & Pîrvu, C. (2022). Simulation of impact on fiberglass laminated packages. International Multidisciplinary Scientific GeoConference: SGEM, 22(6.2), 23-30, <https://doi.org/10.5593/sgem2022V/6.2/s24.04>
3. **Chiper L.**, Ojoc G. G., Pîrvu C., Deleanu L., Simulation of projectile impact on layered package made of unidirectional glass fibers, *U.P.B. Sci. Bull., Series D*, Vol. 83, Iss. 4, 2021, ISSN 1454-2358, pp. 253-266. https://www.scientificbulletin.upb.ro/rev_docs_arhiva/rezeb0_352712.pdf

Articles in peer-reviewed journals indexed in international databases and international conferences

1. **Chiper Titire, L.**, **Ojoc G. G.**, Chiracu I. G., Deleanu L., The influence of introducing the cohesive zone model in simulating the impact of stratified composites, *Journal of Engineering Sciences and Innovation*, 8(1), 2023, pp. 1–16
2. **Chiper Titire L.**, Ojoc G. G., Munteniță C., Deleanu L. (2022) The Influence of Bonding Type of Two Target Models, *Mechanical Testing and Diagnosis*, Volume 1, pp. 12-19,

https://www.mtd.ugal.ro/download/2022-1/2_MTD-Volume-1-2022-Chiper-pp-12-19.pdf

3. Ojoc G. G., **Chiper Titire L.**, Pirvu C. and Popescu C., A ballistic impact model for evaluating a preliminary higher level from simulation and tests on a glass fiber composite, The 10th International Conference on Advanced Concepts in Mechanical Engineering (ACME 2022) 09/06/2022 - 10/06/2022 Online, 2022 IOP Conf. Ser.: Mater. Sci. Eng. 1262 012057, doi:10.1088/1757-899X/1262/1/012057.

4. **Chiper-Titire L.**, Totolici-Rusu V., Ojoc G. G., Influence of material characteristics on impact response for fabrics made of glass and aramid fibers, The 10th International Conference on Advanced Concepts in Mechanical Engineering – ACME 2022, „Gheorghe Asachi” Technical University of Iasi, Romania, June 09 – 10, 2022 ACME, doi:10.1088/1757-899X/1262/1/012045

5. Ojoc G. G., **Chiper Titire L.**, Deleanu L., Muntenita C., Pirvu C., Simulation of the Behavior of 32-Layer Composite Plate for Ballistic Protection, INCAS Bulletin, Volume 14, Issue 4/ 2022, pp. 95 – 109, <https://doi.org/10.13111/2066-8201.2022.14.4.8>

6. Ojoc G. G., **Titire Chiper L.**, Deleanu L., Failure simulation of stratified panel under ballistic impact, Journal of Engineering Sciences and Innovation Volume 7(2), 2022, pp. 143-158, <https://doi.org/10.56958/jesi.2022.7.2.143>

7. Ojoc G. G., **Chiper Titire L.**, Deleanu L., Simulation and analysis of the mechanical behaviour of a gas storage tanks, Mechanical Testing and Diagnosis, 11, (4), 2021, pp. 15-19

Books published

1. Deleanu L., Pîrvu C., Georgescu C., Ojoc G.G., **Titire Chiper L.**, Proiectarea reductoarelor cu roți dințate, Editura GUP, ISBN 978-606-696-222-3, 224 pagini, Galați, 2021
2. **Titire (Chiper) L.**, Munteniță C., G. G. Ojoc, Deleanu L., Aplicații pentru Elemente de Inginerie Mecanică, Galati University Press (GUP), ISBN978-606-696-260-5, 164 pagini,

Bibliography

- [1] Abteew, M. A., Boussu, F., & Bruniaux, P. (2021). Dynamic impact protective body armour: A comprehensive appraisal on panel engineering design and its prospective materials. *Defence Technology*, 17(6), 2027-2049, DOI: 10.1016/j.dt.2021.03.016
- [2] Almohandes, A. A., Abdel-Kader, M. S., & Eleiche, A. M. (1996). Experimental investigation of the ballistic resistance of steel-fiberglass reinforced polyester laminated plates. *Composites Part B: Engineering*, 27(5), 447-458, DOI:10.1016/1359-8368(96)00011-X
- [3] Asemani, S. S., Liaghat, G., Ahmadi, H., Anani, Y., Khodadadi, A., & Charandabi, S. C. (2021). The experimental and numerical analysis of the ballistic performance of elastomer matrix Kevlar composites. *Polymer Testing*, 102, 107311, DOI: 10.1016/j.polymertesting.2021.107311
- [4] Bajya, M., Majumdar, A., Butola, B. S., Arora, S., & Bhattacharjee, D. (2021). Ballistic performance and failure modes of woven and unidirectional fabric based soft armour panels. *Composite Structures*, 255, 112941, DOI: 10.1016/j.compstruct.2020.112941
- [5] Beck, J. (2016). U.S. Patent No. 9,435,614. Washington, DC: U.S. Patent and Trademark Office.
- [6] Bhatnagar, A., Arvidson, B., & Pataki, W. (2006). Prepreg ballistic composites. In *Lightweight ballistic composites* (pp. 272-304). Woodhead Publishing.
- [7] Bilisik, K. (2017). Two-dimensional (2D) fabrics and three-dimensional (3D) preforms for ballistic and stabbing protection: A review. *Textile Research Journal*, 87(18), 2275-2304, <https://doi.org/10.1177/004051751666907>
- [8] Briscoe, B. J., & Motamedi, F. (1992). The ballistic impact characteristics of aramid fabrics: the influence of interface friction. *Wear*, 158(1-2), 229-247, DOI:10.1016/0043-1648(92)90041-6
- [9] Caçoilo, A., Mourão, R., Teixeira-Dias, F., Azevedo, A., Coghe, F., & Valente, R. A. F. (2021). Modelling ballistic impact on military helmets: The relevance of projectile plasticity. *Defence Technology*, 17(5), 1699-1711, DOI: 10.1016/j.dt.2020.09.011
- [10] Chandekar, G. S., & Kelkar, A. D. (2014). Experimental and numerical investigations of textile hybrid composites subjected to low velocity impact loadings. *The Scientific World Journal*, DOI: 10.1155/2014/325783
- [11] Chen, X., Zhou, Y., & Wells, G. (2014). Numerical and experimental investigations into ballistic performance of hybrid fabric panels. *Composites Part B: Engineering*, 58, 35-42, DOI: 10.1016/j.compositesb.2013.10.019
- [12] Chen, X., Zhu, F., & Wells, G. (2013). An analytical model for ballistic impact on textile based body armour. *Composites Part B: Engineering*, 45(1), 1508-1514, <https://doi.org/10.1016/j.compositesb.2012.08.005>
- [13] Choudhury, S., Yerramalli, C. S., & Guha, A. (2023). Analytical modeling of the ballistic impact performance of glass fabric-epoxy composites at low temperatures. *International Journal of Impact Engineering*, 176, 104565, DOI: 10.1016/j.jcomc.2022.100263
- [14] Chu, Y., Chen, X., Sheel, D. W., & Hodgkinson, J. L. (2014). Surface modification of aramid fibers by atmospheric pressure plasma-enhanced vapor deposition. *Textile research journal*, 84(12), 1288-1297, DOI: 10.1177/0040517513515311

- [15] Chu, Y., Chen, X., Wang, Q., & Cui, S. (2014). An investigation on sol–gel treatment to aramid yarn to increase inter-yarn friction. *Applied surface science*, 320, 710-717, DOI: 10.1016/j.apsusc.2014.09.082
- [16] Cunniff, P. (1996). A Semiempirical Model for the Ballistic Impact Performance of Textile-Based Personnel Armor. *Textile Research Journal - TEXT RES J.* 66. 45-58. 10.1177/004051759606600107, DOI: 10.1177/004051759606600107
- [17] D'Amato, E. (2005). Nonlinearities in mechanical behavior of textile composites. *Composite structures*, 71(1), 61-67, DOI: 10.1016/j.compstruct.2004.09.026
- [18] D'Amato, E. (2001). Finite element modeling of textile composites. *Composite structures*, 54(4), 467-475, <https://doi.org/10.1177/0021998314535>
- [19] David, N. V., Gao, X. L., & Zheng, J. Q. (2009). Ballistic resistant body armor: contemporary and prospective materials and related protection mechanisms, DOI: 10.1115/1.3124644
- [20] Dogan, U., & Sunbuloglu, E. (2023). A novel simplified ballistic impact theory for woven composites. *International Journal of Impact Engineering*, 177, 104530, <https://doi.org/10.1016/j.ijimpeng.2023.104530>
- [21] Endruweit, A., Zeng, X., Matveev, M., & Long, A. C. (2018). Effect of yarn cross-sectional shape on resin flow through inter-yarn gaps in textile reinforcements. *Composites Part A: Applied Science and Manufacturing*, 104, 139-150, DOI: 10.1016/j.compositesa.2017.10.020
- [22] Fuqiang, L., Jingru, H., Runhua, L., Liang, Z., & Zheng, W. (2023, June). Numerical Simulation of Anti-penetration Performance of Ceramic/Aramid Fiber/PE-UHMW Composite Armor. *In Journal of Physics: Conference Series* (Vol. 2478, No. 7, p. 072034). IOP Publishing, DOI: 10.1088/1742-6596/2478/7/072034
- [23] Ghazlan, A., Ngo, T., Tan, P., Tran, P., & Xie, Y. M. (2023). A Numerical Modelling Framework for Investigating the Ballistic Performance of Bio-Inspired Body Armour. *Biomimetics*, 8(2), 195, <https://doi.org/10.3390/biomimetics8020195>
- [24] Gilson, L., Rabet, L., Imad, A., & Coghe, F. (2020). Experimental and numerical characterisation of rheological properties of a drop test response of a ballistic plastilina. *Forensic science international*, 310, 110238, DOI: 10.1016/j.forsciint.2020.110238
- [25] Gregori, D., Scazzosi, R., Nunes, S. G., Amico, S. C., Giglio, M., & Manes, A. (2020). Analytical and numerical modelling of high-velocity impact on multilayer alumina/aramid fiber composite ballistic shields: Improvement in modelling approaches. *Composites Part B: Engineering*, 187, 107830, DOI: 10.1016/j.compositesb.2020.107830
- [26] Grujicic, M. (2016). Multiscale modeling of polymeric composite materials for ballistic protection. In *Advanced Fibrous Composite Materials for Ballistic Protection* (pp. 323-361). Woodhead Publishing, DOI: 10.1016/B978-1-78242-461-1.00011-X
- [27] Grujicic, M., Bell, W. C., Arakere, G., He, T., & Cheeseman, B. A. (2009). A meso-scale unit-cell based material model for the single-ply flexible-fabric armor. *Materials & Design*, 30(9), 3690-3704, DOI:10.1016/J.MATDES.2009.02.008
- [28] Grujicic, M., Bell, W.C., Glomski, P.S., Pandurangan, B., Yen, C.-F., Cheeseman, B.A., 2011b. Filament-level modeling of aramid-based high performance structural materials. *Journal of Materials Engineering and Performance* 20, 1401-1413, DOI: 10.1007/s11665-010-9786-y
- [29] Grujicic, M., Bell, W.C., Glomski, P.S., Pandurangan, B., Yen, C.-F., Cheeseman, B.A., 2011c. Multi-length scale computational derivation of Kevlar® yarn-level material model. *Journal of Materials Science* 46, 4787-4802, DOI: 10.1007/s10853-011-5389-8

- [30] Grujicic, M., Pandurangan, B., Snipes, J.S., Yen, C.-F., Cheeseman, B.A., 2013a. Multi-length scale enriched continuum-level material model for Kevlar®-fiber reinforced polymer-matrix composites. *Journal of Materials Engineering and Performance* 22, 681-695, DOI: 10.1007/s11665-012-0329-6
- [31] Grujicic, M., Ramaswami, S., Snipes, J.S., Yavari, R., Lickfield, G.C., Yen, C.-F., Cheeseman, B.A., 2013b. Molecular-level computational investigation of mechanical transverse behavior of p-phenylene terephthalamide (PPTA) fibers. *Multidiscipline Modeling in Materials and Structures*, 9, 462-498, DOI 10.1108/MMMS-11-2012-0018
- [32] Grujicic, M., Ramaswami, S., Snipes, J.S., Yavari, R., Yen, C.-F., Cheeseman, B.A., 2013d. Axial-compressive behavior, including kink-band formation and propagation, of single p-phenylene terephthalamide (PPTA) fibers. *Advances in Materials Science and Engineering 2013*. Article ID 329549. <http://dx.doi.org/10.1155/2013/329549>
- [33] Grujicic, M., Yavari, R., Ramaswami, S., Snipes, J. S., Yen, C. F., & Cheeseman, B. A. (2013). Molecular-level study of the effect of prior axial compression/torsion on the axial-tensile strength of PPTA fibers. *Journal of materials engineering and performance*, 22, 3269-3287, DOI: 10.1007/s11665-013-0648-2
- [34] Grujicic, M., Yavari, R., Snipes, J. S., Ramaswami, S., Yen, C. F., & Cheeseman, B. A. (2014). The effect of plain-weaving on the mechanical properties of warp and weft p-phenylene terephthalamide (PPTA) fibers/yarns. *Journal of materials science*, 49, 8272-8293, DOI 10.1007/s10853-014-8536-1
- [35] Hakan, M., Gunes, R., Apalak, M. K., & Reddy, J. N. (2023). Normal and oblique ballistic impact damage behaviour of functionally graded plates: Experimental and numerical. *International Journal of Impact Engineering*, 181, 104756, DOI: 10.1080/15376494.2020.1717023
- [36] Ha-Minh, C., Boussu, F., Kanit, T., Crépin, D., & Imad, A. (2012). Effect of frictions on the ballistic performance of a 3D warp interlock fabric: numerical analysis. *Applied composite materials*, 19, 333-347, DOI: 10.1007/s10443-011-9202-2
- [37] Hasanzadeh, M., & Mottaghitalab, V. (2014). The role of shear-thickening fluids (STFs) in ballistic and stab-resistance improvement of flexible armor. *Journal of materials engineering and performance*, 23, 1182-1196, DOI: 10.1007/s11665-014-0870-6
- [38] Hassanpour Roubeneh, F., Liaghat, G., Sabouri, H., & Hadavinia, H. (2019). Experimental investigation of impact loading on honeycomb sandwich panels filled with foam. *International Journal of Crashworthiness*, 24(2), 199-210, DOI: 10.1080/13588265.2018.1426233
- [39] Hazzard, M. K., Trask, R. S., Heisserer, U., Van Der Kamp, M., & Hallett, S. R. (2018). Finite element modelling of Dyneema® composites: from quasi-static rates to ballistic impact. *Composites Part A: Applied Science and Manufacturing*, 115, 31-45, <https://doi.org/10.1016/j.compositesa.2018.09.005>
- [40] Hu, Q. R., Shen, X. Y., Qian, X. M., Huang, G. Y., & Yuan, M. Q. (2022). The personal protective equipment (PPE) based on individual combat: A systematic review and trend analysis. *Defence Technology*, DOI:10.1016/j.dt.2022.12.007
- [41] İşmal, Ö. E., & Paul, R. (2018). Composite textiles in high-performance apparel. *In High-performance apparel* (pp. 377-420). Woodhead Publishing, DOI: 10.1016/B978-0-08-100904-8.00019-5
- [42] Jafari, S., & Nia, A. A. (2023). Numerical and analytical investigation of ballistic performance of composite targets with ceramic-polyurea-metal layers and optimization of

- the layer thicknesses. *Journal of the Australian Ceramic Society*, 59(1), 231-244, <https://doi.org/10.1007/s41779-022-00829-9>
- [43] Joo K, Kang TJ., (2008), Numerical analysis of energy absorption mechanism in multi-ply fabric impacts. *Textile Research Journal* 2008;78(7):561–76, DOI: 10.1177/0040517507085194
- [44] Karahan, M. (2008). Comparison of ballistic performance and energy absorption capabilities of woven and unidirectional aramid fabrics. *Textile Research Journal*, 78(8), 718-730, DOI: 10.1177/0040517508090487
- [45] Karahan, M., Jabbar, A., & Karahan, N. (2015). Ballistic impact behavior of the aramid and ultra-high molecular weight polyethylene composites. *Journal of Reinforced Plastics and Composites*, 34(1), 37-48, DOI: 10.1177/0731684414562223
- [46] Karahan, M., Kuş, A., & Eren, R. (2008). An investigation into ballistic performance and energy absorption capabilities of woven aramid fabrics. *International Journal of Impact Engineering*, 35(6), 499-510, DOI: 10.1016/j.ijimpeng.2007.04.003
- [47] Kumar, V., Bajja, M., Majumdar, A., & Dubey, D. K. (2023). Design of Cost-Effective Hybrid Soft Armour Panels Using Strategic Replacement of Backing layers with non-Ballistic Materials: A Parametric Study. *International Journal of Impact Engineering*, 104678, DOI: 10.1016/j.ijimpeng.2023.104678
- [48] Lane, R. A. (2005). High performance fibers for personnel and vehicle armor systems. *Amptiac Quarterly*, 9(2), 3-9.
- [49] Lee, B. L., Walsh, T. F., Won, S. T., Patts, H. M., Song, J. W., & Mayer, A. H. (2001). Penetration failure mechanisms of armor-grade fiber composites under impact. *Journal of composite materials*, 35(18), 1605-1633, <https://doi.org/10.1106/YRBH-JGT9-U6PT-L555>
- [50] Lim, C. T., Shim, V. P. W., & Ng, Y. H. (2003). Finite-element modeling of the ballistic impact of fabric armor. *International Journal of Impact Engineering*, 28(1), 13-31, DOI: 10.1016/S0734-743X(02)00031-3
- [51] Liu, P., Wang, Z., Zhou, H., Zhang, H., & Huang, G. (2023). An analytical model to predict back face deformation of hybrid soft body armors under ballistic impact. *International Journal of Impact Engineering*, 180, 104723, DOI: 10.1016/j.ijimpeng.2023.104723
- [52] López-Gálvez, H., Rodríguez-Millán, M., Feito, N., & Miguelez, H. (2016). A method for inter-yarn friction coefficient calculation for plain wave of aramid fibers. *Mechanics Research Communications*, 74, 52-56.
- [53] Mallick, P.K. (2007). *Fiber-Reinforced Composites: Materials, Manufacturing, and Design, Third Edition (3rd ed.)*. CRC Press. <https://doi.org/10.1201/9781420005981>
- [54] Marques, C. L. M., Kumar, S. R., Goswami, C., & Verma, R. (2021). Numerical simulation of armor materials and optimization using gray relational analysis. *Materials Today: Proceedings*, 44, 4717-4730, DOI: 10.1016/j.matpr.2020.10.942
- [55] Mohamadipoor, R., Zamani, E., & Pol, M. H. (2018). Analytical and experimental investigation of ballistic impact on thin laminated composite plate. *International Journal of Applied Mechanics*, 10(02), 1850020, DOI: 10.1142/S1758825118500205
- [56] Mohammed, M. N., Al-Zubaidi, S., Bahrain, S. H. K., & Sapuan, S. M. (2021). State-of-the-art review on recent advances and perspectives of ballistic composite materials. *Composite Solutions for Ballistics*, 3-54, DOI: 10.1016/B978-0-12-821984-3.00004-8.
- [1] Mohotti, D., Raman, S. N., Ngo, T., & Mendis, P. (2015). Use of coupled smooth-particle hydrodynamics/lagrangian method in the simulation of deformable projectile penetration. Mudric, T., Giacomuzzo, C., Francesconi, A., & Galvanetto, U. (2016). Experimental

- investigation of the ballistic response of composite panels coupled with a self-healing polymeric layer. *Journal of Aerospace Engineering*, 29(6), 04016047, DOI: 10.1061/(ASCE)AS.1943-5525.0000628
- [2] Mudzi, P., Wu, R., Firouzi, D., Ching, C. Y., Farncombe, T. H., & Selvaganapathy, P. R. (2022). Use of patterned thermoplastic hot film to create flexible ballistic composite laminates from UHMWPE fabric. *Materials & Design*, 214, 110403, <https://doi.org/10.1016/j.matdes.2022.110403>
- [3] Naik N.K., Shirao P., Reddy B.C.K., (2006) Ballistic impact behaviour of woven fabric composites: formulation, *International Journal of Impact Engineering*. 32 (9) 15211552, DOI: 10.1016/j.ijimpeng.2005.01.004
- [4] Nilakantan, G., Horner, S., Halls, V., & Zheng, J. (2018). Virtual ballistic impact testing of Kevlar soft armor: Predictive and validated finite element modeling of the V0-V100 probabilistic penetration response. *Defence technology*, 14(3), 213-225, DOI: 10.1016/j.dt.2018.03.001
- [5] Öberg EK, Dean J, Clyne TW., (2015), Effect of inter-layer toughness in ballistic protection systems on absorption of projectile energy. . *International journal of impact engineering*; 76:75–82, DOI: 10.1016/j.ijimpeng.2014.09.006
- [6] Oliveira, M. S., da Costa Garcia Filho, F., Pereira, A. C., Nunes, L. F., da Luz, F. S., de Oliveira Braga, F., ... & Monteiro, S. N. (2019). Ballistic performance and statistical evaluation of multilayered armor with epoxy-fique fabric composites using the Weibull analysis. *Journal of Materials Research and Technology*, 8(6), 5899-5908, DOI: 10.1016/j.jmrt.2019.09.064
- [7] Othman, A. R., & Hassan, M. H. (2013). Effect of different construction designs of aramid fabric on the ballistic performances. *Materials & Design*, 44, 407-413, DOI: 10.1016/j.matdes.2012.07.061
- [8] Pandya, K. S., Kumar, C. V. S., Nair, N. S., Patil, P. S., & Naik, N. K. (2015). Analytical and experimental studies on ballistic impact behavior of 2D woven fabric composites. *International Journal of Damage Mechanics*, 24(4), 471-511, DOI: 10.1177/1056789514531440
- [9] Peroni L., Scapin M.; Fichera C.; Manes A., Giglio M., (2012), Mechanical properties at high strain-rate of lead core and brass jacket of a NATO 7.62 mm ball bullet in numerical simulations of ballistic impacts. *Proc. DYMAT 2012*, 26, 01060, <https://doi.org/10.1051/epjconf/20122601060>
- [10] Pinkos, J., Stempien, Z., & Smędra, A. (2023). Experimental analysis of ballistic trauma in a human body protected with 30 layer packages made of biaxial and triaxial Kevlar® 29 fabrics. *Defence technology*, 21, 73-87, DOI: 10.1016/j.dt.2022.07.004
- [11] Pirvu, C., & Deleanu, L. (2018). Ballistic testing of armor panels based on aramid. *In Ballistics. IntechOpen*, DOI: 10.5772/intechopen.78315
- [12] Pirvu, C., Badea, S., & Deleanu, L. (2014). Influence of several parameters on simulating the ballistic impact on a homogenous plate. *Applied Mechanics and Materials*, 658, 201-206, DOI: 10.4028/www.scientific.net/AMM.658.201
- [13] Porwal, P. K., & Phoenix, S. L. (2005). Modeling system effects in ballistic impact into multi-layered fibrous materials for soft body armor. *International journal of fracture*, 135, 217-249, DOI: 10.1007/s10704-005-3993-9
- [14] Ralph, C., Baker, L., Archer, E., & McIlhagger, A. (2023). Optimization of soft armor: the response of homogenous and hybrid multi-ply para-aramid and ultra-high molecular weight

- polyethylene fabrics under ballistic impact. *Textile Research Journal*, 00405175231194365, <https://doi.org/10.1177/00405175231194365>
- [15] Rezasefat, M., Ma, D., da Silva, A. A., Colombo, C., Amico, S. C., Giglio, M., & Manes, A. (2023). Multi-criteria decision-making analysis and numerical simulation of the low-velocity impact response of inter-ply S2-glass/aramid woven fabric hybrid laminates. *Composite Structures*, 312, 116867, DOI: 10.1016/j.compstruct.2023.116867
- [57] Roylance, D., Hammas, P., Ting, J., Chi, H., & Scott, B. (1995). Numerical modeling of fabric impact. *ASME-Publications-AD*, 48, 155-160.
- [58] Sadegh, A. M., & Cavallaro, P. V. (2012). Mechanics of energy absorbability in plain-woven fabrics: an analytical approach. *Journal of Engineered Fibers and Fabrics*, 7(1), DOI: 10.1177/155892501200700102
- [59] Saleem, I. A., Ahmed, P. S., & Abed, M. S. (2022). Experimental and numerical investigation of Kevlar and UHMWPE multi-layered armors against ballistic impact. *Materials Today: Proceedings*, 56, 2516-2524, DOI: 10.1177/155892501200700102
- [60] Saxtorph, N. M., Gosney, B., & GOSNEY, I. (1972). Krigsfolk Gennem Tiden. Warriors and Weapons of Early Times in Colour... Illustrated by Stig Bramsen.(Translated... by Bob and Inge Gosney). *Blandford Press*.
- [61] Scott, R. A. (Ed.). (2005). Textiles for protection. *Elsevier*, p 229
- [62] Shaktivesh, Nair, N. S., & Naik, N. K. (2015). Ballistic impact behavior of 2D plain weave fabric targets with multiple layers: Analytical formulation. *International Journal of Damage Mechanics*, 24(1), 116-150, DOI: 10.1177/1056789514524074
- [63] Shim, V. P. W., Lim, C. T., & Foo, K. J. (2001). Dynamic mechanical properties of fabric armour. *International Journal of Impact Engineering*, 25(1), 1-15, DOI: 10.1016/S0734-743X(00)00038-5
- [64] Shim, V. P. W., Tan, V. B. C., & Tay, T. E. (1995). Modelling deformation and damage characteristics of woven fabric under small projectile impact. *International Journal of Impact Engineering*, 16(4), 585-605.
- [65] Signetti, S., Bosia, F., Ryu, S., & Pugno, N. M. (2020). A combined experimental/ numerical study on the scaling of impact strength and toughness in composite laminates for ballistic applications. *Composites Part B: Engineering*, 195, <https://doi.org/10.1016/j.compositesb.2020.108090>
- [66] Sikarwar, R. S., Velmurugan, R., & Madhu, V. (2012). Experimental and analytical study of high velocity impact on Kevlar/Epoxy composite plates. *Central European Journal of Engineering*, 2, 638-649, DOI: 10.2478/s13531-012-0029-x
- [67] Sockalingam, S., Gillespie Jr, J. W., & Keefe, M. (2017). Role of inelastic transverse compressive behavior and multiaxial loading on the transverse impact of Kevlar KM2 single fiber. *Fibers*, 5(1), 9, <https://doi.org/10.3390/fib5010009>
- [68] Song, B., Park, H., Lu, W., and Chen, W. (2011). Transverse Impact Response of a Linear Elastic Ballistic Fiber Yarn. *ASME. Journal of Applied Mechanics September 2011; 78(5): 051023*. <https://doi.org/10.1115/1.4004310>
- [69] Soydan, A. M., Tunaboylu, B., Elsabagh, A. G., Sari, A. K., & Akdeniz, R. (2018). Simulation and experimental tests of ballistic impact on composite laminate armor. *Advances in materials science and engineering*, 2018, 1-12, DOI: 10.1155/2018/4696143
- [70] Sun, D., Jiang, J., Zhang, M., & Wang, Z. (2016). Ballistic experiments on the mechanism of protective layer against domino effect caused by projectiles. *Journal of loss prevention in the process industries*, 40, 17-28, <https://doi.org/10.1016/j.ssci.2020.104618>

- [71] Tabiei, A., & Ivanov, I. (2002). Computational micro-mechanical model of flexible woven fabric for finite element impact simulation. *International journal for numerical methods in engineering*, 53(6), 1259-1276, DOI: 10.1002/nme.321
- [72] Tabiei, A., & Nilakantan, G. (2008). Ballistic Impact of Dry Woven Fabric Composites: A Review. ASME. *Applied Mechanics Reviews* 61(1): 010801, DOI: 10.1115/1.2821711
- [73] Tahir, D., Zhang, M., & Hu, H. (2022). Auxetic materials for personal protection: a review. *physica status solidi (b)*, 259(12), 2200324., <https://doi.org/10.1002/pssb.202200324>
- [74] Tam, T., & Bhatnagar, A. (2016), 1 - High-performance ballistic fibers and tapes, Editor(s): Ashok Bhatnagar, In *Woodhead Publishing Series in Composites Science and Engineering, Lightweight Ballistic Composites (Second Edition)*, Woodhead Publishing, 2016, Pages 1-39, eBook ISBN: 9780081004258
- [75] Tarfaoui, M., & Akesbi, S. (2001). A finite element model of mechanical properties of plain weave. *Colloids and Surfaces A: Physicochemical and Engineering Aspects*, 187, 439-448, DOI: 10.1016/S0927-7757(01)00611-2
- [76] Tarfaoui, M., & Akesbi, S. (2001). Numerical study of the mechanical behaviour of textile structures. *International Journal of Clothing Science and Technology*, 13(3/4), 166-175, DOI: 10.1108/EUM0000000005780
- [77] Vescovini, A., Balen, L., Scazzosi, R., da Silva, A. A. X., Amico, S. C., Giglio, M., & Manes, A. (2021). Numerical investigation on the hybridization effect in inter-ply S2-glass and aramid woven composites subjected to ballistic impacts. *Composite Structures*, 276, 114506, DOI: 10.1016/j.compstruct.2021.114506
- [78] Wu, S., Xu, Z., Hu, C., Zou, X., & He, X. (2022). Numerical simulation study of ballistic performance of Al₂O₃/aramid-carbon hybrid FRP laminate composite structures subject to impact loading. *Ceramics International*, 48(5), 6423-6435, DOI: 10.1016/j.ceramint.2021.11.186
- [79] Xie, Z., Chen, W., Liu, Y., Liu, L., Zhao, Z., & Luo, G. (2023). Design of the ballistic performance of shear thickening fluid (STF) impregnated Kevlar fabric via numerical simulation. *Materials & Design*, 226, 111599, DOI:10.1016/j.matdes.2023.111599
- [80] Yang, C. C., Ngo, T., & Tran, P. (2015). Influences of weaving architectures on the impact resistance of multi-layer fabrics. *Materials & Design*, 85, 282-295, DOI: 10.1016/j.matdes.2015.07.014
- [81] Yang, Y., & Chen, X. (2017). Investigation of failure modes and influence on ballistic performance of Ultra-High Molecular Weight Polyethylene (UHMWPE) uni-directional laminate for hybrid design. *Composite Structures*, 174, 233-243, DOI: 10.1016/j.compstruct.2017.04.033
- [82] Yang, Y., & Chen, X. (2019). Influence of fabric architecture on energy absorption efficiency of soft armour panel under ballistic impact. *Composite Structures*, 224, 111015, DOI: 10.1016/j.compstruct.2019.111015
- [83] Yavaş, M. O., Ahmet, A. V. C. I., ŞİMŞİR, M., & AKDEMİR, A. (2015). Ballistic performance of Kevlar49/UHMW-PEHB26 hybrid layered-composite. *International Journal of Engineering Research and Development*, 7(4), 21-27, DOI: 10.29137/umagd.379789
- [84] Yuan, Z., Zeng, H., Xu, W., Qiu, J., Xu, Y., & Chen, X. (2021). Reverse engineering for estimation of shear modulus for yarn models in finite element modelling for ballistic impact. *Composite Structures*, 274, 114371, <https://doi.org/10.1016/j.compstruct.2021.114371>
- [85] Zhang, D., Sun, Y., Chen, L., Zhang, S., & Pan, N. (2014). Influence of fabric structure and thickness on the ballistic impact behavior of Ultrahigh molecular weight polyethylene

- composite laminate. *Materials & Design (1980-2015)*, 54, 315-322, DOI: 10.1016/j.matdes.2013.08.074
- [86] Zhang, R., Han, B., Zhong, J. Y., Qiang, L. S., Ni, C. Y., Zhang, Q., ... & Lu, T. J. (2022). Enhanced ballistic resistance of multilayered cross-ply UHMWPE laminated plates. *International Journal of Impact Engineering*, 159, 104035, DOI: 10.1016/j.ijimpeng.2021.104035
- [87] Zhang, Y. D., Wang, Y. L., Huang, Y., & Wan, Y. Z. (2006). Preparation and properties of three-dimensional braided UHMWPE fiber reinforced PMMA composites. *Journal of reinforced plastics and composites*, 25(15), 1601-1609, DOI: 10.1177/0731684406068400
- [88] Zhou, Y., Ding, S., Zhang, Z., Li, H., Lin, Y., Sun, M., & Wang, M. (2022). The Ballistic responses of thread-quilted plain weaves with increased yarn–yarn friction. *Thin-Walled Structures*, 171, 108762.
- [89] Zhu, D., Vaidya, A., Mobasher, B., & Rajan, S. D. (2014). Finite element modeling of ballistic impact on multi-layer Kevlar 49 fabrics. *Composites Part B: Engineering*, 56, 254-262, DOI: 10.1016/j.compositesb.2013.08.051
- [90] Zochowski, P., Cegła, M., Szczurowski, K., Mączak, J., Bajkowski, M., Bednarczyk, E., ... & Prasula, P. (2023). Experimental and numerical study on failure mechanisms of the 7.62×25 mm FMJ projectile and hyperelastic target material during ballistic impact. *Continuum Mechanics and Thermodynamics*, 35(4), 1745-1767, DOI: 10.1007/s00161-023-01210-2
- [91] *** ANSYS Explicit Dynamics Analysis Guide (2021). ANSYS, Inc., USA
- [92] *** Ballistic Resistance of Personal Body Armor NIJ Standard–0101.04, U.S. Department of Justice Office of Justice Programs National Institute of Justice, 2004, accesibil la adresa: <https://ojp.gov/pdffiles1/nij/183651.pdf>
- [93] *** Catalog Teijin Ballistics Material Handbook QMB1.1-20181001EN
- [94] *** Catalog Teijin Ballistics Material Handbook, 38-14-05/2012
- [95] *** STANAG 2920 PPS (edition 2) - Ballistic Test method for Personal Armour Materials and combat clothing, NATO, 2003.
- [96] *** 2011 Opportunities in protection materials science and technology for future army applications, Committee on Opportunities in Protection Materials Science and Technology for Future Army Applications National Research Council, ISBN 978-0-309-21285-4
- [97] *** Autodesk, Inc. (2021). Autodesk Inventor (Versiunea 2022). <https://www.autodesk.com/products/inventor/overview>
- [98] *** EN 1063:1999 Glass in building. Security glazing. Testing and classification of resistance against bullet attack (under revision)
- [99] *** EN 1522:2004 Windows, doors, shutters and blinds. Bullet resistance. Requirements and classification
- [100] *** EN 1523:2004 Windows, doors, shutters and blinds - Bullet resistance - Test method